


12-2014

QUANTITATIVE ANALYSIS AND IMAGING-BASED INSIGHTS INTO THE CHARACTERISTICS AND MECHANISMS OF YEAST PATTERN FORMATION

LIN CHEN

Follow this and additional works at: http://digitalcommons.library.tmc.edu/utgsbs_dissertations

 Part of the [Medicine and Health Sciences Commons](#), [Other Life Sciences Commons](#), [Other Microbiology Commons](#), and the [Systems Biology Commons](#)

Recommended Citation

CHEN, LIN, "QUANTITATIVE ANALYSIS AND IMAGING-BASED INSIGHTS INTO THE CHARACTERISTICS AND MECHANISMS OF YEAST PATTERN FORMATION" (2014). *UT GSBS Dissertations and Theses (Open Access)*. Paper 524.

This Dissertation (PhD) is brought to you for free and open access by the Graduate School of Biomedical Sciences at DigitalCommons@The Texas Medical Center. It has been accepted for inclusion in UT GSBS Dissertations and Theses (Open Access) by an authorized administrator of DigitalCommons@The Texas Medical Center. For more information, please contact laurel.sanders@library.tmc.edu.

**QUANTITATIVE ANALYSIS AND IMAGING-BASED INSIGHTS INTO THE
CHARACTERISTICS AND MECHANISMS OF YEAST
PATTERN FORMATION**

By

Lin Chen, M.Sc

APPROVED

Gábor Balázsi, PhD., Advisor

Yi Xu, PhD., On-Site Advisor

Krešimir Josić, PhD.

Heidi B. Kaplan, Ph.D.

Jeffrey J. Tabor, PhD.

APPROVED

Dean, The University of Texas Health Science Center at Houston

Graduate School of Biomedical Sciences

**QUANTITATIVE ANALYSIS AND IMAGING-BASED INSIGHTS INTO THE
CHARACTERISTICS AND MECHANISMS OF YEAST
PATTERN FORMATION**

A

DISSERTATION

Presented to the Faculty of
The University of Texas
Health Science Center at Houston
and
The University of Texas
MD Anderson Cancer Center
Graduate School of Biomedical Sciences
in Partial Fulfillment
of the Requirements
for the Degree of
DOCTOR OF PHILOSOPHY

by

Lin Chen, M.Sc.
Houston, TX

December, 2014

DEDICATION

I want to dedicate this work to all my family members for their love and support.

ACKNOWLEDGEMENT

I would like to express by sincere gratitude to my advisor Dr. Gábor Balázs for his exceptional guidance, support and patience during my Ph.D study. I sincerely appreciate his encouragement on exploring interdisciplinary knowledge to answer scientific questions innovatively. His excellent mentorship, the collaborative and diverse research atmosphere in the lab helped me tremendously now and will hereafter.

I would especially like to thank my committee members, Dr. Yi Xu (on-site Advisor), Dr. Krešimir Josić, Dr. Heidi B. Kaplan, Dr Jeffrey J. Tabor, Dr. Ba-Bie Teng and Dr. Kevin A. Morano for their support throughout my training, their innovative ideas and excellent guidance on the projects and excellent advice on the manuscript and dissertation.

I also want to give a huge thank you to my collaborators Dr. Pankaj Mehta, Javad Noorbakhsh, Dr. Rhys M. Adams, Dr. Jennie Kuzdzal-Fick, Dr. Dmitry Nevozhay, Joseph Samaniego-Evans and Germaine Agollah for their excellent work, inspiring discussions on the projects and the manuscript. I thank Richard A. Breckenridge and the Histology Labs at The University of Texas Medical School at Houston for cryosectioning the yeast colonies. My sincere gratitude also goes to my lab members and colleagues in the Department of System Biology at MD Anderson for the interesting discussions and the great atmosphere.

Last but not the least, I would like to thank my family and my friends for their support and love through the good and tough times.

ABSTRACT

QUANTITATIVE ANALYSIS AND IMAGING-BASED INSIGHTS INTO THE CHARACTERISTICS AND MECHANISMS OF YEAST PATTERN FORMATION

Lin Chen, M.Sc

Supervisory Professor: Gábor Balázsi, PhD.

On-Site Advisor: Yi Xu, Ph.D.

Biofilm formation is a common lifestyle adapted by bacteria and fungi in response to various environmental stresses. Bacterial and fungal biofilms adhering to medical devices convey resistance to antibiotics or biocides, causing high rates of clinical infections. Microorganisms are protected from harsh environmental conditions by reduced stress penetration through the complex biofilm architecture with distinct patterns. Although the molecular regulations of surface patterning have been well characterized in bacteria, the mechanisms underlying the complex pattern formation in eukaryotic biofilms remain unclear.

This dissertation aims to investigate the salient features of robust colony expansion in yeast biofilms and the processes driving the complex pattern development.

Various salient features of *Saccharomyces cerevisiae* colony expansion, such as of the change of size, shape, and surface pattern properties were analyzed quantitatively for various combinations of agar and sugar concentrations. I found that the size and irregularity of the *FLO11* expressing colony, and wavelength of the pattern were all monotonically decreasing with agar density. These trends were consistent regardless of sugar sources. Using a mathematical model, I also demonstrated that the differential expansion pattern between the center and the edge of the colony due to the spatial differences in glucose concentration affected the convexity of the expansion curve.

I found that pattern formation in *S. cerevisiae* was not caused by localized cell death as in *Bacillus subtilis* biofilms. Using quantitative measurement and physical models, I found that the surface pattern of *S. cerevisiae* was consistent with hierarchical wrinkling, determined by the physicochemical properties and thickness of the layered structures of the yeast biofilm and the viscoelastic agar. Furthermore, I found that two-dimensional expansion conferred a competitive advantage for *FLO11* sectors during head-to-head competition with *flo11Δ* cells. Overall these results suggested that two-dimensionality of expansion conveyed by *FLO11* directs rapid colony expansion with high irregularity at the rim, hierarchical wrinkling pattern, and competitive advantage during head-to-head competition.

TABLE OF CONTENTS

APPROVAL SHEET	i
TITLE PAGE	ii
DEDICATION.....	iii
ACKNOWLEDGEMENT.....	iv
ABSTRACT	v
TABLE OF CONTENTS	vii
LIST OF ILLUSTRATIONS.....	ix
LIST OF TABLES.....	x
Chapter 1.....	1
Introduction.....	1
1.1 The influence of biofilms on industry and medicine.....	1
1.2 Biofilm development, architecture, and organization.....	6
1.3 Multicellularity in yeast.....	17
Chapter 2.....	23
Salient traits of <i>S. cerevisiae</i> colony expansion in response to various environmental cues	23
2.1 Introduction.....	23
2.2 Materials and Experimental Methods	25
2.3 Results.....	30
2.4 Discussion.....	42
Chapter 3.....	44
Mechanisms Underlying Pattern Formation in <i>S. cerevisiae</i>	44
3.1 Introduction.....	44
3.2 Materials and Experimental Methods	47
3.3 Result	60
3.4 Discussion.....	76
Chapter 4.....	78
Biological function of two-dimensional expansion	78
4.1 Introduction.....	78

4.2 Materials and Experimental Methods	79
4.3 Result	80
4.4 Discussion.....	93
Chapter 5.....	95
Discussion and future directions	95
5.1 Distinct colony expansion conveyed by Flo11p	96
5.2 Hierarchical wrinkling triggers pattern formation in <i>Flo11</i> colony	98
5.3 <i>FLO11</i> directed two-dimensional expansion confers competitive advantage during head-to-head competition	100
Reference	104
Bibliography	124
Vita	125

LIST OF ILLUSTRATIONS

Figure 1 Hierarchical wrinkling in non-biological systems.....	15
Figure 2 Colony size and irregularity for various glucose and agar concentrations.....	31
Figure 3 <i>FLO11</i> colonies expanded faster and were more irregular than <i>flo11Δ</i> colonies on YPGal plates.....	34
Figure 4 Colony characteristics as functions of agar and glucose concentration.....	35
Figure 5 No significant growth difference between <i>FLO11</i> and <i>flo11Δ S. cerevisiae</i> cells in liquid media.....	37
Figure 6 Mathematical model for colony expansion.....	40
Figure 7 Cell death was minimal and uniform during <i>FLO11</i> colony expansion.....	62
Figure 8 Distributions of inter-spoke distances (wavelengths) of <i>FLO11</i> colony.....	64
Figure 9 Analysis of the wavelengths of colony surface patterns.....	67
Figure 10 <i>FLO11</i> -induced wrinkles on the colony surface.....	69
Figure 11 The cross-sectional view of hierarchical wrinkles of a <i>FLO11</i> colony.....	72
Figure 12 The fit of physical models to data on primary and secondary wrinkles.....	75
Figure 13 <i>FLO11</i> cells out-expanded <i>flo11Δ</i> cells during head-to-head competition.....	82
Figure 14 Same-strain controls for competition between <i>FLO11</i> and <i>flo11Δ</i> colonies.....	84
Figure 15 <i>FLO11</i> cells out-expanded <i>flo11Δ</i> cells during head-to-head competition.....	87
Figure 16 Ratio-dependent head-to-head competition between <i>FLO11</i> and <i>flo11Δ</i> cells.....	89
Figure 17 <i>FLO11</i> cells out-expanded <i>flo11Δ</i> cells during head-to-head competition.....	91
Figure 18 <i>FLO11</i> cells out-expanded <i>flo11Δ</i> cells during head-to-head competition.....	92
Figure 19 Summary.....	102

LIST OF TABLES

Table 1 The number of distances measured for primary and secondary wrinkles	50
Table 2 Young's modulus in response to various agar concentrations	55
Table 3 Average wavelengths for primary and secondary wrinkles.....	65

Chapter 1

Introduction

Biofilms, known as the major form of existence for many bacteria in various environments, have gained interest in the 70s (1). Biofilms are multicellular structures developed by microorganisms in response to various environmental cues in nature, in order to adapt to harsh environments (2, 3). A wide range of genetics, microscopy and computational methods have been developed to reveal the complex development of biofilms, which consist of organized structures with layers of specialized cells displaying distinct metabolic states (4-11).

1.1 The influence of biofilms on industry and medicine

Biofilms with distinct patterns have been observed to cause detrimental effect in various industries, from water system, heat-exchange system, food industry and dentistry to medicine (4, 12-20). The prevalence of biofilms not only results in high economic costs for cleaning the contaminated devices, but also imposes emergent threats to human health (12).

1.1.1 The corrosion of water systems by biofilms

The components of water distributions systems, such as water pipes and drinking water devices, are found to be the habitats for various biofilms, such as those

caused by *Campylobacter* (21), *Escherichia coli* (22-31), *Pseudomonas aeruginosa* (25, 30, 32, 33), which cause contamination to the drinking water, resulting in increasing health concerns (16, 34). For instance, on water pipe surfaces, sulfate-reducing bacterial (SRB) biofilms reduce sulfate to hydrogen sulfide, resulting in the mobilization of ions due to differential physicochemical properties (4, 35-40). Therefore, the adherence of SRB biofilms to the water pipe surfaces could cause severe metal corrosion of the water distribution systems, resulting in a burden for the economy (4, 17, 27).

1.1.2 Biofilm contamination in food industry

Pathogenic bacteria, existing in the form of biofilms, are known to cause contamination to food processing systems (17, 41-44). The Center for Disease Control and Prevention (CDC) reported 48 million cases of foodborne diseases in 2013 in USA (CDC 2013). After pasteurization, the attachment of biofilms, composed of *Staphylococcus aureus* (45), *Listeria monocytogenes* (46, 47), *Klebsiella oxytoca* (48), *Bacillus cereus* and *Pseudomonas fluorescens* (49), to the milk processing components that were made of various materials (45, 50), results in the persistent contamination of the milk products. Biofilms could also gradually accumulate in the ready-to-eat meat, resulting in severe problems for food safety and quality (51). Biofilm contamination in the food industry also occurs through the food processing equipment, food processing environment and food handler (52, 53).

The contamination of biofilms, composed of *Legionella pneumophila*, *Staphylococcus xylosum*, *Listeria monocytogenes*, to food industry is also associated with their capacity to attach to a diverse range of the materials important to food processing environments, from stainless steel, polyethylene, polypropylene, acetal resin, rubber to glass (12, 44, 54-57).

The capability of biofilms to attach to various materials leading to persistent contamination in the food industry, is related to the physicochemical interactions between biofilms and the substrates, the nutrients in the environment, as well as the biofilm architecture development upon attachment (54, 55, 58-60). Therefore, understanding the mechanisms underlying the biofilms architecture development and their physical interactions with the surface are critical to the development of potential treatments for biofilms in the food industry.

1.1.3 Medical relevance of biofilms

Biofilms, in the form of dental plaques, cause various dental infectious diseases, ranging from caries to periodontal disease (19, 20, 61-63). Dental plaques are formed by the attachment of mixed species, such as the initial establishment of *Streptococci*, followed by the accumulation of *Actinomyces*, and then the attachment of anaerobic Gram-negative bacteria (62, 64). The mixed species interact with each other through lectin bonds to aggregate and assemble into biofilms (65-69). The adhered biofilms in the mouth are resistant to the physical stress caused by the salivary flow shear force

(61).

Besides dental plaques, biofilms also impose threats to public health as a dominant causes for health-care related nosocomial infections, with 2 million cases including about 100,000 deaths annually (2, 53, 70-77). Biofilms cause high mortality rates through adherence to hospital medical equipment, invasive devices, such as pyrolytic carbon heart valves, catheters, intubations, and prostheses, made from various materials ranging from metal, rubber, plastic to glass (53, 78, 79).

Therefore, understanding of the process of complex biofilm formation on biomaterial and abiotic surfaces will promote the treatment or cleaning process to remove persistent biofilms in food industry or medical devices (12).

1.1.4 Drug resistance of biofilms

The organization and morphology are critical for controlling infections caused by biofilms grown on organs or medical devices (78). The phenotypic variants of *S. aureus* biofilm with distinct colony morphologies render different sensitivity and persistence to antibiotics, suggesting the importance of biofilm structures to the *S. aureus* persistence (80). The distinct morphology of the *Pseudomonas aeruginosa* biofilm adapted in the cystic fibrosis-affected lung plays a role in the aggravation of the disease (81). The phenotypic variant of *P. aeruginosa*, rugose small-colony variants (RSCV) with a rougher colony than wild type, demonstrates higher resistance to a wide range of antibiotics, ranging from tobramycin, tetracyclin to kanamycin (82). *Uropathogenic*

strains of Escherichia coli (UPEC), which is the major cause of urinary tract infections (UTIs), organizes into biofilm-like structures encased in matrix with close interaction with the environment, resulting in billions of cost in medical expense and afflicting the public health (83-86). This organized structure contributes to the persistence of bladder infections despite of diversity in host defense (86, 87).

Bacterial biofilms are known to confer antibiotic resistance via many mechanisms including expressing multi-drug resistant pumps. The multiple antibiotic resistance (*mar*) gene encoding efflux pumps confers multidrug resistance in *E. coli* to a large spectrum of biocides, ranging from various toxic chemicals, antibiotics to disinfectants (88).

In addition to the conventional drug resistance pumps, biofilms can also provide physical shield to protect microbes from various antibiotics and biocides. For instance, *E. coli* and *P. aeruginosa* biofilms that do not express *mar* or *mexAB-oprM* multidrug pump genes still confer resistance to antibiotics, such as ciprofloxacin (89-91).

Actually, the multicellular biofilm structure conveys a conspicuous advantage in protecting microbes within the biofilm, which requires thousands-fold-higher concentrations of antibiotics compared to planktonic microbes (92, 93). The complex structure of the biofilms and the physical properties of the extracellular matrix (ECM) contribute to the antibiotic resistance and persistence of biofilm infections (92). The biofilm matrix significantly enhances drug resistance through the reduction of antibiotic penetration inside the biofilms (92). For instance, *Klebsiella pneumoniae* biofilm

markedly reduces the penetration of ampicillin and ciprofloxacin compared to planktonic cells (94, 95). The exopolysaccharides of the *P. aeruginosa* biofilm also serve as a barrier, which significantly inhibit the penetration of polypeptides and aminoglycosides drugs, such as gentamicin and amikacin (96-99).

The architecture with diverse metabolic states in the heterogeneous biofilms also contributes to its drug resistance (92). Biofilm structures, such as voids, markedly increase the oxygen transfer at the surface of the biofilm and create a gradient of oxygen with the minimal level at the bottom layer of the biofilm (100, 101). The cells with low metabolic activity in the deeper layers of the biofilms, associated with oxygen limitation, are critical for the antibiotic resistance in *P. aeruginosa* (101). The spatial differential distribution of substrates in the biofilm microenvironment also leads to gradients of metabolic products and pH levels, which reduce the sensitivity of the biofilm to aminoglycoside antibiotics (102-104).

Therefore, this dissertation investigated the adhesin-mediated biofilm development and architecture organization, as well as the adherence of the biofilm to surfaces with various physical properties, which are important to the biofilm eradication in various industries.

1.2 Biofilm development, architecture, and organization

As the structures and development of biofilms in various microorganisms have been suggested to be associated with drug resistance and environmental stresses,, the

complexity of biofilms structures have raised increasing interests a(5, 105).

The complexity, the differentiation and the organization of biofilms into a variety of patterns and morphological structures, as well as the consequent behaviors to convey expansion advantage, resistance to antibiotics, and persistence in infection have been extensively studied and found to be critical to the treatment, as well as to establish a model for the complex development in higher organisms (2, 4, 5, 106, 107). Biofilms enable the sharing of common goods via physiological cooperation to combat environmental variations (5). The transportation of nutrients through channels of the biofilm shares similarity with the circulation system in higher organisms (10, 108, 109). The physical stress and forces are critical for bacterial biofilm pattern formation, therefore, understanding multicellular traits and the architecture of the patterning in biofilm will shed light on the spatial organization and physicochemical interactions that shape the development in higher organisms (2, 110).

1.2.1 Biofilm development

Biofilm development undergoes various stages, including the initial attachment to surfaces or adjacent cells, then further development and maturation upon stable attachment, followed by the detachment, and eventually dispersal to release pathogenic planktonic cells to the environment leading to persistence in infection (111, 112).

The initial attachment of biofilms involves the motility of cells, the physical

property of surfaces, the adherence of cells to surfaces upon external stimulations, leading to the enhancement in ECM synthesis, which is composed of DNAs, polysaccharides, adhesins, lipids and various proteins (5, 113-118). For instance, the initiation of the *P. aeruginosa* biofilm attachment is sensitive to the external stimuli through signaling pathways, resulting in a monolayer of cells attached to the surfaces initially (2, 118-122). Surface roughness and the hydrophobicity of the surface materials contribute strongly to the attachment speed and area (123).

Following the initial attachment and EPS production, biofilms gradually develop into a matured form with high resistance to antibiotics and persistence in infection (124, 125). Biofilms undergo maturation through the production of various secondary metabolites, such as arginine, as well as the exchange or release of genetic materials, such as DNA from dead cells (2, 126-134). The matured biofilms possess a structured polymeric network with enhanced biocides resistance (135). Cells within matured biofilms also cooperate to adapt to various environmental stresses. Multidrug pumps and antibiotics degrading enzymes are increasingly expressed by biofilms under stresses (2, 136-142). Due to the diversity in the composition of the biofilm EPS, obtaining effective treatments to eradicate the matured biofilms is difficult (Sutherland et al., 2001).

The detachment stage of biofilm development involves the segregation and release of cells from the biofilm upon sudden deprivation of nutrients (2). Biofilm detachment is dependent on the various enzymes that degrade the EPS, as well as the

physical shear stress (2). Biodegradation of the EPS through polysaccharases, lyases, proteases (65), and the interruption, as well as promotion of quorum sensing (143, 144) can be used to disturb the matured biofilm (145).

1.2.2 Environmental cues that affect biofilm formation

Complex biofilm development in various species is sensitive to different environmental conditions, resulting in morphogenesis adapted to nutrient deprivation, physical property of the surface, temperature, oxygen and pH gradients (53, 146-150).

The formation of biofilms is sensitive to the change, limitation and balance of nutrients, such as carbon, nitrogen source and phosphorus (65, 151). Upon nutrient deprivation, *Pseudomonas sp. strain S9* enhances the production of EPS with reduced association to the cell surfaces, leading to the increase in the viscosity of the biofilm (152). In contrast, *P. aeruginosa* increases the EPS and alginate production to facilitate the attachment to the abiotic surface, and utilizes extracellular DNA as the nutrient source during starvation (145, 153-155). The balance between various nutrients is also important to biofilm formation. The lack of lactose results in significant increase in the biomass production in *Citrobacter sp.* that overexpresses phosphatase, while the deprivation of nitrogen or phosphorus causes the reduction in the wet biomass of the biofilm (156).

Biofilms cells also sense the osmolality changes in their environments (157, 158). In a high salt environment, *E.coli* lowers its own motility by reducing the expression of

the flagella gene, which encodes flagellin (fliC), meanwhile increasing the expression of porin gene *ompC*, and enhancing the EPS colonic acid production (157, 159), leading to enhanced biofilm development (160, 161).

1.2.3 Biofilm architecture

Biofilms develop complex and distinct structures during development in response to various environments. The complex architecture is structured by the secreted ECM that supports and protects cells within the organized structure (65, 162). The dynamic organization of the polysaccharides and the interaction with a mixture of macromolecules, such as DNA, lipids and proteins form the EPS, contribute to the structured and diverse architecture of the biofilm (65, 163, 164).

EPS, a complex gel-like structured network connected via hydrogen bonds, serves as stable mechanical support for the cells that adhere to each other within the biofilm (4, 65, 113, 164, 165). Within the biofilm environment, water is trapped by the EPS network and serves as the solvent for a variety of substances, such as nutrients and ions that are transported within the biofilm (113, 166). The matrix of the biofilm also provides support for enzymes to utilize the macromolecules and nutrients that could benefit the cells within the biofilm (113).

It was recently reported that *E. coli* biofilms forming inside the agar demonstrates a novel multicellular behavior, which is composed of multilayered and equally spaced “coronal spikes” forming in a ring shape (167). The coronal morphology is organized

and facilitated through cell-cell aggregation and cell-cell clumping, which increases the viscoelasticity property of the sessile community to exploit the environment for food sources more thoroughly (167). The crowning behavior is suppressed by glucose, independent of the well-known transcriptional regulatory network consisted of cAMP-CRP complex (167).

It was reported that *E. coli* biofilms have the capacity and plasticity to spatially organize its architectures in response to a variety of physical and chemical changes in the environment (167-169). For instance, Peterson et al. visualized via confocal-laser-scanning-microscopy that *P. aeruginosa* biofilms undergo efficient rearrangement and regain the architecture after transient deformation due to external stress, whereas a strain deficient of EPS production lacks the capacity to retain the colony morphology and structure (65, 169).

The physical properties of the biofilms contribute to the adherence and colonization of biofilms to various surfaces (4, 170). Hydrophobicity and the charges on the cell membranes are critical for the physicochemical property of biofilms and their adherence to different surfaces (171-173).

The hydrophobicity on the surface of the *Streptomyces coelicolor* cells is important for the hyphae formation and biofilm development (174). Bacteria also express various kinds of lipoproteins or lipopeptides as biosurfactants to establish initiation, development and maintenance of the structures of biofilms (175-177). Biosurfactants, such as rhamnolipid, secreted by *P. aeruginosa*, increase the solubility

of organic substances in the environment to facilitate nutrient uptake and also promote the shedding of the biofilms membrane bound lipopolysaccharide (LPS) to obtain a hydrophobic membrane surface during biofilm migration at later development phases (177-179). The enhancement of hydrophobicity and viscosity via biosurfactants also facilitates the rapid expansion of the biofilm (180)

1.2.4 Biofilm patterns

An essential trait of the biofilm architecture is the sophisticated patterns developed on biofilm surfaces (181). Differentiated colony morphological patterns, named morphotypes, are systematically categorized as chiral, tip-splitting and vortex (182). The T subtype demonstrates a complex morphology, with faster spreading on hard agar (182). Even within the same branch of the complex pattern, the bacterial density is non-uniformed (182). The morphological phenotypes are sensitive to environmental cues and employ adaptation via morphotype transitions. Ben-Jacob et al showed that *Bacillus subtilis* biofilms develop distinct morphology in response to chemical concentrations in the environment (181). The microscopic organization of the colony is denser and compact at the edge of colony on higher agar concentration and sparser with increasing inter-bacterial distances at lower peptone and agar levels (181). It is suggested that the limited availability of peptone induces chemotaxis, resulting in the development of macroscopically distinct morphological changes, from compact and dense structure at high peptone level, to large colony with thick and equally spaced

branches with high level of ramification at intermediate peptone concentration, to small and compact colony with thin and dense branches at low peptone levels (181). The balance between the diffusion of substrate and the growth was suggested to contribute to the surface patterns, texture and organization of the biofilm, indicated by computational simulations (183). The mechanism underlying *B. subtilis* biofilm formation was suggested to be caused by buckling by local cell death to release mechanical stress accumulated within the biofilm during development (11).

Distinct surface patterns are also observed in eukaryotic cells. Smooth, semi-fluffy and fluffy colonies, are found in feral *S. cerevisiae* strains in response to diverse environments (184). The structural complexity of the pattern is determined by the ECM, the significant composites of which are Aqy1, a water channel aquaporin protein to retain water, and *FLO11* that adheres to cells and surfaces (184). It is, therefore, important to uncover the mechanisms underlying surface pattern formation, which is significant for eukaryotic biofilm formation (185, 186).

1.2.5 Pattern formation in non-biological systems

In comparison to pattern formation in biofilms, Ben-Jacob, et al. found that similar morphological characteristics occur in non-biological systems (181). The compact pattern with intense ramified branches resembled the dynamic Hele-Shaw pattern of granular substances after injecting air to the center (187, 188). The fractal pattern is also observed in thin oil layer, similar to the diffusion limited aggregation

simulation (189).

It is known that physical stresses in materials could induce hierarchical wrinkling, leading to multiple orders of wrinkling pattern formation (Figure 1) (190, 191).

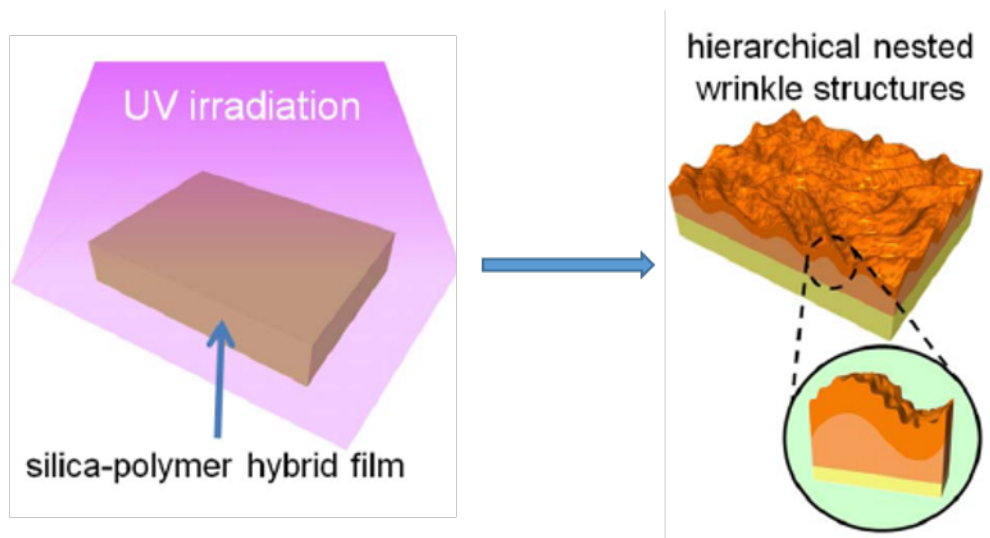


Figure 1. Hierarchical wrinkling in non-biological systems. Silica film generates hierarchical wrinkles on top of the photomonomer substrate upon stress, such as irradiation (Modified from Tokudome et al., 2012). [Permission to reprint obtained from Journal (191)].

The top elastic layer generates nested wrinkles with wavelengths at several length scales, ranging from nanometers to millimeters due to the stretching relative to the substrate layer, in response to stress (Figure 1) (190, 191).

The wavelengths of the wrinkles of the elastic layer on top of the viscoelastic thick substrate layer is derived theoretically by $\lambda = h * (E_y / E_a)^{1/3}$, where h is the height of the top elastic layer, E_y and E_a are the Young moduli of the top skin layer and the substrate measured by sharp atomic force microscope (AFM) respectively (190). The wrinkling process is triggered by mechanical stress accumulation within the biofilm. The wavelength of the wrinkles depends on the Young's Modulus of the top film and substrate, the height of the top film, and thickness of substrate if the substrate is thin (Figure 1) (190, 191).

Viscoelastic soft polymer networks, such as agar, undergo rearrangement under stress. The viscoelastic substrate maintains both the elastic property, as well as the viscous property. Elasticity is the capability of the cross-linked polymer networks of substance to reverse the deformations caused by mechanical stresses (192-194). Dynamic nanoindentation and scanning electron microscope (SEM) are used to measure the viscoelastic mechanical properties of the elastic agar (195).

Similar to non-biological materials, the architecture of the biofilms is also associated with biophysical properties of the biofilm (196). EPS, composed of strong cohesive polymer networks, contributes to the physicochemical property of the biofilm to endure the hydrodynamic shear force (168, 197). The elasticity of the biofilm has

been measured by AFM (196, 197). Understanding the physical properties underlying the complex patterns is critical to the removal and disinfection process of the adhesive biofilm (197).

The attachment, maturation and detachment of the biofilm to various surfaces are dynamic processes involving chemical binding as well as physical interactions between cells and surfaces (118). However, how the physicochemical interaction influences the development of biofilm architecture remains unclear. Therefore, it is important to reveal the association of the mechanical and physicochemical properties of the biofilm and various environments, and its contribution to biofilm architecture development. Therefore, I hypothesize that the physicochemical properties of the biofilm and the agar substrate contribute to the pattern formation through hierarchical wrinkling. This dissertation systematically and quantitatively characterized the colony expansion traits, such as the size and the irregularity of the colony on various agar and nutrient conditions. Furthermore, I determined the dependence of pattern formation on environmental cues by quantifying the wavelengths of the patterning in various conditions, and found that the wavelengths were decreasing with agar density. This study provided evidence that the hierarchical wrinkling, dependent on the physicochemical properties of the biofilms and the agar, causes pattern formation.

1.3 Multicellularity in yeast

Pattern formation during biofilm development is one of the most important social

behaviors employed by feral and non-standard yeast strains (4, 186, 198). Wild yeast strains demonstrate great capacity in coping with various environmental stresses by forming multicellular structures (199-201). The complex and dynamic multicellular structure confers prominent traits, such as stratification of specialized cells (9), and resistance to antibiotics through cooperation (201).

1.3.1 Multicellular behaviors

Wild yeast strains exhibit diverse multicellular behaviors through cooperation (199). Cell clumping conveys a remarkable advantage in survival under nutrient deprivation by expressing invertase to enhance sucrose breakdown into monosaccharides (199, 200). In the brewing industry, yeast cells form flocs and sediment to the bottom at the end of the fermentation process, which benefits the separation of flocs from bulk products (202). The flocculation process is directed by a series of cell-to-cell and cell-to-surface adhesion genes, including *FLO11*, *FLO5*, *FLO8*, and *FLO1* (203-206). Flocs improve the adaptation of cells to environmental stresses, such as the pH level, temperature, oxygen level, and nutrient deficiency (202). The protection of cells within the flocs from harsh environments, such as antibiotics and ethanol stress, depends on the development of architectures that exclude potential cheaters, which utilize without contributing to the common goods, to the exterior of the flocs to shield the rest of the flocs from stresses (201, 202, 207).

1.3.2 Biofilm formation directed by *FLO11* and its regulation in *S. cerevisiae*

One remarkable multicellular phenotype of feral and non-standard *S. cerevisiae* is biofilm formation (146, 186). Reynolds and Fink found that the presence of the adhesin Flo11p is sufficient for a complex pattern formation and rapid colony expansion during biofilm development on soft agar (0.3%) (146, 186).

The *FLO11* gene is also known as *MUC1*, which regulates pseudohyphal growth, and is homologous to the STA gene and SGA gene, encoding secreted and sporulation-specific glucoamylases in yeast (208-210). Flo11p is similar to the transmembrane adhesin in mammalian cells, known as mucin, which is the major component of mucous barrier and functions in tumor adhesion, progression, and invasion (211-214).

Flo11p is an adhesin, independent of sugar, which contains an N-terminal peptide binding domain, conveying hydrophobicity to the cell membrane, followed by a central domain consisting of threonine and serine repeats, generating variants of the adhesin, and a C terminal domain of a glycosylphosphatidylinositol (GPI) anchor, providing the anchoring of the adhesin onto the cell wall (207, 215-222).

In response to environmental stresses, the adhesion conveyed by *FLO11* allows the attachment of yeast to biomaterials and abiotic surfaces, and to neighboring cells through calcium dependent cell-cell adhesion (9, 186, 204, 210, 223-225).

FLO11, one of the largest promoters in yeast with 3 kb in length (226), is regulated through the convergence of various signaling pathways integrating diverse

environmental cues (227).

To sense the environment and undergo phenotypic switches to adapt to the stress robustly and quickly, *S. cerevisiae* regulates *FLO11* gene expression by the transcription factor Mot3 (228). The switch of Mot3 to the prion state [MOT3⁺] conveys heritable and immediate changes to the multicellular behaviors of *S. cerevisiae*, such as invasive and filamentous growth, to adapt to environmental stresses, such as starvation, hypoxia and high ethanol level (228). In addition, *FLO11* transcription is also upregulated post-transcriptionally in response to environmental cues, such as the deprivation of nutrients (229). The mRNA of *FLO11* repressors, such as *NRG1* and *NRG2*, is reduced by mRNA deadenylation by exonuclease Ccr4, resulting in the upregulation in *FLO11* expression (229). The heterogeneity of morphological phenotypes is associated with various states of *FLO11* expression, regulated by noncoding RNA, which is modulated by Flo8p, Sfl1p and chromatin silencer Rpd3L (229, 230).

The responses of *S. cerevisiae* to nitrogen deprivation, high osmolality and alcohols in the environment converge to the MAPK pathway (231-235). The MAPK pathway controls *FLO11* expression through the initiation of ammonium permease Mep2 activation upon nitrogen starvation stress (236). The subsequent signaling proteins are activated in the MAPK cascade, from MAPKKK Ste11, MAPKK Ste7, to MARK Kss1 (237, 238). The MAPK relay eventually leads to invasive and filamentous yeast growth through the activation of *FLO11* via transcription factors Ste12 and Tec1

(239-241).

High concentration of environmental carbohydrates, such as glucose or sucrose, evokes Ras/cAMP/PKA pathway to activate *FLO11* gene expression either through the activation of Flo8p, an important transcription activator of *FLO11*, or through the inhibition of transcription repressor Sfl1 that silences *FLO11* chromatin through histone deacetylase Hda1 (242, 243). In addition to the traditional transcription activation, chromatin remodeling facilitates the fast fluctuation of *FLO11* promoter activity to adapt to the diverse environmental changes (244). *FLO11* directed morphogenesis in *S. cerevisiae* could also be regulated through feedback loops. Aromatic alcohols, such as phenylethanol, tryptophol, are repressed by high ammonium concentration. The feedback between Aro9, Aro10 and aromatic alcohols through Aro80p, together with the activation of Aro9, Aro10 under high cell density by Aro80p, resulting in the filamentous morphology through Tpk2p activated Flo11p pathway (245).

It is known that *S. cerevisiae* undergoes morphogenetic switch in response to various environmental cues by integrating various complex transcriptional and posttranscriptional modulations (246-248). However, it is still unclear how *FLO11* mediates complex pattern formation in *S. cerevisiae*, an important morphological trait of the biofilm consisting of a central hub with intense primary wrinkles and radial secondary wrinkles. Understanding the mechanisms underlying the organized pattern development in *S. cerevisiae* via mathematical and physical models and characterizing the significant traits of the *S. cerevisiae* biofilm surface structure will reveal how

physicochemical stress shapes organized multicellular structure development in various organisms.

This dissertation investigates different characteristics of the *FLO11* directed biofilms expansion in various conditions, and further illustrates how patterns develop upon physical and mechanical stress during colony expansion, as well as the benefits of forming the structured patterns during colony expansion.

Chapter 2

Salient traits of *S. cerevisiae* colony expansion in response to various environmental cues

2.1 Introduction

Many important traits of social behaviors are eliminated from laboratory yeast strains for easy handling and genetic manipulation. Wild *S. cerevisiae* strains that express cell surface adhesins have the capacity of developing various multicellular behaviors, from flocculation, clump formation, to biofilm development (186, 200, 201, 249-253). Quantitative analysis on the features of the multicellular structure is important to reveal critical physicochemical processes that cause structural development in *S. cerevisiae*. Furthermore, the mathematical models and systematic analysis developed to elucidate colony development in yeast could be used as a model system to understand the complex developmental process and its regulation in higher organisms, such as adhesin mediated carcinogenesis (254, 255).

Various morphological changes in *S. cerevisiae* are sensitive to environmental cues through complex genetic regulation converging on *FLO11* (9, 256). *FLO11* directs rapid expansion of the *S. cerevisiae* biofilm upon nutrient deprivation (186). During the deprivation of nitrogen source, *FLO11* modulates pseudohyphal formation in diploid cells due to sustained attachment between mother and daughter cells in the unipolar axial orientation (257-260). *FLO11* also regulates invasive growth in haploid cells in

response to dextrose deficiency in the environment (261, 262). Another remarkable multicellular behavior directed by *FLO11* is biofilm formation, composed of complex pattern development and rapid mat expansion in semisolid agar surfaces (186).

The genetic networks that convert the environmental cues to the modulation of morphological changes through *FLO11* are well studied (260, 262-264). However, the morphology of the biofilm and the patterning have only been identified in very low agar density within a short time course. The detailed characterization of the morphological changes in response to various environmental cues requires further identification of environmental factors that affect the morphological changes. In this chapter, quantitative analysis methods were used to systematically characterize, during the entire biofilm development time course, the morphological changes of yeast colonies in response to various conditions, such as different sugar sources, different agar and sugar concentrations..

Based on the analysis of the colony expansion features, I found that the expansion curve had distinct convexity upon different initial glucose concentration. In a previous report, a glucose gradient was observed across the colony during expansion (146). Glucose level is gradually decreasing from the rim to the center of the colony, which confers a better cell-surface adherence in the center compared to the rim due to the repression on Flo11p by high glucose concentration (146). In this chapter, the unique colony expansion properties were identified by a mathematical model to be associated with heterogeneous modes of growth upon different nutrient levels.

In this chapter, further analysis of the morphological traits also indicated changes associated with agar density, continued in chapter 3 to identify how the physical properties contribute to the complex and organized pattern formation.

2.2 Materials and Experimental Methods

2.2.1 Strains, Media and Growth conditions:

The haploid *S. cerevisiae* strains TBR1 (Σ 1278b, mat α , *FLO11*, tryp) and TBR5 (Σ 1278b, mat α , *flo11* Δ , tryp) were used. To characterize colony expansion characteristics, a volume of 0.5 μ l of *FLO11* or *flo11* Δ cells (at OD around 0.3) were inoculated onto YPD agar plates (20 ml media per plate, Fisher scientific, Cat#: 0875714G) at various high (1.5%, 3.0%, 6.0%) agar concentrations in combination with glucose (0.5%, 1.0%, 2.0%).

2.2.2 Plate Imaging and Microscopy:

Plates with yeast strains were imaged under a Biorad imager or Leica MZ6 stereo microscope with Nikon DS-Fi1 camera and Nikon Digital sight DS-U3 camera controller and analyzed for colony size.

2.2.3 Image Processing.

To analyze images for the study of colony shape, Javad Noorbakhsh from the Department of Physics, Boston University, used an image processing procedure consisting of two stages of dish detection and colony detection to analyze the images I

obtained experimentally. To detect the Petri dish, he assumed that the dish was perfectly circular and used an algorithm that searched for circular objects with sizes close to the dish size. This algorithm functions by looping through different threshold values and binarized the image. It then chooses the threshold value that produces the most circular object (through minimizing a cost function) and thresholds the image to detect the dish. The dish is then removed from the image, leaving only the colony and a background.

To detect the colony, images were binarized by thresholding. The threshold was determined for each image by producing its intensity histogram. Each histogram contained two main peaks that corresponded to background and foreground. The threshold value was determined by finding the local minimum between these two peaks. This procedure was successful at accurately detecting colonies in almost all images. The few images missed by the algorithm were analyzed through choosing the threshold manually.

2.2.4 Analysis of the colony expansion time course and the non-circularity of the colony rim.

Javad Noorbakhsh performed the P2A analysis on the images I obtained experimentally. The P2A method thresholded the image to find the colony boundary and then derivatives (Equation 1.1).

$$P2A = \frac{P^2}{4 \times \pi \times A} \quad (1.1)$$

where P was the perimeter of the colony in pixels calculated by the function `bwperim` in Matlab in 8-connected mode. A was the area of the colony calculated by counting the total number of pixels in the colony. Note that P2A had been defined, such that it was invariant under scaling of the image and only responded to the changes in the shape of the colony boundary. Furthermore its value was equal to one for a perfect circle and would increase as the colony boundary became more irregular. Thus, P2A was used to measure the deviation of the shape of the colony rim from a circle.

2.2.5 Mathematical modeling of differential growth of the *FLO11* directed biofilm.

The growth of the center of the colony was modeled by the modification on the Michaelis-Menten equation (265). Glucose (G) formed complex (C) with a mother cell (N_o), then the glucose (G) was converted to a daughter cell (N_n) (Equation 1.2).



The mother cell (N_o), glucose (G) and daughter cell (N_n) in this equation resembled the enzyme, substrate and product in the Michaelis-Menten equation respectively. Equation (1.3) was different form the Michaelis-Menten equation in the sense that the daughter cell (N_n) generated from Equation (1.2) became a mother cell (N_o) and re-entered Equation (1.2) to repeat the process until glucose was used up in the center of the colony.



The initial condition was the initial glucose (G_0) provided to the colony from the media, which was retained in the daughter cells (N_n), mother cells (N_o), the complex (C), and the remaining glucose (G), while not in the initial cells inoculated to the plate (N_i) (Equation 1.4). The total number of cells in the center is composed of both the mother cells and daughter cells (Equation 1.5).

$$N_n + G + C + N_o - N_i = G_0 \quad (1.4)$$

$$N_T = N_o + N_n = G_0 + N_i - C - G \quad (1.5)$$

The following ordinary differential equations (Equation 1.6 - 1.9) described the changes of glucose (G), the complex (C), the mother cell (N_o) and daughter cell (N_n) over time. The rates of reactions for complex formation, complex decomposition, daughter cell generation, and the conversion from daughter cell to mother cell were indicated by f , b , c , v respectively.

$$\frac{dG}{dt} = -f * G * N_o + b * C \quad (1.6)$$

$$\frac{dC}{dt} = f * G * N_o - b * C - c * C \quad (1.7)$$

$$\frac{dN_o}{dt} = -f * G * N_o + b * C + c * C + v * N_n \quad (1.8)$$

$$\frac{dN_n}{dt} = c * C - v * N_n \quad (1.9)$$

It has been reported previously that the rim of the *FLO11* colony had access to a sufficient level of glucose during colony expansion (146). Therefore, the growth on the rim of the colony was modeled as linear growth due to sufficient glucose. Specifically, the mother cell generated a daughter cell in the orientation from the center to the rim

(Equation 2.0). The extension of the rim of the colony over time was associated with the growth rate (g) and the diameter of the cell (D) (Equation 2.0).

$$\frac{dR}{dt} = g * D \quad (2.0)$$

The size of the *S. cerevisiae* cell was 4.5 μm , which was measured by Nexcelom Vision CBA version 2.1.4.2 on the thresholded image with only single cells (See Methods in Chapter 4), and was the same as in previous reports (266).

In order to find the relationship between the colony radius and the cell number, which represented the growth at the rim and the center of the colony respectively, experimental data was used. Specifically, the image of the colony was used for obtaining the radius of the colony at certain time points, when the total cell number of the entire colony was measured through OD_{600} . The entire colony, with radius of the colony measured, was collected with a specific amount of media, followed by $\text{OD}_{600 \text{ nm}}$ measurement. The cell number was then calculated using the ratio that 1ml of cells with $\text{OD}_{600 \text{ nm}}$ at 1.0 indicating $1.5 * 10^7$ number of cells (267). Then the ratio of the cell number and colony radius (mm) was $2.2 * 10^7 \text{ mm}^{-1}$.

2.2.6 Growth rate measurement for *FLO11* and *flo11* Δ .

FLO11 and *flo11* Δ cells were inoculated to yeast extract peptone galactose (YPGal) media with 0.5% galactose, at the same starting $\text{OD}_{600 \text{ nm}} = 0.005$. Three independent replicates were initiated from three different colonies of *FLO11* or *flo11* Δ . The optical density of the cultures was mostly measured at interval of 2- to 4- hours for the 57 hour assay. The cultures were incubated in a 311DS Shaking Incubator. Growth

curve was plotted in Graphpad Prism. The distribution of the *FLO11* and *flo11* Δ cells composed of both the clump form due to incomplete separation and single cells form was obtained by Nexcelom Vision CBA version 2.1.4.2. *FLO11* and *flo11* Δ cells with or without clumps were imaged by Nexcelom with threshold on the diameter of the object. The image of single cell was obtained from disguising the clumps from the image containing both clumps and single cells with Matlab script, and then the diameters of single cells of *FLO11* and *flo11* Δ were counted in Nexcelom.

2.3 Results

2.3.1 The influence of the environment and *FLO11* on colony size.

How the presence of a functional *FLO11* gene influences colony expansion under various nutrient conditions on agar plates was first investigated. To address this question, the areas of *FLO11* and *flo11* Δ colonies that expanded under nine different combinations of YPD agar (1.5%, 3.0%, and 6.0%) and glucose (0.5%, 1.0%, and 2.0%) concentrations were obtained. *FLO11* colonies (Figure 2A, C) expanded faster than *flo11* Δ colonies (Figure 2B, C) and reached larger maximum size in all conditions tested, in agreement with previous observations in soft agar (186).

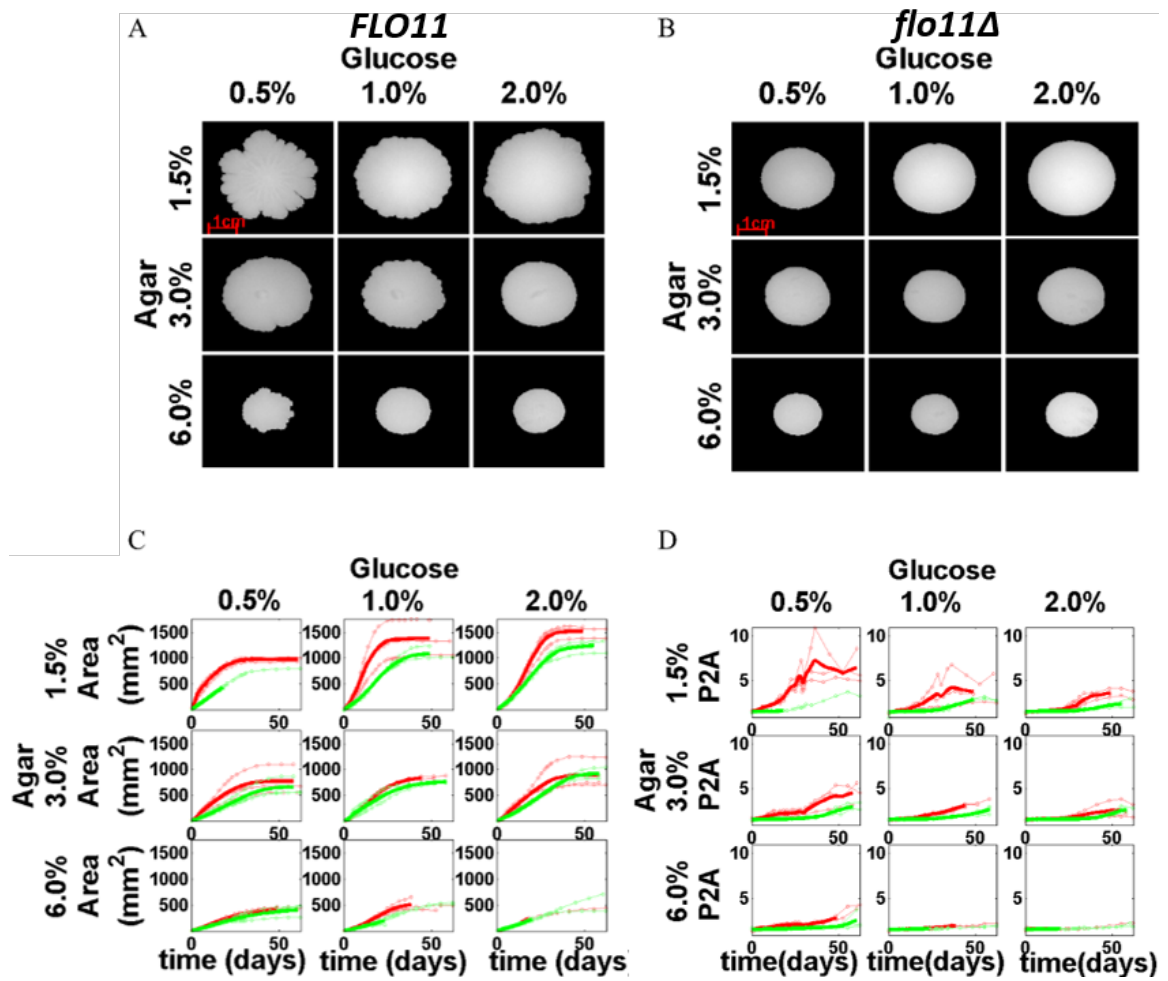


Figure 2. Colony size and irregularity for various glucose and agar concentrations. (A, B) Images of *FLO11* (A) and *flo11Δ* (B) on YPD plates containing different glucose (0.5%, 1.0%, 2.0%) and agar (1.5%, 3.0%, 6.0%) concentrations around day 20. (C, D) The expansion of colony area (C) and the irregularity (D) of *FLO11* (red curves) and *flo11Δ* (green curves) colonies over the 60-day time course. *FLO11* colonies (red curves) demonstrated higher maximum colony size (C) with higher irregularity (D) at the colony rim than the *flo11Δ* colonies (green curves) in all conditions tested. The maximum colony size (C) of both *FLO11* (red curves) and *flo11Δ* (green curves) colonies increased with glucose and inversely depended on agar concentrations. The irregularity of *FLO11* (D) (red curves) inversely depended on both the agar and the glucose concentrations, compared to the minimal irregularity of *flo11Δ* (D) (green curves) colonies throughout the time course at all conditions tested. Thinner curves were different replicates and thicker curves were their average up to a time when all the replicates were present. (Analysis performed by Javad Noorbakhsh)

To further investigate whether similar trends appear independent of sugar sources, galactose was used in replacement of glucose. Colonies expanded on surfaces at conditions (0.5%, 1.0% and 2.0% galactose (Figure 3), in combination with 1.5%, 3.0% and 6.0% agar) the same as on glucose (Figure 2) surfaces.

In order to elucidate the critical environmental conditions that affected colony expansion, the detailed features of colony expansion were captured among various conditions. The maximum colony area increased with the glucose concentration, but had an inverse dependence on agar density, regardless of *FLO11* status (Figure 2). The time that colonies took to reach the maximum colony area increased with agar density, with no consistent dependence on glucose concentration for colonies on different agar density surfaces, regardless of *FLO11* status (Figure 4E, F).

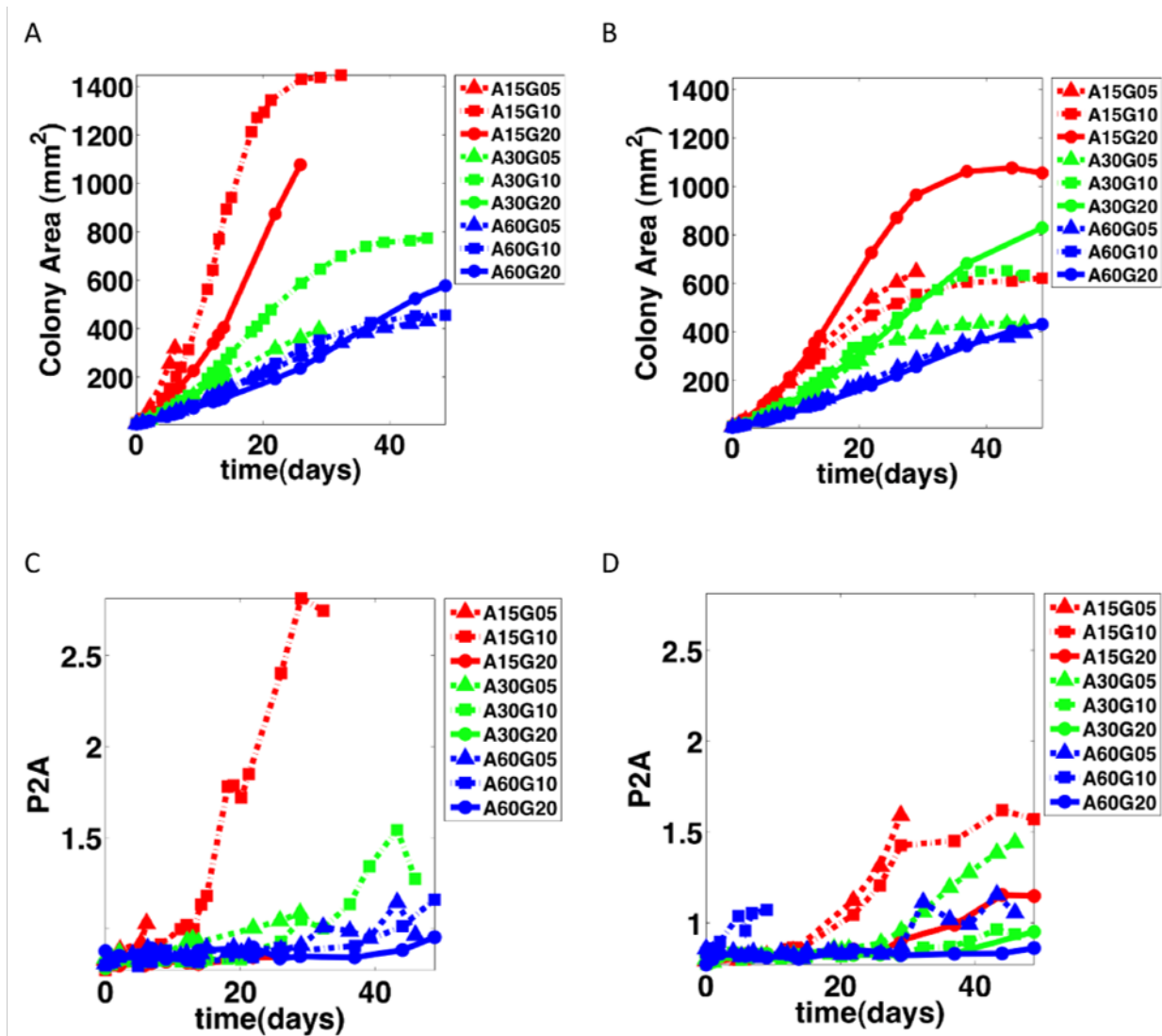


Figure 3. *FLO11* colonies expanded faster and were more irregular than *flo11Δ* colonies on YPGal plates. (A-D) On YPGal plates with galactose as the sugar source, the colony size (A) and the irregularity of *FLO11* colony measured by P2A (C) increased along the time course, with higher value compared to *flo11Δ* (B, D) at most conditions. The conditions included three agar densities at 1.5%, 3.0%, 6.0% (as A15, A30 and A60 respectively in the figure legend) and three glucose concentrations at 0.5%, 1.0%, and 2.0% (as G05, G10, and G20 respectively in the figure legend). (Analysis performed by Javad Noorbakhsh)

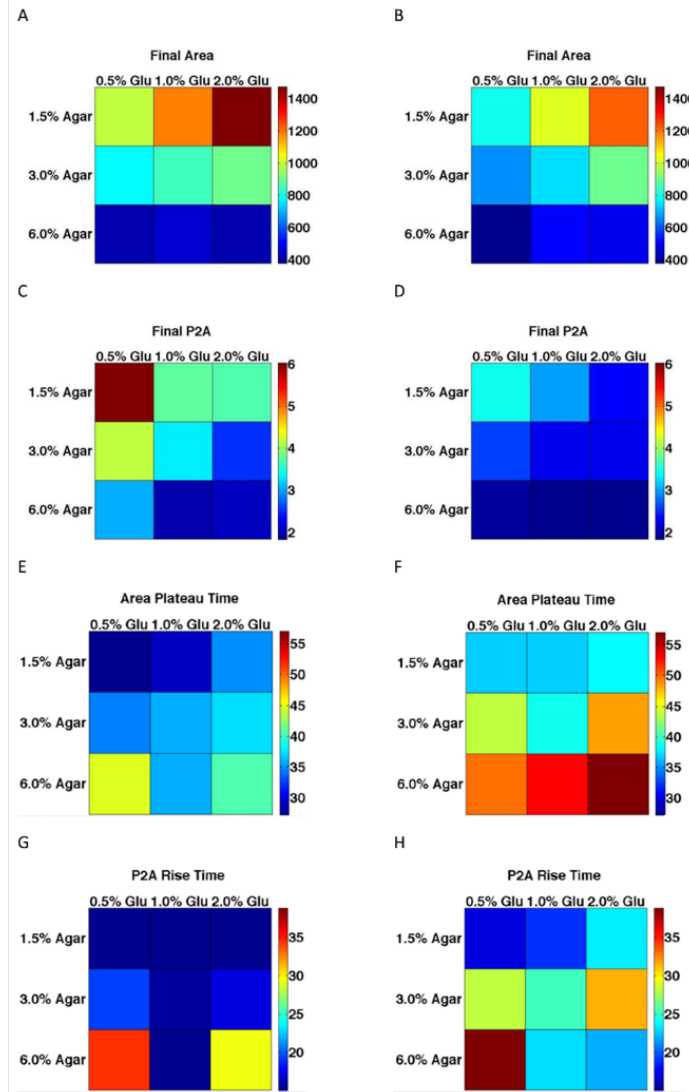


Figure 4. Colony characteristics as functions of agar and glucose concentration. (A-D) The maximum colony area (A, B) and the irregularity of the colony rim (C, D) of both *FLO11* (A, C) and *flo11Δ* (B, D) colonies inversely depended on agar density. The maximum colony area (A, B) increased and the maximum irregularity of the colony rim (C, D) decreased with glucose concentration, regardless of *FLO11*. (E-H) Colonies approached the maximum area (E, F) and the irregularity (G, H) faster at lower agar density regardless of *FLO11*. (Analysis performed by Javad Noorbakhsh)

FLO11 colonies expanded to reach larger colony sizes at each condition (Figure 2, 3). The above observations suggested that the properties of *FLO11* colony expansion followed similar trends on different sugar sources (Figure 2, 3).

I further tested whether faster *FLO11* colony expansion could be related to faster growth rate and/or larger cell size of *FLO11* compared to *flo11* Δ cells. *FLO11* and *flo11* Δ cells grew at comparable rates in liquid cultures (Figure 5) arguing against a significant difference in their growth rates.

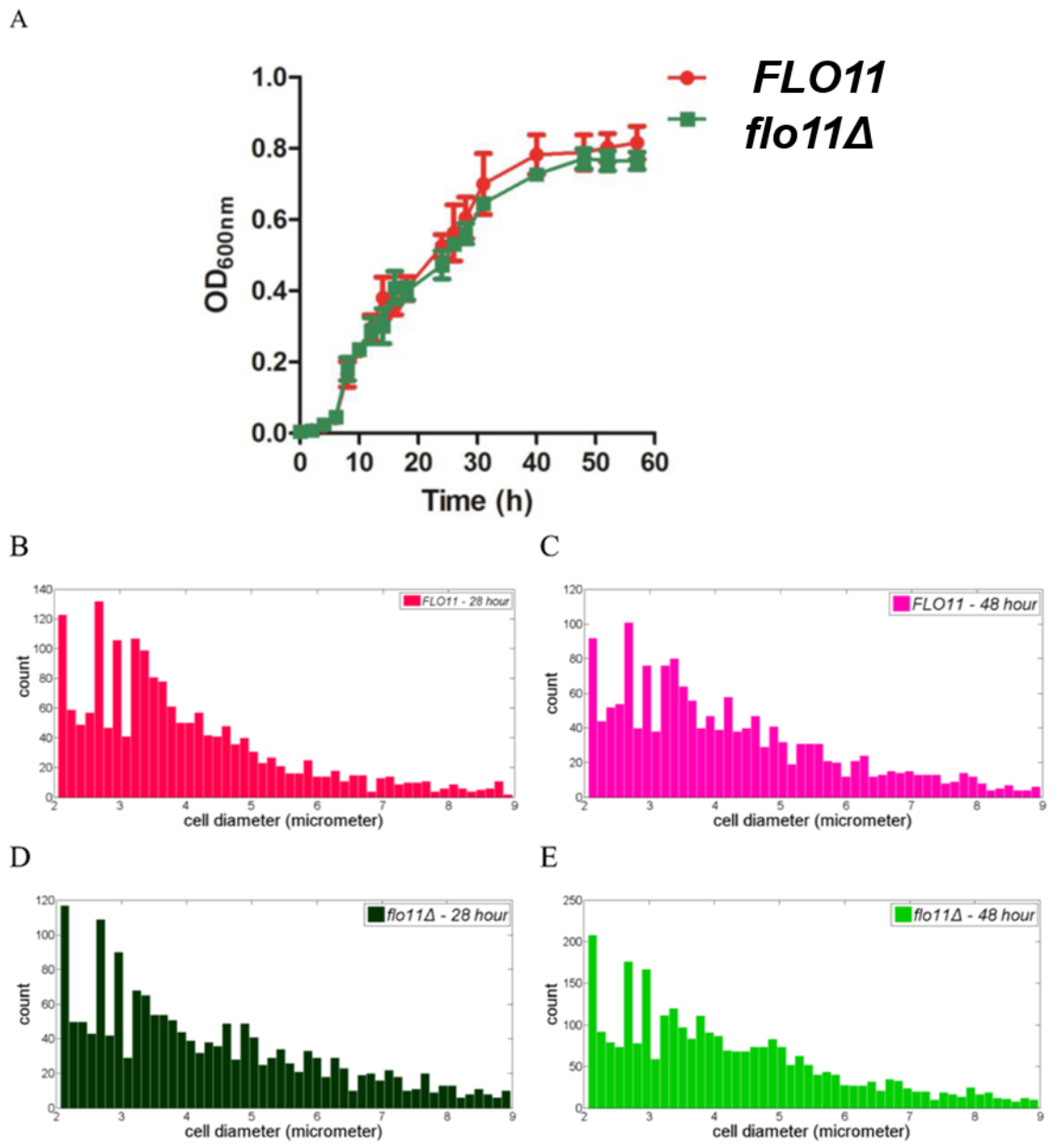


Figure 5. No significant growth difference between *FLO11* and *flo11Δ* *S. cerevisiae* cells in liquid media. On 0.5% galactose YPGal liquid media, (A) No significant difference throughout the 57-hour growth curves between *FLO11* and *flo11Δ* cells. Three independent replicates of *FLO11* (red) and *flo11Δ* (green) were shown as error bars for the average curve. (B, C, D, E) The distributions of cells and clumps diameters between *FLO11* (B, C) and *flo11Δ* (mutant) (D, E) at 28 hours (B, D) in exponential growth and at 48 hours (C, E) in stationary phase were similar.

Moreover, *FLO11* and *flo11* Δ cells had similar cell size distributions (Figure 5). *FLO11* and *flo11* Δ cells also had similar cell size at 4.5 μ m. The distribution of the *FLO11* (Figure 5B, C) and *flo11* Δ (Figure 5D, E) cell and clump diameters were similar at either exponential (Figure 5B, D) or stationary phase (Figure 5C, E). Therefore, some other mechanisms, such as the *FLO11* directed two dimensional growth due to close attachment to the surface, might underlie the faster expansion of *FLO11* colonies compared to *flo11* Δ colonies in the same agar and sugar conditions.

2.3.2 The influence of the environment and *FLO11* on colony shape.

The second colony characteristic investigated was the colony shape, quantified by analyzing the irregularity of the colony rim (see *Methods*). The dimensionless P2A ratio, defined as $P^2/4\pi A$, where P is the perimeter, and A is the area of the segmented object. The P2A ratio takes its minimal value of 1 for a perfect circle, and increases as the object becomes more irregular. The P2A method is more sensitive to small fluctuations at the colony rim.

At each combination of glucose and agar concentrations, P2A method indicated more pronounced colony rim fluctuations in *FLO11* colonies compared to *flo11* Δ colonies (Figure 2D). The irregularity at the rim of *FLO11* colonies increased over time for all colonies. The maximum irregularity reached at the end of the time course decreased with both agar and glucose concentrations (Figure 2D, 4C, D). The irregularity of the colonies rims saturated at a much earlier time than the area of the

colonies, regardless of *FLO11* status (Figure 4G, H). The trends of the expansion of *FLO11* colonies over a wide range of agar levels and sugar concentrations were consistent between trials, and were independent of sugar sources (Figure 2, 3).

These findings indicated that the characteristics of colony expansion, such as expansion rates and the non-circularities on the boundary of *FLO11* colonies were robust and consistent between trials, which were dominated mainly by *FLO11* expression and the expansion conditions, such as agar densities and glucose levels (Figure 5, 6).

2.3.3 Heterogeneous modes of cell growth within the colony determine the convexity of the expansion curve in response to various glucose levels.

Colony expansion was modeled as heterogeneous cell growth, which consisted of growth in the colony center (a modified Michaelis-Menten equation) and linear growth on the rim of the colony (Figure 6A). The ratio of the cell number to the radius (mm) of the colony was $2.2 * 10^7 \text{ mm}^{-1}$ (See Methods in Chapter 2). The time dependence of glucose (G), daughter cells (N_n), mother cells (N_o), the cell-sugar complex (C), and the radius (R) of the colony (Equation 2.0-2.4) were derived from Equation 1.6-2.0. The parameters were $f = 0.3$; $b = 0.0001$; $c = 0.01$; $v = 0.01$; $g = 0.000167$.

$$\frac{dG}{dt} = -f * G * N_o + b * (K * G * N_o) \quad (2.0)$$

$$\frac{dN_n}{dt} = c * (K * G * N_o) - v * (G_o - C - G - N_o + N_i) \quad (2.1)$$

$$\frac{dN_o}{dt} = -f * G * N_o + (b + c) * K * G * N_o + v * (G_o - C - G - N_o + N_i) \quad (2.2)$$

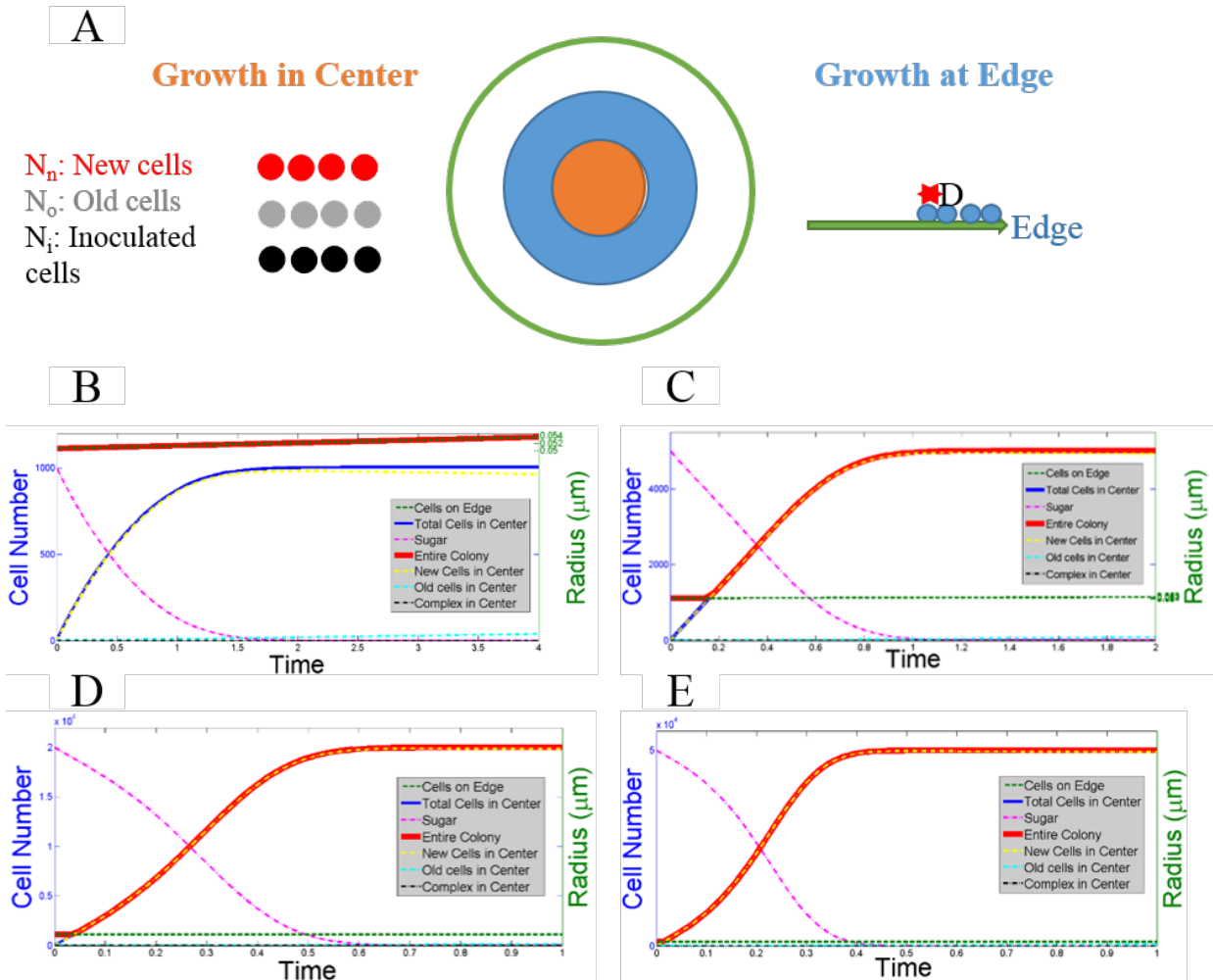


Figure 6. Mathematical model for colony expansion. (A) Schematic on the different modes of growth on the center composed of initial inoculated cells (N_i), old cells (N_o) that generate new cells (N_n), and on the edge composed of cells generated from center to edge. (B) Cell growth at the edge of the colony (green line) was observed as it exceeded expansion of cells in the center throughout the time course. (C-E) The expansion of cells in the center (blue line) represented the entire colony (yellow line) at certain time point when the center approached and pushed the edge when the colony grew to certain size. The expansion curve was concave at lower glucose concentration (C), and became more convex with the increase in glucose level (D, E). The cells on the edge, total cells in the center, the sugar level, the cells of the entire colony, the daughter cells (New Cells), the mother cells (Old Cells) and the complex in the center were represented in green, blue, magenta, red, yellow, cyan and black curves respectively.

$$\frac{dC}{dt} = f * G * N_o - (b + c) * (K * G * N_o) \quad (2.3)$$

$$\frac{dR}{dt} = g * 4.5 \quad (2.4)$$

Initial glucose (G_o) (Equation 1.4) corresponded to the starting glucose level that was initiated in the plate in the experiment (Figure 2). When colony expanded on media with very low glucose concentration, the center of the colony expanded slowly, and was not able to approach the rim of the colony, therefore linear growth at the edge of the colony was observed (Figure 6B).

At medium initial glucose level, the expansion in the center was more rapid than the colony rim after a certain time point. Therefore, the behavior of the entire colony was represented by the center of the colony after an initial lag, replacing the behavior of the edge of the colony that was observed initially. Therefore, the overall colony expansion curve was concave at the intermediate glucose level in this colony expansion model (Figure 6C), which agreed with the experimental data on the concave colony expansion curve on 0.5% glucose concentration (Figure 2C).

With the increase in the starting level of glucose, the center of the colony pushed the edge from very early time, leading to the representation of the expansion curve of the entire colony by the cells in the center for most of the time course (Figure 6D, E). Thus, the overall expansion curve switched from concave at medium initial glucose concentration (Figure 6C), to more and more convex curve when the initial glucose was increasing (Figure 6D, E), which agreed with the trend observed experimentally (Figure

2).

The mathematical model on the heterogeneous cell growth between the center and the rim of the colony captured the trend of the convexity change of the expansion curve in response to various initial glucose concentrations observed in the experiment (Figure 2, 6). The findings suggested that the observed unique property of the expansion curve may be due to the distinct modes of growth within the colony, depending on whether the center of the colony could overtake the edge during colony expansion.

2.4 Discussion

Microbial biofilm formation has received considerable attention. In the 1990s there was a surge of interest in quantitative characterization of microbial colony as physicists forged connections to non-equilibrium growth phenomena (181, 268, 269). Although many recent studies describe phenomenological associations of various molecular and physical processes with biofilm development, it is unclear whether there is a dependence of the salient traits of the colony expansion on various environmental cues. The mechanism underlying the distinct expansion behavior on different environmental conditions still remains unclear.

Deeper understanding of colony development requires systematic imaging on pattern development, quantitative data analysis from images, and mathematical models. This work represents a step in this direction by systematically extracting and quantifying

features in expanding yeast colonies.

This Chapter used quantitative methods to analyze the salient features of yeast colonies during their expansion on agar plates: colony size and rim irregularity. By comparing *FLO11* cells to otherwise isogenic *flo11* Δ cells, it was observed that the *FLO11* gene increased the rate of colony expansion, enhanced rim irregularity in all the sugar and agar concentrations tested. These trends were consistent among three different trials with glucose (Figure 2), as well as a trial with galactose, indicating the robustness of colony expansion features, which was independent of the sugar source (Figure 3). Seeking a unifying explanation for these experimental observations, I proposed a simple mathematical model to capture these differences. The model qualitatively reproduced colony expansion curves under different growth conditions.

Overall, this chapter not only quantitatively characterized the salient traits of *S. cerevisiae* colony expansion that the value of both colony size and the irregularity of the colony rim of *FLO11* were higher than *flo11* Δ colonies at various of glucose and high agar concentrations, but also identified that the convexity of the distinct expansion curve observed in the quantitative analysis to be defined by the differential growth modes within the colony in response to various initial glucose levels.

The inverse association of the colony size and the irregularity with agar density revealed in this chapter suggested that the physical properties of the biofilm and the substrate were also important for the biofilm formation and organized patterning, which was further investigated in Chapter 3.

Chapter 3

Mechanisms Underlying Pattern Formation in *S. cerevisiae*

3.1 Introduction

3.1.1 Biofilm architecture development in microorganisms.

Biofilms in various species undergo complex spatiotemporal development to form organized structures. *E.coli* biofilms exhibit heterogeneously structured layers of cells, with the outside layer composed of ovoid cells at stationary phase and the inside layer of a growth zone formed by actively dividing cells (270). Similar structures are observed in eukaryotes, as in *S. cerevisiae* biofilms, where metabolically active cells in the cavity of the biofilm are encased and protected by the ECM (9). The high level of organization of biofilms in adaption to nutrient limitation resembles a simplified version of the differentiation and organization of specialized cells in higher organisms (9, 270).

Biofilms also form complex surface architectures composed of spatially organized surface patterns, with cell-free channels, which transport water, dissolvable nutrients and waste products within the biofilm (10, 271, 272). This nutrient transportation through interconnected channels within the biofilm shares common traits with the simplified circulation system in higher organisms (272).

3.1.2 Hierarchical model in non-biological system.

The complex patterning extending to multiple scales is also observed in non-biological systems (190, 273, 274). Theories of elastic skin-viscoelastic substrate (ESVS) sandwich systems indicated that an elastic thin surface Polydimethylsiloxane (PDMS) film on the substrate generates hierarchical wrinkles over several scale when exposed to ultraviolet and ozone radiation (190). The disturbance of the equilibrium between the stresses accumulated in the top elastic skin layer and the viscoelastic bottom substrate layer results in the wrinkling pattern extending to several scales, where the strains accumulated saturate the scale of the previous wrinkle (190, 273, 274).

The hierarchical wrinkling model derived from non-biological systems in previous reports showed that the wavelengths of the patterns at different scales are associated with the Young's Modulus of both the elastic top thin film and the bottom viscoelastic substrate layer, the height of the thin top film of the previous wrinkle, and the thickness of thin substrate (190, 195). Hierarchical wrinkling in non-biological systems suggest the importance of the physical properties of surface and substrate layers to pattern development (Equation 2.6, 2.7).

3.1.3 Physicochemical property of biofilm.

The physical properties, such as the hydrophobicity and tension accumulated through the interaction between the biofilm and the abiotic surface, are not only

important to the biofilm attachment to low energy surfaces, but are also critical to the pattern development of the biofilm (257, 275).

The capability of biofilms attaching to various biological and abiotic surfaces in nature is associated with its physicochemical property (12, 276), which is contributed by the viscous matrix that encases the cells (275). The ECM is composed of networks of interconnected polysaccharides, the modification of which could alter the hydrophobicity, dynamics and stability of the biofilm, resulting in the change in the elasticity, in order to protect the biofilm from mechanical shear stress (4).

In Gram-negative bacteria, the hydrophobicity of the matrix could be enhanced through the alterations of the O-antigen of the lipopolysaccharide, in order to confer attachment to hydrophobic abiotic surfaces (2, 277). It has been reported that the acetylation of the polysaccharide of the *Rhizobium meliloti* cells in a biofilm promotes the organization of the polysaccharides network, resulting in higher elasticity (278, 279). The alteration of the physical properties of the matrix in *Arthrobacter viscosus* cells is triggered by deacetylation of the alginate via carboxylesterase (280).

The physical properties are critical to the biofilm development and pattern formation, and I also found that agar density played an important role in determining the biofilm expansion features (Figure 2, 4, 8). Therefore, I investigated whether yeast biofilms developed patterns due to hierarchical wrinkling, similar to non-biological systems. The cross-sectional view of the yeast colonies in previous studies suggested that yeast biofilms are composed of layered structures of cells and ECM (9). I

hypothesized that the primary wrinkle is triggered on the top layer of cells, which interacts with ECM substrate. As stress accumulated, cells with ECM could generate secondary wrinkles on top of the agar substrate. The ESVS model for yeast is composed of ESVS Thin model and ESVS Thick model specifically, depending on the thickness of the substrate (see *Methods*) (190, 274, 281).

In this Chapter, I quantitatively analyzed the pattern formation on different agar densities and glucose concentrations, and fitted the data with the ESVS Thin and Thick model. I found that ESVS Thin model fitted the primary wrinkle and ESVS Thicker model fitted the secondary wrinkle much better than the agar-independent model. These findings suggested that the yeast biofilm is much more complicated than non-biological ESVS systems, as it is composed of multi-layered structures of cells, and ECM with different physical properties, which interact with the agar substrate, leading to complex pattern formation.

3.2 Materials and Experimental Methods

3.2.1 Strains, media and growth conditions.

For manual measurement of the wavelength in pattern formation, a volume of 0.5 μ l of *FLO11* or *flo11* Δ parental strains (at OD_{600 nm} 0.5) in liquid culture were inoculated onto yeast extract peptone dextrose (YPD) media agar plates (6-well plate, BD, Cat#: 353046) at various low (0.3%, 0.6%, 0.9%) and high (1.5%, 3.0%, 6.0%) agar concentrations in combination with various glucose concentrations (0.5%, 1.0%, 2.0%).

For each colony, the arc-length distances between primary wrinkles or secondary wrinkles were measured, at a certain radius that was positioned both within the colony and close to the outside rim. Primary wrinkles or secondary wrinkles were distinguished by the random positioned short first degree structure and the radially positioned thick secondary wrinkles bundled from thin secondary wrinkles, respectively. The number of arc-length distances of primary wrinkles were measured corresponding to each agar concentration, which were obtained over the range of glucose concentrations. The arc-length distances of primary or secondary wrinkles were measured for *FLO11* colonies expanding on all agar concentration tested. Based on the strong influence of agar on the secondary wrinkles pattern formation on *FLO11* colony, which is slightly effected by the change of glucose concentration, the arc-length distances measured on each agar level consisted of three glucose conditions. There were three replicates for most agar and glucose combinations. The total number of arc-length distances for primary and secondary wrinkles measured on each agar level were listed in Table 1.

3.2.2 Detection of death patterns in *S.cerevisae*.

Since *FLO11* colonies expand rapidly with stable patterns forming on 0.6% agar and 1.0% glucose YPD plates, this agar surface was then used as the substrate for the detection of cell death pattern during mat formation. 5 μ M sytox (SYTOXR Green Nucleic Acid Stain, Life Technologies) was added to the YPD agar to detect the viability

of cells during pattern formation. A time-lapse movie examining cell death in a *FLO11* colony was created by imaging with bright field and FITC filter under Nikon Eclipse Ti microscope for forty one hours with 10 minute intervals. The negative controls were *FLO11* colonies expanding on 0.6% agar and 1.0% glucose YPD plate without sytox, in the presence or absence of 3% hydrogen peroxide. 3% hydrogen peroxide was applied in the YPD plate as a positive control for cell death, as it was previously reported that the survival rate of *S. cerevisiae* was below 0.01 under the treatment of 0.017% hydrogen peroxide (Jamieson, 1992). The positive control was YPD plate with 5 μ M sytox and 3% hydrogen peroxide added at 15 hours. The contrast was adjusted to the same level for experimental images and controls.

	0.3% Agar	0.6% Agar	0.9% Agar	1.5% Agar	3.0% Agar	6.0% Agar
Number of Primary Wrinkles measured	147	207	158	169	106	51
Number of Secondary Wrinkles measured	49	116	80	87	73	42

Table 1. The number of distances measured for primary and secondary wrinkles.

3.2.3 Colony freezing and cryosectioning.

To culture colonies for cryosectioning, a volume of 0.5 μ l of *FLO11* or *flo11* Δ (at OD₆₀₀ around 0.3) were inoculated onto YPD agar plates (6-well plate, BD Falcon, Cat#: 353046) with 1.0% glucose in combination with various agar concentrations (0.6%, 1.5%, or 3.0%). At day 9 after inoculation, the colonies were cut for frozen blocks for cryosectioning. Radial and across- secondary wrinkles blocks that were oriented parallel or perpendicular to the direction from the center to the rim of the colony were cut out of the colonies with a scalpel and then immersed in clear frozen section compound (VWR, CA95057-83B). The blocks were frozen in a HistoChill Cryobath (SP Scientific, FTS system), and then sectioned with 4 μ m thickness for each cross section slice. Each block was cryosectioned at radial or across- secondary wrinkles orientation for six slices, respectively.

3.2.4 Plate imaging and microscopy.

For manual measurement of the wavelength in pattern formation, colonies on 0.3% agar density were imaged at day 4, and colonies on 0.6%, 0.9%, 1.5%, 3.0%, 6.0% agar concentrations were imaged with a Leica MZ6 stereo microscope with Nikon DS-Fi1 camera at day 24. For cryosectioning, colonies were imaged under the Leica microscope before and after removing blocks for frozen and cryosectioning, and the cryosectioned slices were imaged under a Nikon Eclipse TE2000-E microscope with a 4X magnification objective using a QIClick camera and montaged via Photoshop CS.

3.2.5 ESVS model for *S.cerevisiae* colony.

To investigate the mechanisms underlying the hierarchical wrinkling patterns of the *S.cerevisiae* colony expanding on the surfaces with various agar concentrations, I applied “The Hierarchical Wrinkling Pattern Model for Viscoelastic Skin and Substrate” ESVE model from the Genzer group to correlate the wavelengths of *S. cerevisiae* colonies (“skin”) to various agar (“substrate”) concentrations (Efimenko et al., 2005; Fu et al., 2009; Nayar et al., 2012). The wavelengths of the hierarchical wrinkles of colonies depend on the Young's Modulus of both the colonies (“skin”) and the agar (“substrate”) surfaces (Efimenko et al., 2005; Fu et al., 2009).

The Young's modulus for each agar surface in the model (*see Methods*) was obtained from previous report from Hodge group through nanoindentation, (Nayar et al., 2012). Specifically, the Young's modulus was calculated from:

$$E = \sqrt{(E' + E''^2)} \quad (2.5)$$

where the storage modulus E' and the loss modulus E'' were the dynamic modulus, measured by Nayar et al., 2012. The Young's Modulus E in correspondence to various agar concentrations are shown in Table 2 (Nayar et al., 2012).

To obtain the wavelengths of the hierarchical wrinkles of the colony in the model (*see Methods*), the height of the smooth yeast skin and the primary wrinkle were measured respectively. The height of the smooth colony and primary wrinkles, which were 80 μm and 350 μm measured from cryosectioned colonies (on YPD media with

1.5% agar and 1.0% glucose), were used in the following model to obtain the wavelength of the primary wrinkles and secondary wrinkles.

The hierarchical wrinkling model showed that the wavelengths of the secondary wrinkles of *S. cerevisiae* colonies were decreasing with the increase of agar levels, which indicated the dominance of agar in determining the wavelengths of secondary wrinkles.

We then applied the ESVS Thin Substrate (Equation 2.6) and Thick Substrate (Equation 2.7) model to obtain the wavelengths of the pattern for yeast colony respectively.

$$\lambda = (hH)^{\frac{1}{2}} \left(\frac{Y_{yeast}}{a^2x^2 + bx} \right)^{\frac{1}{6}} \quad (2.6)$$

$$\lambda = h \left(\frac{Y_{yeast}}{a^2x^2 + bx} \right)^{\frac{1}{3}} \quad (2.7)$$

where x indicates the percentages of agar, λ is the predicted wavelength of the wrinkling pattern in *S. cerevisiae*. The heights of yeast cell layer (h) and ECM substrate (H), used in ESVS Thin Substrate model (Equation 2.6) were both $80 \mu\text{m}$, the yeast Young's modulus was 112 KPa, the coefficient a , b for x were $1.81\text{e-}007$ and 3.2051 respectively. The heights of yeast cell and ECM layer used in ESVS Thick Substrate model (Equation 2.7) were $325 \mu\text{m}$, the yeast Young's modulus was 8000 KPa, the coefficient a , b for x were 798500 and 3823 respectively, which was obtained from fitting a quadratic polynomial equation (Equation 2.8) to the data on the Young's Modulus of agar versus various agar densities from Nayar 2012 (195).

$$f(x) = ax^2 + bx + c \quad (2.8)$$

where a , b , c were 798500, 3923, 83.3 from the fit respectively, the R-square was 0.999. Geometric mean of wavelengths were used. The height for calculating the wavelengths of primary and secondary wrinkles were measured from the cross section of the *FLO11* colony. I also verified that the fitting of the model to the data is not affected by the change in yeast Young's Modulus over a wide range of values.

Agar\ Young Modulus of Agar	E'	E''	E
0.5%	148 5KPa	1KPa	148KPa
1.0%	160KPa	3KPa	160KPa
2.0%	500KPa	8KPa	500KPa
5.0%	2274 15KPa	22KPa	2274.1KPa

Table 2. Young's modulus in response to various agar concentrations (Modified from Nayar et al., 2012).

3.2.6 Manual measurement on the wavelength of colony patterns.

For each colony, the arc-length distances between the primary or secondary wrinkles were measured, at a certain radius that was positioned in the outside rim of the colony. The primary and secondary wrinkles were distinguished as the randomly positioned short first-degree structures or the radially positioned thick bundles of thin wrinkles respectively. The arc-length distances of primary and secondary wrinkles were measured for *FLO11* colonies on each combination of agar and glucose concentrations. Based on the strong influence of agar on the wavelengths of secondary wrinkles on *FLO11* colony, which was slightly effected by the change of glucose concentration, the arc-length distances measured on each agar level consisted of three glucose conditions with replicates. Most agar and glucose combinations had three replicates. The total number of arc-length distances of primary or secondary wrinkles measured for each agar density were shown in Table 1. The wavelengths of the wrinkles were obtained from Equation 2.9, 3.0.

$$\lambda = \frac{d}{2} \times \theta \quad (2.9)$$

$$\theta = 2 \times \arcsin \left(\frac{d_i}{d} \right) \quad (3.0)$$

where d was the diameter of the circle that harbored the measured arc-length distances; d_i : the arc-length distance between primary wrinkles or between secondary wrinkles; θ : angles between primary or secondary wrinkles; λ : wavelength for primary or secondary wrinkles. The distances (d_i) between adjacent primary or secondary wrinkles were measured around a circle near the colony rim. The diameter of the circle (d) and

the diameter of the plate in the image were also measured. Knowing the actual diameter of the plate (3.5 cm), we could therefore estimate the actual radius of the circle (d), as well as the inter-secondary wrinkles and inter-primary wrinkle distances (d_i). The analysis on wavelength was performed in Matlab R2010b.

3.2.7 Fast Fourier Transformation analysis on secondary wrinkles frequencies.

Images were converted to grayscale and colonies were segmented based on pixel brightness and radius, using a Gaussian mixture model. Yeast colonies were converted to radial coordinates using the *imgpolarcoord* Matlab file written by Juan Carlos Gutierrez and Javier Montoya. The image data lines at each radius within a section were Fast Fourier Transformed (FFT). The mean and standard deviations of the FFT intensities within each section were then calculated, and used to create the mean spectra and the standard deviation of the spectra. Finally, the heights of the peaks were calculated as $s(k) = \log_{10} t(m, k) + \log_{10} t(-n, k)$, with a *t*-statistic defined in Equation 3.1.

$$t(j, k) = \max \frac{\mu(k) - \mu(k - j)}{\sqrt{\frac{\sigma(k) + \sigma(k - j)}{N}}} \quad (3.1)$$

where $m, n \in \{1, 2, 3\}$. The mean and standard deviation of spectral intensity corresponding to k are $\mu(k), \sigma(k)$. N is the number of spectra used to calculate $\mu(k)$ and $\sigma(k)$. Peak with highest s was chosen as the frequency of secondary wrinkles. Wavelengths were then calculated by dividing the outermost perimeter of a section by the number of secondary wrinkles (or oscillations) corresponding to the corresponding

frequency. The Fast Fourier Transformation was performed by Rhys Adams.

3.2.8 Comparison of fitting between ESVS Thin and Thick model and agar-independent model to wavelengths of pattern of *FLO11* colony.

ESVS model includes the ESVS Thin and Thick model and agar-independent model, which were fitted to the manual measured wavelength for the hierarchical wrinkles (including both the primary and secondary wrinkles) with one parameter, such as the Young's Modulus of substrate or yeast free.

The ESVS Thin model and Thick model were used based on the thickness of the substrate (Equation 3.2, 3.3) (273, 274).

$$\lambda = (hH)^{\frac{1}{2}} \left(\frac{E_m}{E_p} \right)^{\frac{1}{6}} \quad (3.2)$$

$$\lambda = h \left(\frac{E_m}{E_p} \right)^{\frac{1}{3}} \quad (3.3)$$

h , H , E_m , E_p represented the height of the top film and substrate, the Young's Modulus of the top film and substrate respectively. Incorporating the height of the yeast biofilm and the association of agar density and the Young's Modulus of agar (195), the ESVS model with the free parameter, which was the Young's Modulus for ECM substrate or the Young's Modulus for the yeast biofilm, suggested the relationship between the wavelengths of the primary wrinkle for ESVS Thin (Equation 3.4) and Thick model (Equation 3.6), or secondary wrinkle for ESVS Thin (Equation 3.5) and Thick model (Equation 3.7) respectively, which were fitted to the data. The Young's Modulus of the yeast used was 0.019 KPa, which was the bacterial biofilm Young's Modulus (282).

The height of the agar 6236(μm) in Equation 3.7 was calculated by Equation 3.8,

$$\lambda = (80(\mu\text{m}) \times 80(\mu\text{m}))^{\frac{1}{2}} \times \sqrt[6]{\frac{112\text{Kpa}}{(a^2x^2+b^2x)(\text{KPa})}} \quad (3.4)$$

$$\lambda = (325(\mu\text{m}) \times 6236(\mu\text{m}))^{\frac{1}{2}} \times \sqrt[6]{\frac{112(\text{Kpa})}{(a^2x^2+b^2x)(\text{KPa})}} \quad (3.5)$$

$$\lambda = (80(\mu\text{m})) \times \sqrt[3]{\frac{112\text{KPa}}{(a^2x^2+b^2x)(\text{KPa})}} \quad (3.6)$$

$$\lambda = (325(\mu\text{m})) \times \sqrt[3]{\frac{112\text{KPa}}{(a^2x^2+b^2x)(\text{KPa})}} \quad (3.7)$$

$$V_{\text{Agar}} = \pi R^2 H \quad (3.8)$$

where R is the radius (1.75 cm) of the 6-well plate (BD Falcon, Cat#: 353046), V_{Agar} is the volume of the agar (6 ml).

The agar-independent model was shown in Equation 3.9. The fittings were performed with Matlab curve fitting tool – cftool.

$$c \times x^0 \quad (3.9)$$

3.3 Result

3.3.1 Pattern formation in *S. cerevisiae*.

The characteristic investigated in this chapter was pattern formation on colony surfaces during expansion. Initial patterns in *FLO11* colonies typically appear as irregular wrinkles developing into a “hub”, a thickening mass of cells in the colony center. After a few days, as the colony expanded beyond the wrinkled hub, wrinkles emerge in the radial direction, some of which bundled into thicker secondary wrinkle-like structures. As the colony area increases, radial secondary wrinkles appear *de novo* between two existing secondary wrinkles or by branching, with apparently quasi-regular spacing. In contrast, *flo11* Δ colonies appear smooth, without any obvious surface patterns (Figure 2B).

To determine whether the distances between primary and secondary wrinkles are regular, and whether they depend on agar and glucose concentrations, the surface patterns of individual colonies were measured manually. The narrow distributions of inter-wrinkle distances suggested regular spacing for the primary wrinkle, as well as the secondary wrinkle (Figure 8). Additionally, through colony expansion, the spacing between primary and secondary wrinkles were regular and were maintained to be constant during expansion. Moreover, the number of primary and secondary wrinkles increased towards the colony edge, indicating that pattern formation had a tendency to preserve inter-primary wrinkle and inter-secondary wrinkles arc-lengths rather than

arc-angles (Figure 2).

3.3.2 The absence of localized cell death pattern in *S. cerevisiae*.

Next I investigated the mechanisms underlying wrinkle formation. Considering recent evidence for non-uniform cell death causing bacterial colony wrinkling (11), I tested whether it played a role in the formation of yeast colony surface patterns. By incubating yeast colonies on media with SYTOXR Green Nucleic Acid Stain, the pattern of cell death was indicated by green fluorescence. In contrast to bacteria, I observed uniform and minimal distribution of cell death from inoculation throughout colony maturation when expanding on plate with SYTOXR Green Nucleic Acid Stain (see *Methods*), arguing against the role of non-uniform cell death in pattern formation by yeast colonies (Figure 7).

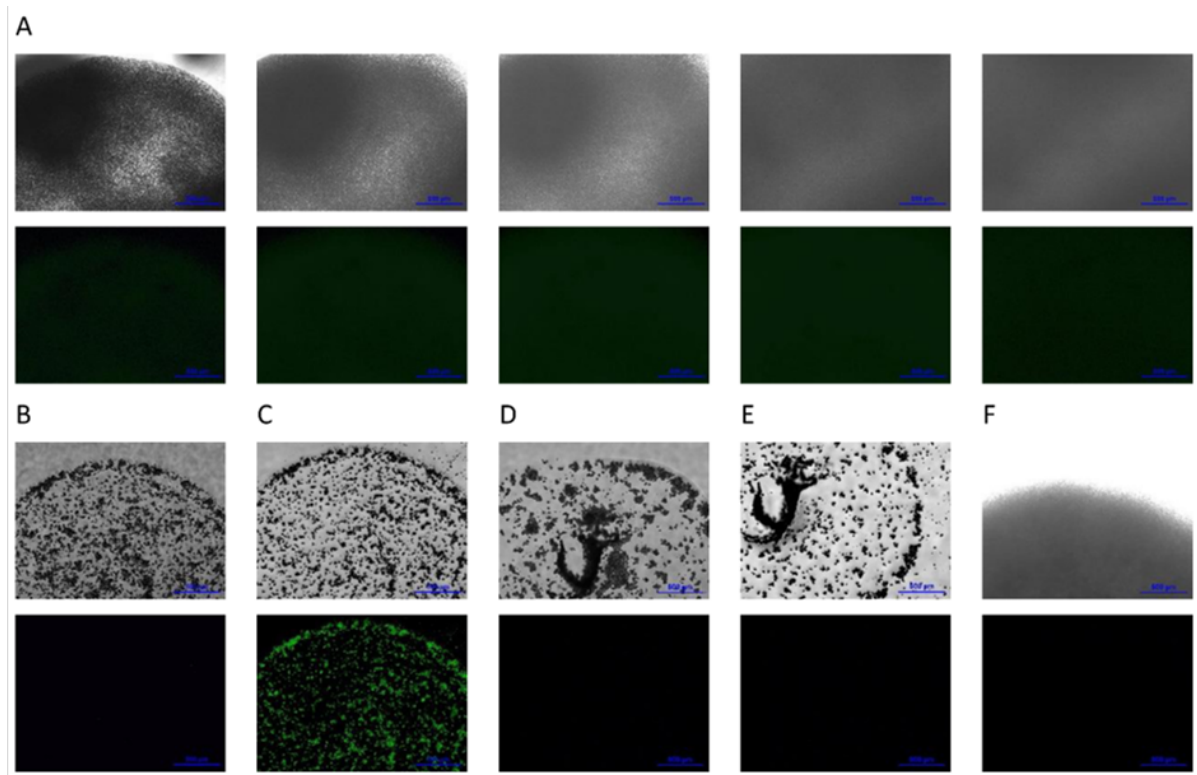


Figure 7. Cell death was minimal and uniform during *FLO11* colony expansion. (A) No particular death pattern has been detected on 0.6% agar and 1.0% glucose YPD plate with 5 μ M Sytox green nucleic acid, at 19:40 hours, 26:20 hours, 30:50 hours, 41:40 hours and 67:40 hours after inoculation. (B-C) *FLO11* colony incubated with 5 μ M Sytox was imaged before (at 14 hours after inoculation) (B) and after adding of 3% H_2O_2 (at 15 hours after inoculation) (C) as positive control. Minimal cell death was detected (bottom panel) in the former, and uniform cell death was observed for the latter at 36 hours. (D-E) In the absence of Sytox as a negative control, no fluorescence was observed before (at 20 hours) (D) or after (at 42 hours) (E) adding 3% H_2O_2 at 21 hours. (F) No fluorescence was observed for *FLO11wt* colony with neither Sytox nor H_2O_2 . (A-F) Bright field and FITC channel were shown on the top and bottom panels respectively.

The positive control of 3% H₂O₂ treated *FLO11* colony expanding on 5 μ M sytox YPD plate showed bright fluorescence (Figure 7). Thus, *FLO11* colony develops wrinkling formation in the absence of specific cell death pattern.

3.3.3 The wavelength of patterning measured manually

. The results revealed regular spacing for the primary wrinkles, as well as thicker secondary wrinkles (Figure 8). This process was maintained following physical laws in order to preserve the dominant frequency of wrinkles along with the colony expansion. As the patterns developed by the yeast biofilms preserve arc-lengths rather than arc-angles (Figure 2), the wavelength could be used as a marker for pattern formation. To determine whether the distances between primary and secondary wrinkles have a dependence on agar and glucose concentrations, I investigated colony surface patterns of individual colonies by manual measurement. The secondary wrinkles development started initially with thin and short secondary wrinkles, which bundled together to form thick secondary wrinkles, the frequencies of which were determined by agar levels, rather than glucose concentrations (Figure 8).

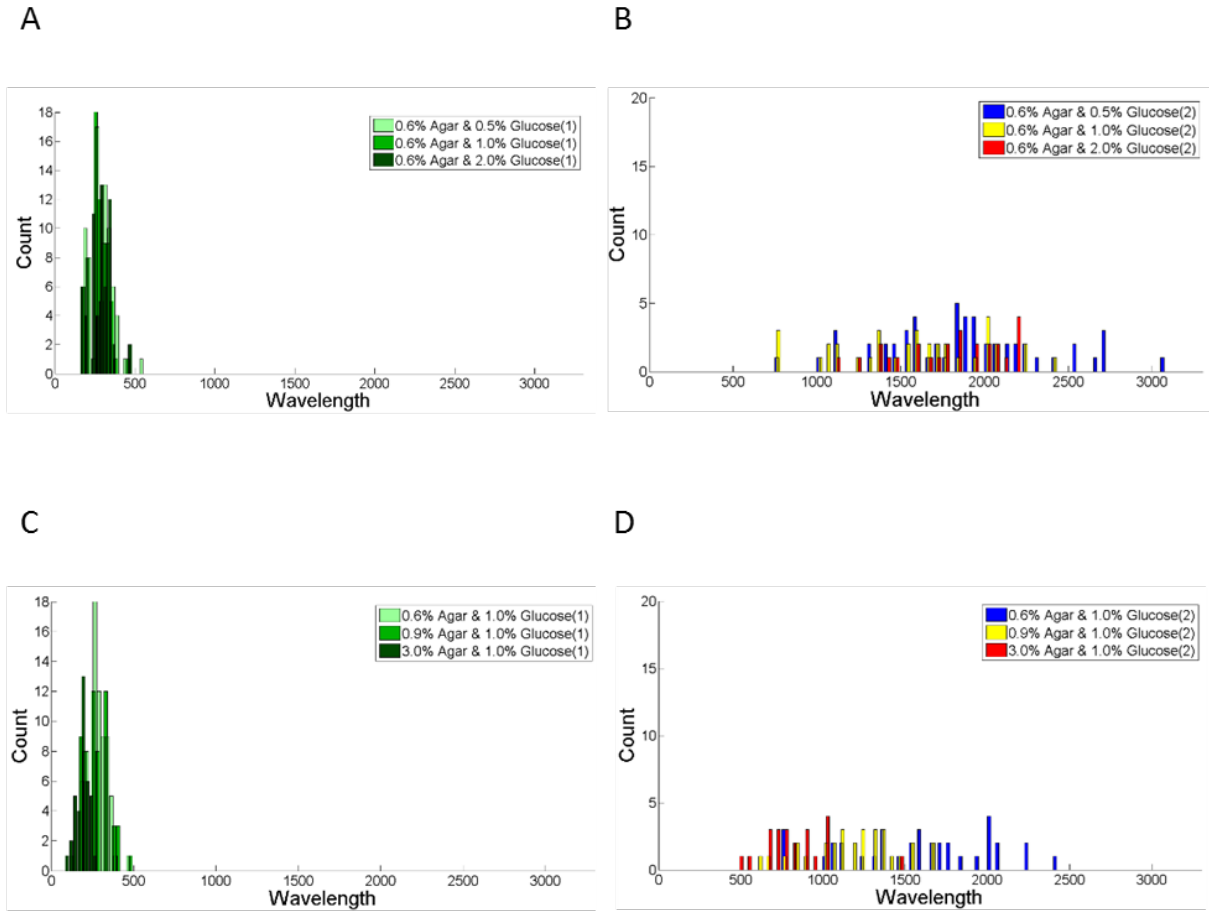


Figure 8. Distributions of inter-spoke distances (wavelengths) of *FLO11* colony. (A, B) The distribution of wavelength of both wrinkles (1) (A) and spokes (2) (B) were insensitive to the change of glucose concentrations. (C, D) The distribution of wavelength of spokes (2) (D) from manual measurements shifted to shorter wavelength with the increase in agar density. The wavelength of the wrinkles (1) (C) was insensitive to the change of agar levels. Primary wrinkle and spokes were indicated by (1) and (2) respectively in the figure legend. The unit for the wavelength in all panels were μm .

	0.3% Agar	0.6% Agar	0.9% Agar	1.5% Agar	3.0% Agar	6.0% Agar
Average Wavelength of Primary Wrinkles (μm)	414	304	292	298	236	281
Average Wavelength of Secondary Wrinkles (μm)	3617	1747	1339	1100	730	574

Table 3. Average wavelengths for primary and secondary wrinkles.

Therefore, the results suggested that the viscoelasticity of the agar is critical to the wavelength of the patterns. Thus, this chapter further analyzed and characterized the wavelengths of the pattern formation. The measured wavelengths for the shorter-wavelength wrinkles changed very slightly with the increase of agar levels. On the contrary, the average wavelengths of the longer-wavelength wrinkles were highly affected by the concentrations of agar (Table 3). The wavelengths decreased sharply with the increase of agar concentrations across the range of low agar levels (0.3%, 0.6%, 0.9%, 1.5%, and 3%), while they approached a plateau from 3% to 6% agar levels (Figure 9). In concordance with ESVS model, this study suggested that the evenly distributed wrinkles in our pattern-forming *S. cerevisiae* are generated due to the hierarchical wrinkling of the colony in correspondence to the Young's Modulus properties of the complex yeast biofilm and the agar surface (Efimenko et al., 2005; Fu et al., 2009).

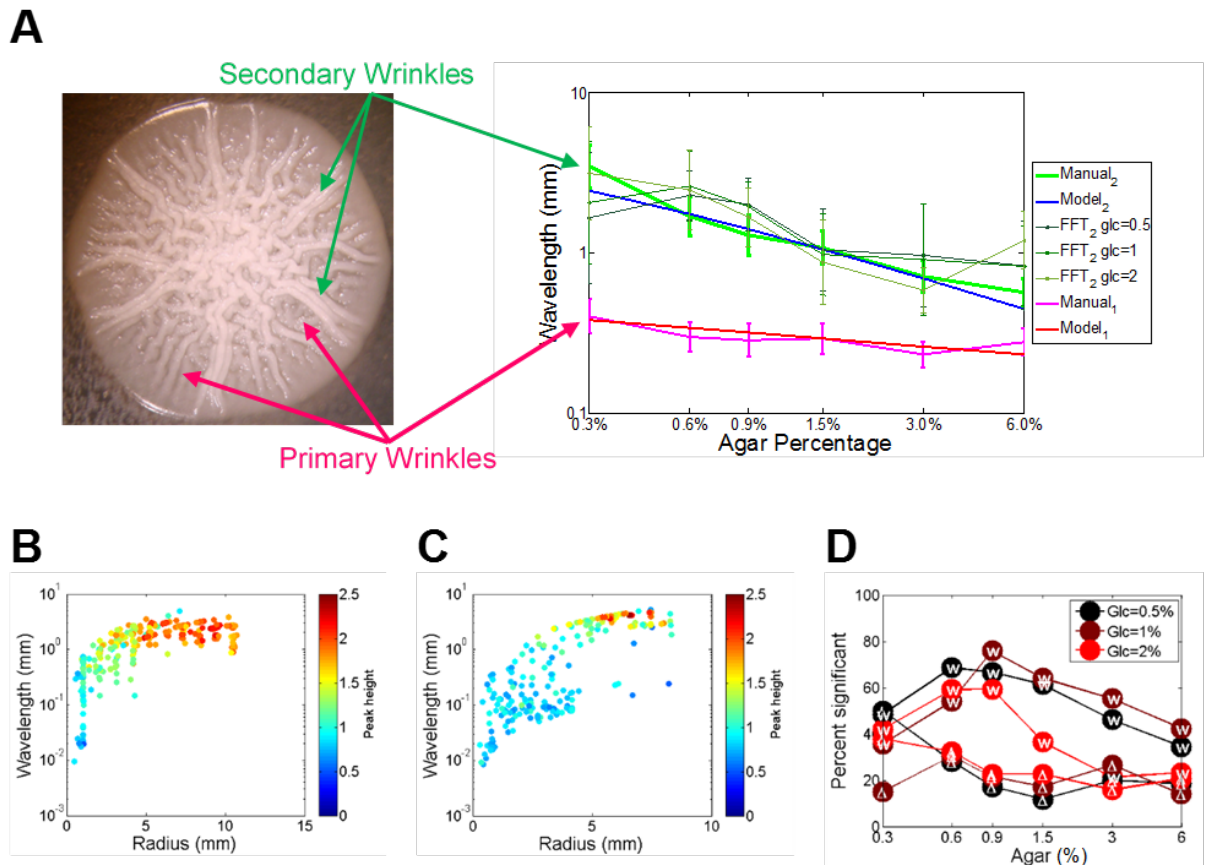


Figure 9. Analysis of the wavelengths of colony surface patterns. (A) The wavelengths of spokes (2) measured manually decreased with increasing agar density, while the wrinkles wavelengths (1) from both manual measurements, and FFT estimates from the 3 glucose concentrations were insensitive to the change of agar density. The wavelength of the wrinkles was shorter than that of the spokes among all agar levels tested. The wavelength of spokes measured experimentally was fitted by ESVS model. The inserted image showed the distances between adjacent primary wrinkles (red line) or two secondary spokes (green line) measured at the outer radii. (B) The Secondary wavelengths plotted as a function of section radius, independent of time for *FLO11* colony at 0.5% glucose and 0.9% agar. (C) Same as (B), but for a *flo11Δ* colony at 0.5% glucose and 0.9% agar. FFT measurement was applied only on the secondary spokes. Each dot (C, D) represented a colony from a replicate and a time point. (D) The percent of significant points (defined as peak height > 1.5) was plotted as a function of agar. The numbers (*FLO11* or *flo11Δ*) are shown in white inside of the circles. FFT analysis was performed by Rhys Adams.

3.3.4 Hierarchical wrinkles of yeast pattern

A striking observation was the existence of two different scales in the surface patterns of the *FLO11* colonies (Figure 10). This pattern is similar to the hierarchical wrinkling observed in a related mechanical system: the wrinkling in a thin elastic film on top of a viscoelastic substrate during substrate shrinkage (Figure 1)(190, 191). The shrinkage of the substrate relative to the film should cause similar strain as the stretching of the growing yeast colony relative to the agar substrate.

Therefore, I considered two different modes of colony expansion depending on the presence/absence of a functional *FLO11* gene. If *FLO11* was present, presumably cells were constrained to grow two-dimensionally into a multi-layered structure, as an elastic skin made of cells and extracellular matrix attached to the viscoelastic agar (283). In contrast, cells without *FLO11* were assumed to expand in three dimensions without any constraints due to the absence of strong attachment to the agar.

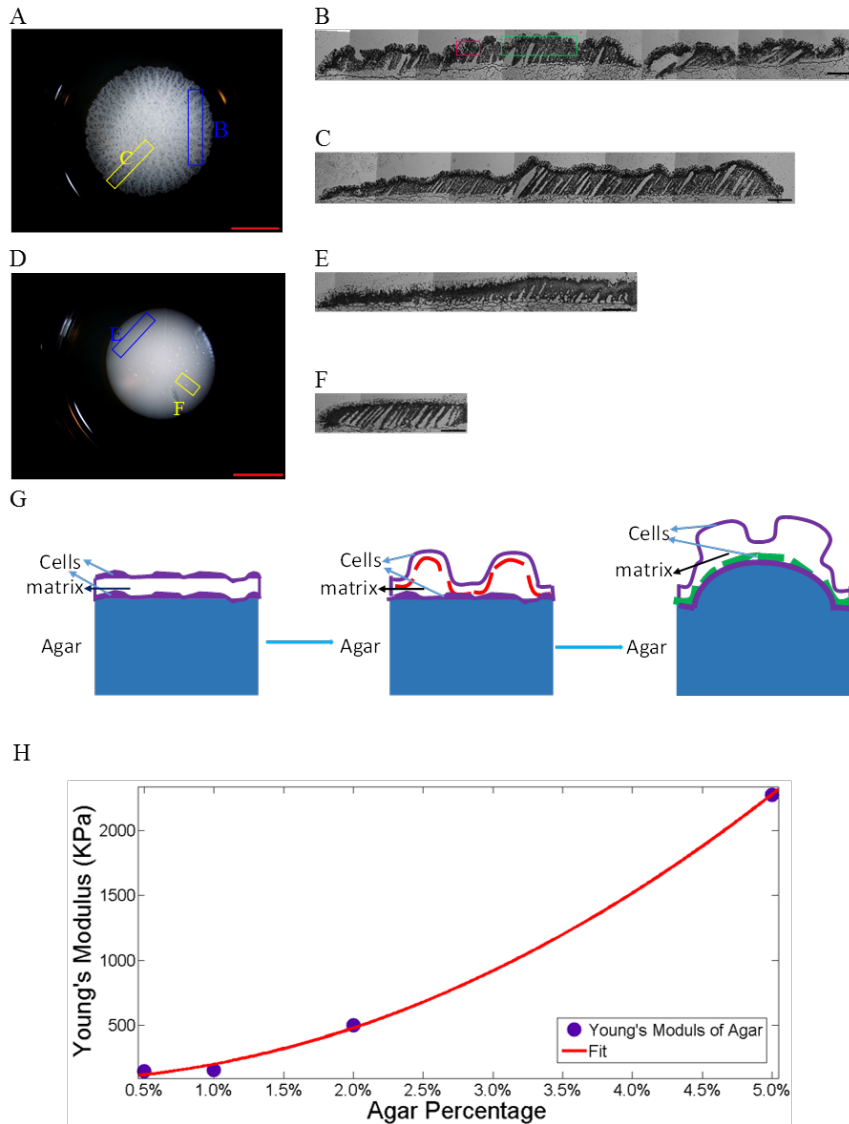


Figure 10. *FLO11*-induced wrinkles on the colony surface. (A, D) Frozen blocks oriented across-spokes (blue box indicating estimated location) and radially (yellow box indicating estimated location) were cut from the *FLO11* (A) or *flo11Δ* (D) *S. cerevisiae* colonies on 1.5% agar and 1.0% glucose YPD plates. The scale bar was 7500 μm. (B) Montage of the cryosections oriented across-spokes of a *FLO11* colony (A) indicating wrinkles (red box) and spokes (green box). (C) Radial cryosectioning of the *FLO11* colony (A). (E, F) Montage of the cryosections oriented across-spokes (E) or radially (F) for a *flo11Δ* colony (D). The scale bar (B, C, E, F) was 500 μm. (G) A schematic showing primary wrinkle formation (red dashed line), the saturation of which upon increasing stress leads to the higher degree spokes formation (green dashed line). Agar on which the colony expands is shown in blue. (H) The Young's Modulus of the substrate material – varies on various agar percentages (Modified from Nayar et al., 2012). [Reprinted from (195) under the Creative Commons License].

Cryosections of *FLO11* and *flo11Δ* colonies suggested that hierarchical wrinkles occurred in and only in *FLO11* colonies. The cryosectioning of the *FLO11* colonies grown on various agar concentrations (0.6%, 1.5%, 3.0%) demonstrated two degrees of wrinkling patterns as compared to the smooth and dome-shaped *flo11 Δ* colonies, which were flat without any wrinkling structure on the cross-sectional view in both radial or across- secondary wrinkles orientation on all agar concentrations tested (Figure 10, 11).

The radial oriented cryosections showed shorter-wavelength wrinkles on top of comparatively flat surface (Figure 10C, F). The apparent longer-wavelength secondary wrinkles viewed from across-secondary wrinkles cryosections suggested the emergence of secondary wrinkles that extended from the center to the rim of the colony (Figure 10B, E). On various agar surfaces (0.6% to 1.5% to 3.0%), the wavelengths of secondary wrinkles decreased along with the agar concentration (0.6% to 1.5% to 3.0%) (Figure 10).

3.3.5 ESVS model on yeast pattern formation.

Theories of elastic skin-viscoelastic substrate (ESVS) sandwich systems can capture two limiting cases [38]. First, if the thicknesses of the skin and substrate are comparable then the wavelength depends on H , the substrate thickness (Equation 3.2). If the stress continues to increase, the amplitude of primary wrinkles increases until saturation, after which secondary wrinkles start forming according to the similar formula,

independent of the thickness of the substrate (Equation 3.3) (190). This process of hierarchical wrinkling can continue until wrinkles appear at several length scales (190).

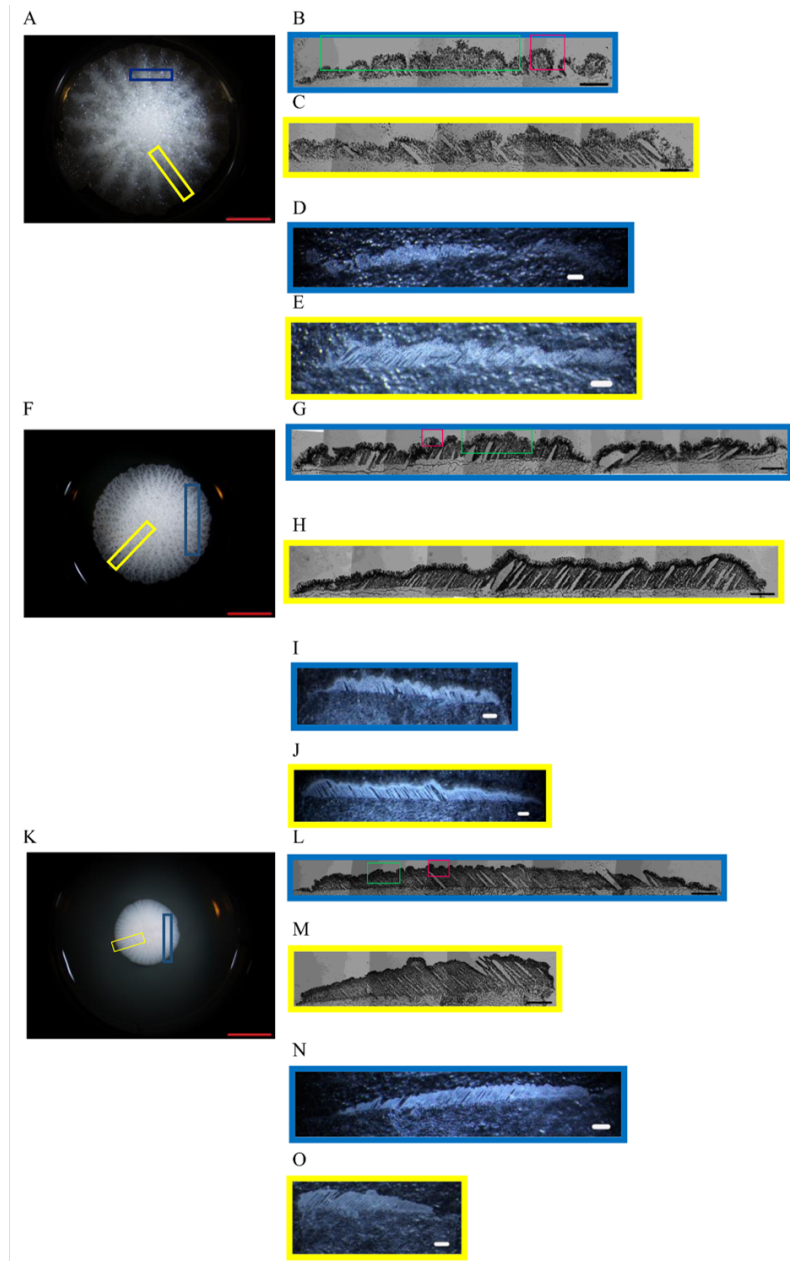


Figure 11. The cross-sectional view of hierarchical wrinkles of a *FLO11* colony. (A, F, K) *FLO11* colonies on 0.6%, 1.5%, or 3.0% agar were cryosectioned at across-spokes (blue indicated estimated location) and radial (yellow indicated estimated location) orientations. Scale bars were 7.5 mm. (B, D, G, I, L, N) On 0.6%, 1.5%, or 3.0% agar, the cross-sectional view of the across-spokes (blue) oriented section from *FLO11* colonies, two degrees of wrinkling composed of shorter-wavelength wrinkles at the surface of the colony (red box) and the longer-wavelength spokes underneath it (green box). (C, E, H, J, M, O) On 0.6%, 1.5%, or 3.0% agar, only shorter-wavelength wrinkles were shown on the radial (yellow) cross-sectional view of the *FLO11* colonies. (B, C, G, H, L, M) Images were taken under Nikon Eclipse TE2000-E Microscope, (D, E, I, J, N, O) Images were taken under Leica MZ6 stereo microscope (See Methods). Overall, the hierarchical wrinkles were observed on *FLO11* colonies on various agar conditions. (B-E, G-J, L-O) Scale bar were 500 μ m.

If the theory for hierarchical wrinkling in ESVS sandwich systems applies to *FLO11* colonies, the spatial frequencies should follow formulas as describe above. Indeed, fitting these models indicated that inter-secondary wrinkles spacing had an inverse dependence on the agar density as expected from the physical ESVS theory of wrinkling when the substrate is thick (Figure 9A). In contrast, only the thin substrate ESVS model could fit the spacing of primary wrinkles, which was less agar density-dependent (Figure 12). These findings suggested that primary wrinkle formation does not directly involve the agar, but another thin substrate that sits below the top layer of cells. The density and thereby the elasticity of the matrix could nonetheless correlate with the density of agar, which must be the source of water for the matrix. Indeed, confocal microscopy previously suggested the existence of at least 4 layers (agar, yeast attached to agar, extracellular matrix, and yeast exposed to air) in yeast colonies (9). Therefore, the prime candidate for the thin substrate is the extracellular matrix squeezed between two cell layers. The spacing of both the spokes and primary wrinkles was independent of glucose concentrations (Figure 8, 11A), as expected from the ESVS model. The wavelengths corresponding to dominant frequencies had a tendency to stabilize around specific values towards the outer radii of *FLO11* colonies (Figure 9B, C). These wavelengths were the most significant and tightly peaked within Fourier spectra for a wide range of agar concentrations (0.6-1.5%) (Figure 9A, D). Except for the lowest agar concentration (agar=0.3%), wavelengths obtained for *FLO11* colonies were consistently more significant than for those obtained for *flo11* Δ colonies (Figure

9D). Finally, the dominant wavelengths (even if sometimes non-significant) tended to decrease with increasing agar concentration, resembling the agar-dependence of inter-spoke arc-lengths (Figure 9A), and were only moderately affected by the glucose concentration (Figure 8).

3.3.6 ESVS model fitted the data on wavelengths of the hierarchical wrinkles better than an agar-dependent model.

In order to further validate that ESVS model explains pattern formation well, I compared the fitting of the ESVS model and the agar-independent model (*see Methods*) (273, 274) to the data on the wavelengths of both primary and secondary wrinkles.

The ESVS Thick model fitted the hierarchical wrinkling data with R-square of -0.24 and 0.89 for primary and secondary wrinkles respectively, while ESVS Thin model fitted the primary and secondary wrinkles with R-square of 0.63 and 0.6 respectively. However, the agar-independent model had R-square of 0 for both primary and secondary wrinkles.

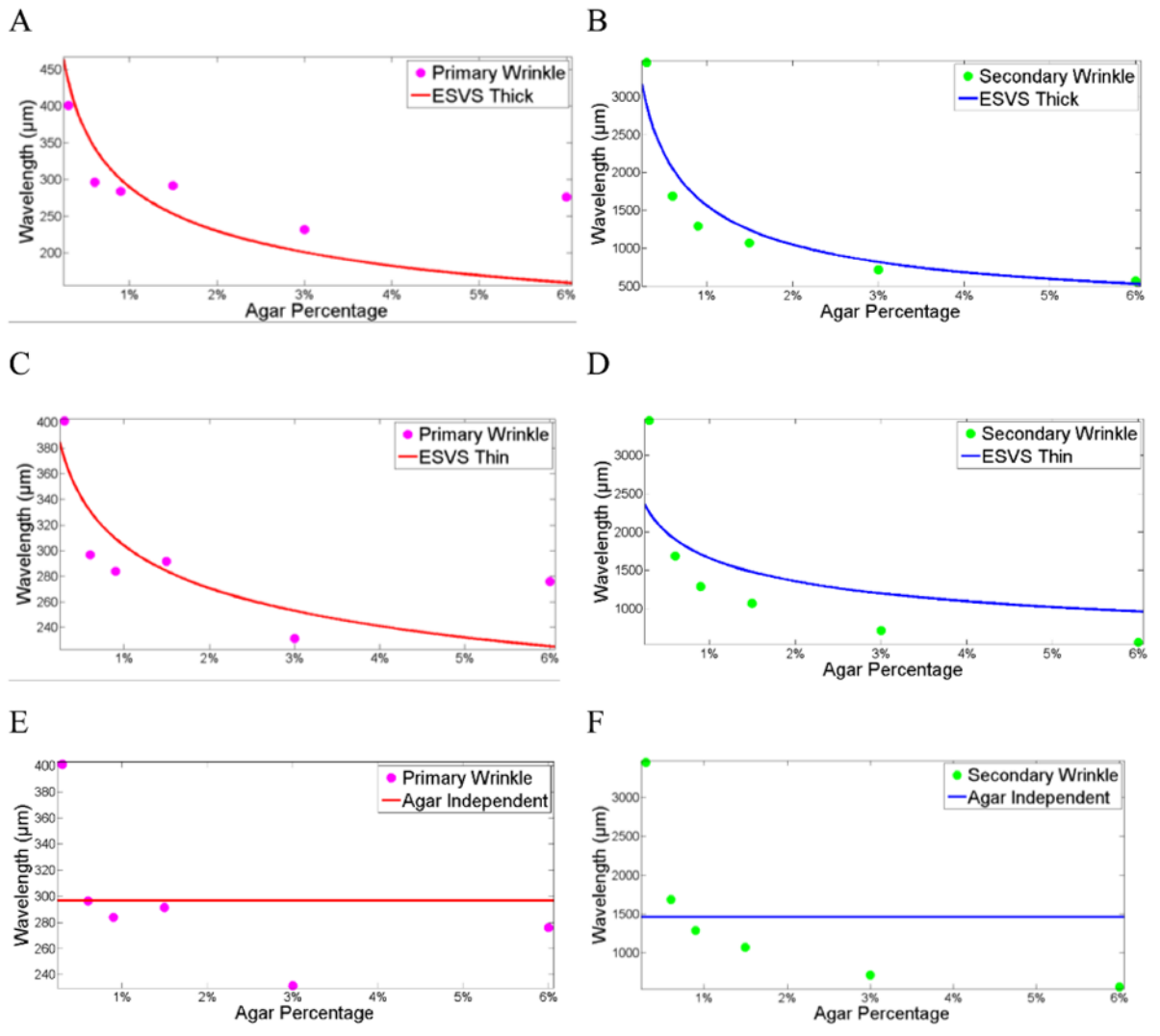


Figure 12. The fit of physical models to data on primary and secondary wrinkles. On YPD media with various agar densities (0.3%, 0.6%, 0.9%, 1.5%, 3.0%, and 6.0%), the geometric mean of wavelength of the primary (A, C, E) and secondary wrinkles (B, D, F) were plotted in magenta and green respectively. (A, B) ESVS Thick model fitted primary (A) and secondary wrinkles (B) with R-square at -0.24 and 0.89 respectively. (C, D) ESVS Thin model fitted primary (C) and secondary wrinkles (D) with R-square at 0.63 and 0.6 respectively. (E, F) Agar-independent model fitted primary (E) and secondary wrinkles (F) with R-square at 0 for both.

Therefore, the ESVS model exhibited better fitting to the primary and secondary wrinkles comparing with the agar-independent model (Figure 12). Specifically, the ESVS Thin model and Thick model explained the primary and secondary wrinkles well respectively (Figure 12). This further indicated that the physical property of the yeast biofilm and substrate are critical for both scale of wrinkles, and the hierarchical wrinkling triggers the pattern formation in yeast (Figure 12).

3.4 Discussion

In this Chapter, it was indicated that the wrinkling pattern observed on the yeast colony surface is triggered by hierarchical wrinkling similar to sandwich systems consisting of an elastic skin on top of a viscoelastic substrate. Microbial biofilms typically contain an extracellular matrix secreted by cells, creating a connective medium across the colony that acts as an elastic skin (284). It is indicated from this study that the expansion of the *FLO11* colony that attached closely to the agar can cause strain, which generates pattern through hierarchical wrinkling.

The agar-independent model didn't fit the wrinkling pattern at all suggesting that the physical properties of the yeast biofilm and the substrate are critical to the pattern development. Furthermore, the distributions of the wavelengths of the primary and secondary wrinkles along agar densities were fitted well by the ESVS Thin and Thick model respectively (Figure 12). These findings suggested that, due to the complexity of the sandwich system composed of layered cells and ECM in yeast, the wrinkling pattern

at two different scales were generated through the interaction between the corresponding substrate and top layers. Specifically, upon stress, the primary wrinkle of cells on top of the enriched ECM is generated through the wrinkling of both layers, while the secondary wrinkle of cells with ECM expanding on the agar substrate is then generated if stress keeps accumulating.

The differential growth in the center and the colony rim were identified to contribute to distinct colony expansion in response to different nutrient levels in Chapter 1, the ESVS model could be further modified to distinguish the effect of the compact center, as well as the less dense rim on the elasticity of the biofilm.

In previous studies, the differentiation of biofilms into organized architectures in nature is found to result in both the physiological and the spatial separation of specialized cells. The structures of biofilms are sensitive to the environment and develop distinctively upon different stresses (3, 285-288), The limitation in oxygen, nutrients, and the stresses from antibiotics in the environment shape the colony morphology by organizing in to layers of metabolically active or inactive cells with differential diffusion rates to better protect the actively dividing cells, in order to provide better survival strategy in harsh environments (289, 290). It is therefore interesting to further investigate whether the stresses in nature could alter the wavelengths of pattern formation and the colony morphology through the quantitative analysis methods developed in Chapter 2 and 3, to better understand the crosstalk between physiological activity and the spatial organization of the multicellular structure.

Chapter 4

Biological function of two-dimensional expansion

4.1 Introduction

Biofilm wrinkling in other organisms has been shown to perform specific biological functions. For example, wrinkling is induced under anoxic environment, increasing the oxygenation in *Pseudomonas aeruginosa* colonies (148). The channels underneath wrinkles are suggested to transport liquid within *Bacillus subtilis* biofilms (10).

In previous chapters, *FLO11* was suggested to enable the biofilm cling to the surface closely and fit cells in a very thin film, leading to rapid colony expansion (Figure 2). Therefore, it is also important to understand whether the two-dimensional expansion could convey an advantage during colony expansion, in order to benefit cells to approach nutrients in the environment more efficiently.

Previously, Korolev and colleagues (291, 292) showed that two differently labeled *S. cerevisiae* strains should segregate into single-colored sectors as initial spatial non-homogeneities amplify through a “founder effect” during colony expansion. The boundaries of such single-colored sectors should reveal any competitive advantage between the two strains (or lack thereof).

In this chapter, I demonstrated that despite that *FLO11* and *flo11* Δ cells exhibited comparative growth rate and similar size in the liquid culture (Figure 5),

FLO11 directed two-dimensional growth conveyed expansion advantage during head-to-head competition with *flo11* Δ cells on semi-solid surface. Specifically, the sectors of *FLO11* had outward curvature against adjacent *flo11* Δ sectors, despite of labeling method or initial mixing ratio of the two strains. *FLO11* sectors sustained the surface patterning indicating two-dimensional growth and maintained the advantage until taking over the colony, leaving the *flo11* Δ cells to annihilation in the center of the mixed colony. This finding suggested that the unique modes of expansion conveyed by *FLO11* could benefit the colony in the process of nutrient foraging.

4.2 Materials and Experimental Methods

4.2.1 Strains, media and growth conditions.

For competition experiment, a volume of 0.5 μ l liquid culture of mixed populations with OD_{600 nm} at 0.3 of *FLO11* and *flo11* Δ (one of which was labeled by mCherry) at 1:1 ratio were inoculated in the center of yeast extract peptone galactose (YPGal) plates with 1.0% agar and 0.5% galactose, which were incubated at 30°C.

4.2.2 Fluorescently labeled strains.

We integrated GFP or mCherry into the native GAL1 locus of TBR1 or TBR5 strains respectively, using the histidine auxotrophic marker. Transformation was performed with a modified lithium acetate procedure (Gietz & Schiestl, 2007; Gietz et al., 1995). Synthetic drop-out media (SD -his -tryp) was used for selection (all reagents

from Sigma, Inc.). *FLO11*, *FLO11*-mCherry, *flo11* Δ , and *flo11* Δ -mCherry strains were incubated under 30°C to reach stationary phase, shaking at 300 rpm (311DS Shaking Incubator).

4.2.3 Plate Imaging and Microscopy:

The mCherry transformation into cells were confirmed for fluorescence under Nikon Eclipse TE2000-E microscope with QIClick camera with 20X or 40X objectives under TxRed filters for 8 days. The competition mixes and controls were imaged under a Leica microscope with a Nikon camera at day 5 after inoculation. For the competition experiment, *FLO11*-GFP, *FLO11*-mCherry, *flo11* Δ -GFP, and *flo11* Δ -mCherry strains were transformed, inoculated at various ratios (1:1, 1:3, 3:1), and imaged by Nikon Eclipse TE2000-E microscope with QIClick camera, and Leica MZ6 stereo microscope with Nikon DS-Fi1 camera and Nikon Digital sight DS-U3 camera controller.

4.3 Result

4.3.1 Competition between *FLO11* and *flo11* Δ

Considering that *FLO11* colonies expanded faster in all sugar-agar combinations than their *flo11* Δ counterparts when the colonies were expanding separately (Figure 2), I tested whether the two-dimensional expansion of *FLO11* cells could still convey a competitive advantage over the *flo11* Δ strain during expansion. In particular, I wanted to know if inter-strain interactions could mitigate the growth advantage of *FLO11* strains,

which could not be predicted by single strain expansion (Figure 2).

Specifically, if the sectors occupy approximately the same arc-angle $\theta(r)$ around the colony's periphery over time (Figure 13A), there is no competition. However, if the arc-angle $\theta(r)$ occupied by the unlabeled strain, for instance, increases at the expense of the arc-angle occupied by the other strain labeled by mCherry, then the unlabeled strain is determined to have a competitive advantage (Figure 13B), and vice versa (Figure 13C).

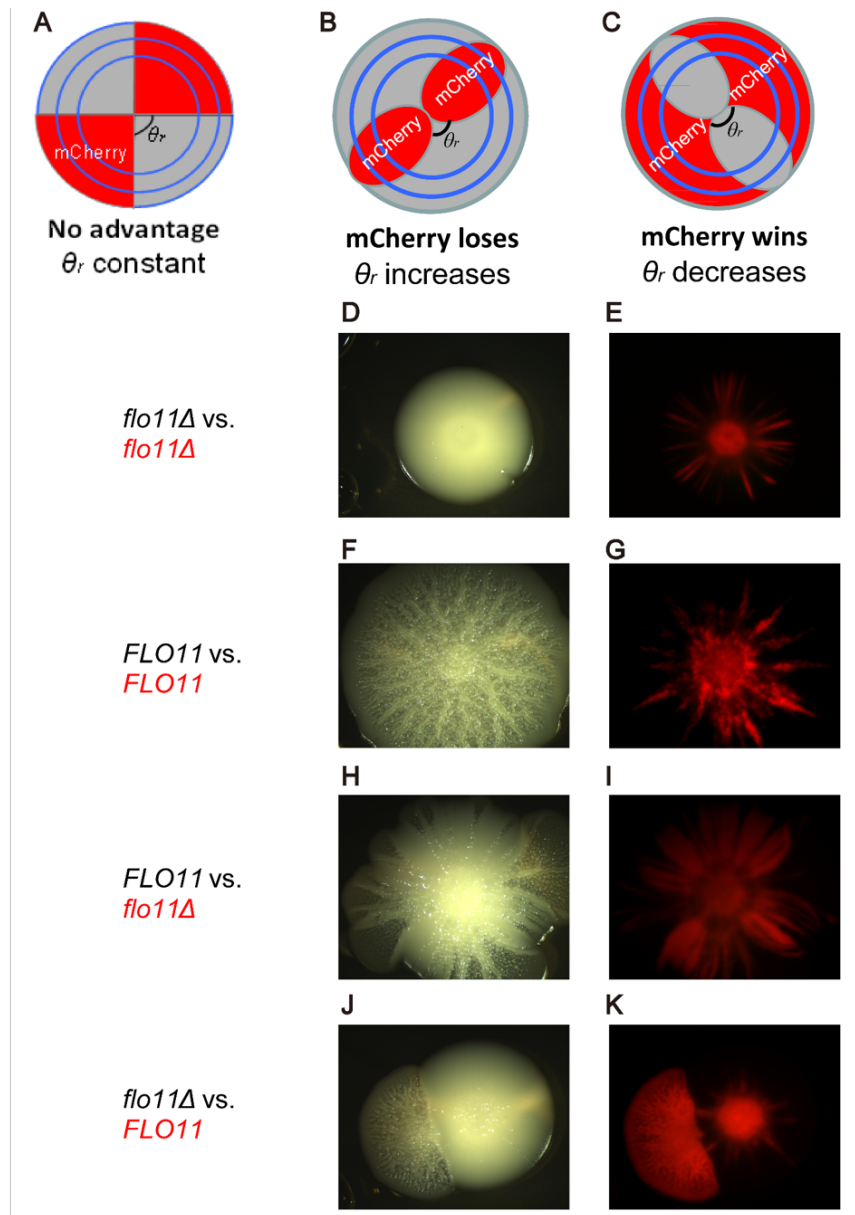


Figure 13. *FLO11* cells out-expanded *flo11* Δ cells during head-to-head competition. On 1.0% agar, 0.5% galactose YPGal plates, (A, B, C) Schematic showing the range expansion of mixed populations segregated into sectors with constant or gradually changing sector angles along the radius due to the difference of fitness between the particular sector and the adjacent sectors (Hallatschek et al., 2007; Korolev et al., 2012). (D, E) Minimal competitive advantage is observed between isogenic cells of unlabeled and mCherry labeled *flo11* Δ sectors. (F, G) Minimal competitive advantage was observed between unlabeled and mCherry labeled *FLO11* sectors. (H, I) Unlabeled *FLO11* sector out-expanded mCherry labeled *flo11* Δ sectors with a conspicuous increase in the unlabeled sector angle, in comparison to minimal competition between isogenic cells (D-G). (J, K) Reverse labeling of (H, I) showed that mCherry labeled *FLO11* sectors overtook the mixed colonies after some time, despite of the initial lack of expansion advantage against unlabeled *flo11* Δ sectors. Bright field (D, F, H, J) and mCherry (E, G, I, K) were shown respectively. Contrast is adjusted in Adobe Photoshop CS for mCherry images.

I used these theoretical results to judge whether two-dimensional expansion of *FLO11* cells was associated with an advantage during head-to-head competition. To examine competition in mixed colonies, I labeled either *FLO11* cells or *flo11* Δ cells, by placing a chromosomally integrated mCherry reporter under the control of an extra copy of the *GAL1* promoter into each strain (*Methods*). 1:1 mixes of labeled *FLO11* cells and unlabeled *flo11* Δ cells, vice versa (Figure 13) and single strain controls (Figure 14) were prepared, and inoculated onto agar plates. As the colony rim was not highly irregular initially (Figure 2), and the competitive advantage was observable before the colonies became highly irregular (Figure 2, 13), the theory by Korolev et al. should apply. Moreover, since the theory refers to the shapes of sectors inside the colony (i.e., inward- or outward-curving sector boundaries), then the moderate irregularity at the colony rim should not affect the claims on the competitive advantage/disadvantage.

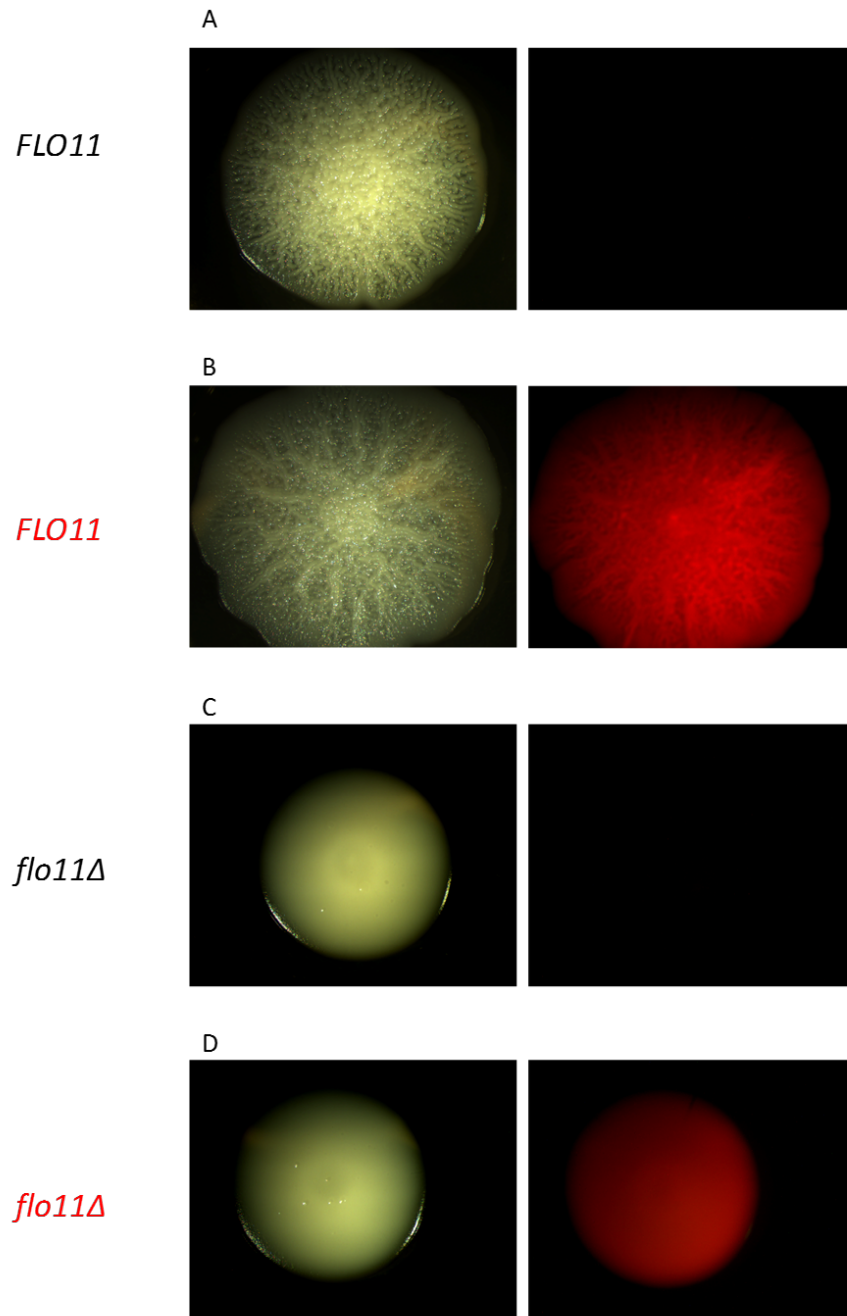


Figure 14. Same-strain controls for competition between *FLO11* and *flo11Δ* colonies. (A) On 1.0% Agar YPD plates with 0.5% galactose, unlabeled *FLO11* expanded with regular pattern formation. (B) Pattern forming mCherry labeled *FLO11* colony was visualized by mCherry fluorescence throughout the colony (right panel). (C) Unlabeled *flo11Δ* colony expanded without pattern. (D) mCherry labeled *flo11Δ* colony was visualized by mCherry fluorescence (right panel) with no pattern formation. Contrast is adjusted in photoshop for mCherry images.

I found that well-mixed liquid cultures (1:1 ratio) inoculated onto agar plates, resulted in distinct red and unlabeled sectors (Figure 13). Examining the sectors that formed when mCherry-labeled *FLO11* cells were mixed with unlabeled *FLO11* cells (or when mCherry-labeled and unlabeled *flo11* Δ cells were mixed), revealed a lack of significant competition, except for a small fitness cost associated with mCherry expression (Figure 13D-G). Importantly, the mixtures of labeled and unlabeled *FLO11* cells preserved the colony expansion and pattern formation characteristics of *FLO11* strains grown alone under the same conditions (Figure 13). These data, taken together with the similarity of *FLO11* and *flo11* Δ cell sizes and growth rates in liquid cultures (Figure 5), indicated that the two-dimensionally constrained expansion mode of *FLO11* cells gives them advantage over *flo11* Δ cells when they expand on agar plates.

When a mixture of *flo11* Δ (labeled) and *FLO11* (unlabeled) cells were inoculated onto a plate, *FLO11* sectors not only preserved the surface patterning (visualized in bright field), but also displayed a strong outward curvature at the expense of *flo11* Δ sectors (Figure 13H, I). The arc-angle θ of the *flo11* Δ colony (mCherry labeled) decreased with the radius (Figure 13I) compared to the control mixtures (Figure 13D-G). Interestingly, however, mCherry-labeled *FLO11* cells seemed to gain competitive advantage against *flo11* Δ cells only after colonies grew for a substantial time, indicating that a sufficiently large sector of these cells had to be established, or the sugar levels on the plate had to drop before they could outcompete *flo11* Δ cells. Once that happened, not only did the *FLO11* gene convey a competitive advantage, but the

FLO11 cells eventually enveloped the *flo11* Δ sector (visualized by mCherry in Figure 16I) by coalescing with the adjacent *FLO11* sector (Figure 13H). This halted the spread of the *flo11* Δ colony (Figure 13I).

Overall, *FLO11* gene directed two-dimensional expansion conveyed a competitive advantage in head-to-head competition with *flo11* Δ . The widening of *FLO11* sectors along the radius, and the envelopment of the outside rim of *flo11* Δ cells by *FLO11* cells indicated that *FLO11* cells robustly out-competed *flo11* Δ cells during colony expansion (Figure 16). The result was consistent among three different replicates (Figure 13, 17, 18).

4.3.2 Competition between *FLO11* and *flo11* Δ labeled by GFP or mCherry

We observed similar behavior with reverse labeling (Figure 13J, K). We further confirmed these observations with *FLO11* and *flo11* Δ strains labeled either by GFP or by mCherry.

When the mixtures of *FLO11* and *flo11* Δ cells competed on 1% agar and 1% galactose YPGal plates, the mCherry labeled *FLO11* sectors out-expanded the GFP labeled *flo11* Δ sectors, which were annihilated at the later time points (Figure 15A). The reverse labeling confirmed the competitive advantage of the GFP labeled *FLO11* colony at the later time point, despite the absence a significant advantage initially (Figure 15B). Therefore the above results of the out-expansion of *FLO11* against *flo11* Δ cells was consistent between different labeling methods (Figure 13, 15).

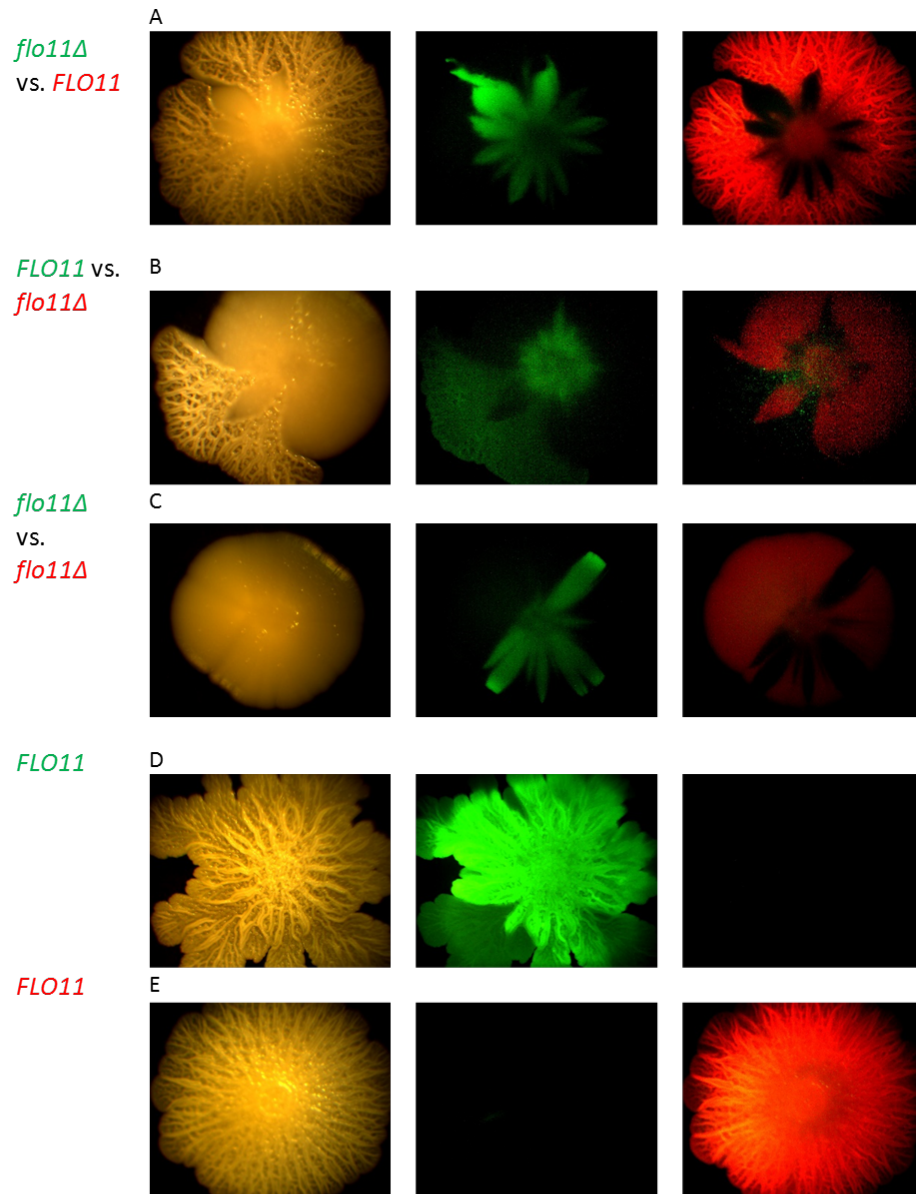


Figure 15. *FLO11* cells out-expanded *flo11Δ* cells during head-to-head competition. On 1% Agar and 1% galactose YPD plate, (A) The mixture of mCherry labeled *FLO11* out-expanded GFP labeled *flo11Δ* cells, which were annihilated eventually. (B) The reverse labeling revealed the out-expansion of GFP labeled *FLO11* sectors over mCherry labeled *flo11Δ* sectors from a later time point, despite of initial limitation of *FLO11* cells in the center of the mixed colony. (C) The mixture of *flo11Δ* colonies labeled with GFP or mCherry respectively showed minimal competition. (D) GFP labeled *FLO11* colony visualized by GFP fluorescence formed pattern on 1% agar surface with 0.5% galactose. (E) On 1% agar and 1% galactose surface, mCherry labeled *FLO11* colony was visualized by mCherry fluorescence. (A-E) Bright field, GFP and mCherry were shown on the left, middle and right columns respectively. The out-expansion of *FLO11* sectors over *flo11Δ* cells were consistent and independent of fluorescence labeling (Figure 13).

4.3.3 Ratio dependent competition between *FLO11* and *flo11*Δ.

Extending from the head-to head competition between *FLO11* and *flo11* Δ (Figure 13), we studied the dependence of competition on the mixing ratio between the two strains. Expanding on the 1.5% agar YPGal plates with 1.0% galactose, the mixture of *FLO11* colonies not only robustly preserved their pattern formation in the sectors, but also out-expanded the *flo11* Δ cells at all mixing ratios (1:3, 3:1, or 1:1) (Figure 16).

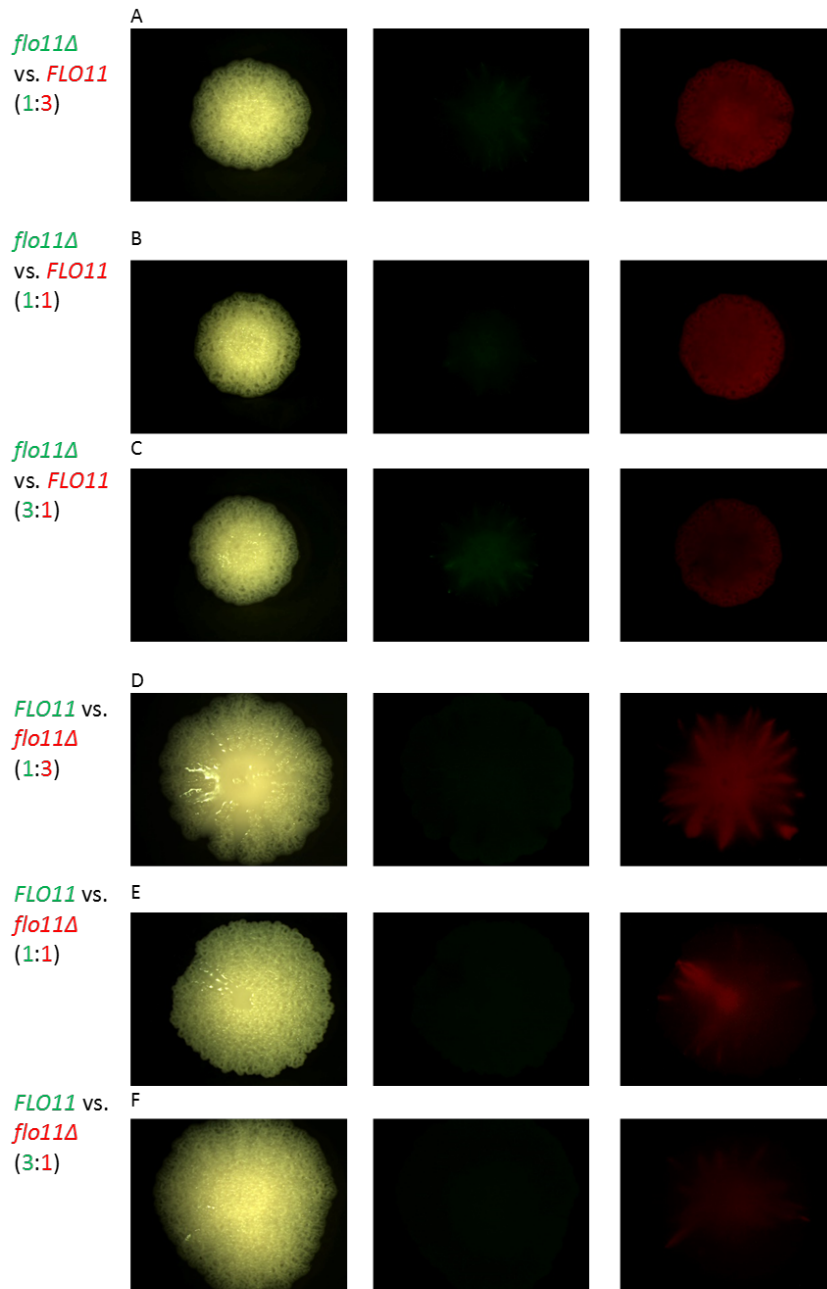


Figure 16. Ratio-dependent head-to-head competition between *FLO11* and *flo11Δ* cells. On 1.5% agar YPD plates with 1.0% galactose, (A) *flo11Δ* and *FLO11* labeled by GFP (middle panel) or mCherry (right panel) respectively were mixed at the ratio of 1:3 (A), 1:1 (B), 3:1 (C), and imaged at day 4. (A-C) Evident expansion advantage of mCherry labeled *FLO11* was observed initially at lower mutant ratio (A). The increase in the mutant ratio delayed the evident advantage of *FLO11* to later time, eventually led to the annihilation of *flo11Δ* cells (C). (D-F) Reverse labeling of *FLO11* and *flo11Δ* labeled by GFP (middle panel) or mCherry (right panel) respectively were mixed at the ratio of 1:3 (D), 1:1 (E), 3:1 (F), and imaged at day 7. *FLO11* exhibited expansion advantage robustly at all mixed ratios, and the strength of the advantage was ratio dependent.

The GFP labeled *flo11*Δ revealed a competitive disadvantage from the start time point and throughout the competition, in the sense that the *flo11*Δ (GFP labeled) sectors showed decreased sector angles along the expanding radius (Figure 16 A-C). The higher the mixing ratio to start with, the more rapid the decrease of the *flo11* Δ (GFP labeled) sectors (Figure 16). Over all mixing ratios tested, *FLO11* cells revealed robust competitive advantage over its mutant counterpart, as all *flo11* Δ sectors were annihilated by the *FLO11* (mCherry labeled) cells eventually (Figure 16A-C).

Varying the percentage of *flo11* Δ versus *FLO11* cells did not alter these results (Figure 16A-C). With a higher initial *FLO11* percentage, the competitive advantage of the *FLO11* colony over the *flo11* Δ colony was even more evident (Figure 16A-C).

The reverse labeling confirmed this advantage. *flo11* Δ (mCherry labeled) sectors showed sharply decreased sector angles as the mixed colonies expanded at all ratios tested (1:3, 1:1, 3:1), which indicated the competitive advantage of the *FLO11* sectors (Figure 16D-F). The competitive advantages conveyed by two-dimensional expansion of the *FLO11* sectors were ratio dependent (Figure 16).

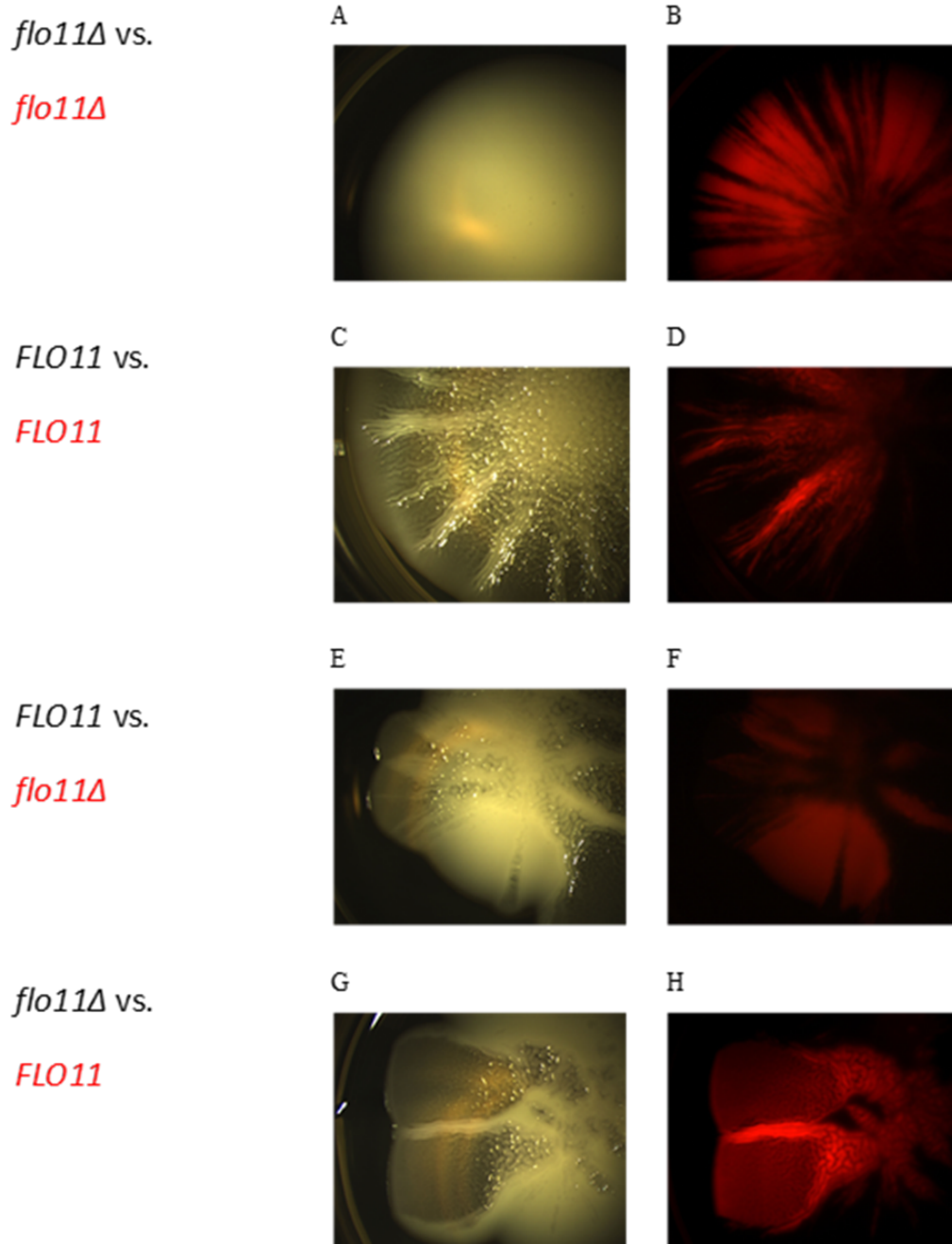


Figure 17. *FLO11* cells out-expanded *flo11Δ* cells during head-to-head competition. Replicate #2 of competing *FLO11* and *flo11Δ* cells on 1.0% agar, 0.5% galactose YPD plates. (A, B) Minimal competition between isogenic strains of unlabeled and mCherry labeled *flo11Δ* sectors. (C, D) Minimal competition was observed between unlabeled and mCherry labeled *FLO11* sectors. (E, F) unlabeled *FLO11* sector out-expanded mCherry labeled *flo11Δ* sectors with a conspicuous increase in the unlabeled sector angle. (G, H) Reverse labeling of (E, F). Bright field (A, C, E, G) and mCherry (B, D, F, H) were shown respectively. Contrast is adjusted in Adobe Photoshop CS for mCherry images.

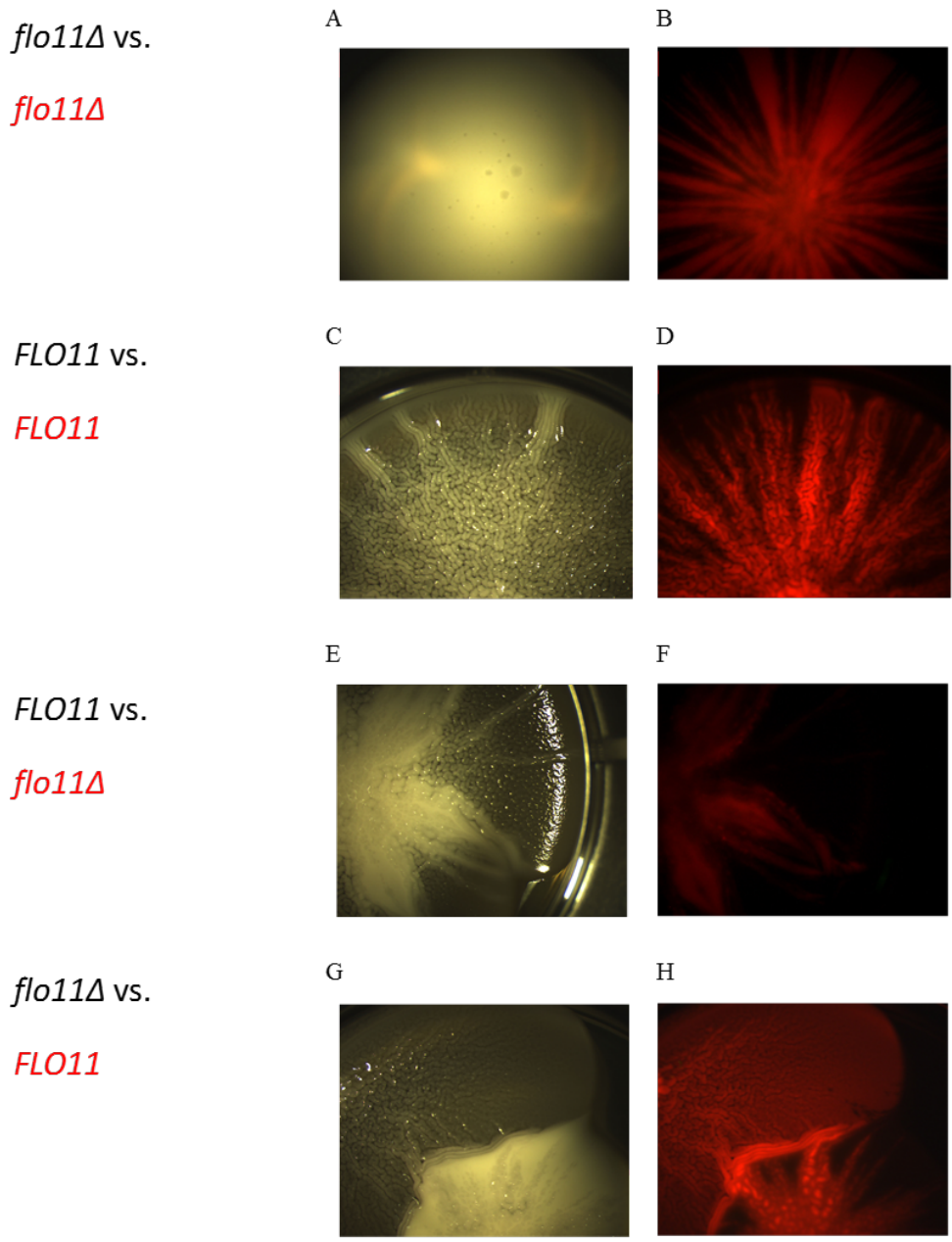


Figure 18. *FLO11* cells out-expanded *flo11Δ* cells during head-to-head competition. Replicate #3 of competing *FLO11* and *flo11Δ* cells on 1.0% agar, 0.5% galactose YPD plates. (A, B) Minimal competition between isogenic strains of unlabeled and mCherry labeled *flo11Δ* sectors. (C, D) Minimal competition was observed between unlabeled and mCherry labeled *FLO11* sectors. (E, F) unlabeled *FLO11* sector out-expanded mCherry labeled *flo11Δ* sectors with a conspicuous increase in the unlabeled sector angle. (G, H) Reverse labeling of (E, F). Bright field (A, C, E, G) and mCherry (B, D, F, H) were shown respectively. Contrast is adjusted in Adobe Photoshop CS for mCherry images.

4.4 Discussion

In this Chapter, I showed that the pattern forming *FLO11* cells were able to expand with advantage against *flo11* Δ cells during head-to-head competition (Figure 13-18). This advantage is likely to be conferred by the modes of growth of pattern forming colony that enable the *FLO11* cells to expand as a thin film in two dimensions, which facilitates the occupancy of larger area, compared to *flo11* Δ cells expanding in three dimensions.

Identifying the modes of expansion, the underlying mechanisms of patterning and the related features of pattern formation quantitatively facilitate the understanding on the biological function of the yeast biofilm. Without a physical sciences perspective, molecular and cell biological considerations will be insufficient to understand the intricacies of biofilm formation. Overall, this work is an example for how the adhesin mediated complex pattern formation could provide a competitive advantage spatially, which is not simply due to growth advantage in the environment with sufficient nutrients.

In this study, the results agreed among different labeling methods. However, the reverse labeling revealed a delay in exhibiting the advantage of pattern forming cells when *FLO11* cells were labeled by mCherry (Figure 13J, K). The burden of expressing this fluorescent protein was also observed in the controls (Figure 13D-G), where *FLO11*-mCherry cells revealed moderate disadvantage. Further quantitative analysis could be performed to normalize the competitive advantage conferred by *FLO11*, to take into account the cost from expressing the fluorescent markers.

Future experiments could be performed to include a variety of environmental stresses, such as pH, oxygen and nitrogen starvation, to further illustrate the benefit of generating patterns for survival in harsh environments (146, 202, 228, 237, 247, 257, 293-296). The change of the angle of the *FLO11* sectors along the radius could be quantitatively analyzed and systematically characterized, in order to compare the advantage of pattern forming *FLO11* cells on various environments.

Chapter 5

Discussion and future directions

The multicellular structure development by microbes has received a surge of interest over recent decades (297, 298). The diverse cooperative behaviors adopted by microbial cells have been utilized as model systems to study the complex structural and functional development of multicellular architecture (299-301). Genetic engineering, microscopic imaging and mathematical modeling of the spatial organization of distinct patterns in various bacteria reveal the importance of chemical gradients in shaping the self-organization of complex patterns through quorum sensing (302-304), long range inhibition and short range activation (305), and chemotaxis (306). However, it remains unclear how the physicochemical properties contribute to the distinct biofilm colony expansion in response to various nutrients levels, and trigger the emergence of complex patterns in eukaryotes.

Therefore, I investigated how the hierarchical wrinkling mediated by the physical property of the biofilm and agar substrate triggered pattern formation in yeast. This dissertation further developed quantitative methods to systematically characterize the biofilm expansion and identified the wavelengths of the patterns, followed by mathematical modeling in combination with microscopic imaging methods that uncovered the underlying unifying mechanisms for distinct colony expansion and complex pattern formation (Figure 19).

5.1 Distinct colony expansion conveyed by Flo11p

Previous studies identified that Flo11p drives rapid colony expansion on semi-solid surfaces within a short time course (146, 186, 307). To comprehensively understand how the traits of yeast colony expansion change on various environmental conditions, I extended the study to a range of glucose concentrations in combination with various agar densities in an around 60-day time course. I observed rapid colony expansion with high irregularity formed at the colony rim directed by Flo11p, in comparison to small, circular and smooth *flo11Δ* colonies at all conditions tested (Figure 2-4). The above traits followed similar trends consistently on glucose and galactose, indicating the robustness of colony expansion independent of sugar source.

The quantitative analysis revealed distinct colony expansion curves, depending on different sugar concentrations, as the convexity of the expansion curve increased with glucose concentration. Reynolds et al previously reported a spatial distribution of glucose along the radius of the colony with its maximum at the colony rim (146). The microscopic imaging on colony expansion further suggested that there could be a differential modes of growth between the center and the edge of the colony during expansion. I used a mathematical model that distinguished the growth in the center and linear growth at the edge of the colony to qualitatively reproduce the colony expansion curve with increase in convexity in response to higher glucose concentration. The result indicated that the differential modes of growth between the center and the edge of the colony in response to the gradient of nutrients along the colony expansion explains the

distinct colony expansion curves observed experimentally (Figure 6). Future versions of the mathematical model need to incorporate the spatial effects of *FLO11* on colony expansion to distinguish the two-dimensional and three-dimensional expansion in the presence or absence of *FLO11* respectively.

Future experiment and analysis are needed to study the effect of environments, such as glucose and galactose (146) that influence the colony morphology, colony expansion rate and irregularity, in a broad spectrum of conditions, including anaerobic environment, various pH value and aromatic alcohols, to quantify the association between environmental cues and multicellular behaviors .

The anaerobic environment is closely associated with multicellular structural development from bacteria to tumors. *P. aeruginosa* undergoes morphological changes including wrinkling in order to maintain global redox homeostasis (148). Angiogenesis is adopted by tumors to increase oxygen circulation during hypoxia (308). Under anaerobic environment, I found that the *S. cerevisiae* colony exhibit neither fast colony expansion nor complex and organized patterns in comparison to the colony with access to oxygen. It could be further investigated whether a minimal oxygen level or particular media are required to maintain basic features of colony expansion, such as colony area, irregular rim and patterning, by using a gradient of oxygen concentration (mixture of oxygen and nitrogen) and various media.

Similar to glucose gradients within the colony, there is also a gradient of pH level observed along the radius of the colony (146). In a previous report, high pH values

disturb adhesion over the entire colony and direct a more circular colony rim (146). Future experiments could be done to quantitatively analyze the change of rim irregularity in response to various pH concentrations.

Aromatic acids, positively auto-regulating their own expression through transcription factor Aro80p, are also found to be positive regulators for *FLO11* driven pattern formation (245). Future experiments on finding the inhibitor of aromatic acid synthesis in *S. cerevisiae*, which in turn could be activated by aromatic acid, will provide evidence for the long-range inhibition and short-range activation theory for pattern formation (309-311).

5.2 Hierarchical wrinkling triggers pattern formation in *Flo11* colony

The colony expansion mediated by adhesin *FLO11* enables the close attachment of the biofilm to the agar surface by squeezing cells in two dimensions. The constraints in dimensionality during colony expansion lead to rapid colony expansion with complex pattern development (Figure 19).

The pattern development is composed of small primary and large secondary wrinkles extending from the center to the edge of the colony. The wavelength of primary and secondary wrinkles remain constant, kept consistent through the initiation of a new secondary wrinkle in the middle of two secondary wrinkles or branching out from a previous secondary wrinkle as the colony expands radially. To reveal the underlying mechanism for pattern formation, I utilized the wavelengths as the marker for the

pattern. The wavelength of the secondary wrinkle is inversely correlated with the density of agar, in the absence of a clear dependence on glucose concentration, which suggests a correlation between the physical property of the colony and the organized surface pattern (Figure 9).

Similar patterns are observed in non-biological systems, where elastic thin skin generates wrinkles at several length scales on top of a viscoelastic substrate in response to stress (Figure 1) (190, 191, 273, 274, 312). This dissertation demonstrated that similar to the non-biological system, the constraint in the dimensionality of yeast colony expansion generates patterns due to hierarchical wrinkling. More complicated than the non-biological system, this dissertation illustrated that the yeast biofilm may generate primary wrinkle through the interaction between top cell layer and ECM substrate, both of which are thin layers, while the secondary wrinkle is generated through the cells with ECM expanding on top of the thick agar substrate. The understanding on the physical properties of the multi-layered sandwich system, which results in complex pattern formation, not only reveals novel mechanisms underlying biological patterning, but also provides valuable tools to study complex multicellular structure development. Further experiment and analysis, such as AFM, could also be used to measure mechanical strains accumulation and the initiation of the wrinkling pattern during biofilm development to further elucidate the critical role of physical properties in generating patterns. To assess the effect of adherence on wrinkling pattern formation in response to mechanical stress accumulation, future experiments

could focus on how the change of the adherence between cell and agar surfaces, as well as the alteration of the viscoelastic properties of the substrate could influence the wrinkle formation.

5.3 *FLO11* directed two-dimensional expansion confers competitive advantage during head-to-head competition

This dissertation illustrated that two-dimensional growth conveys competitive advantage during colony expansion, independent of labeling methods (Figure 19). The higher ratio of *FLO11* and *flo11* Δ cells with different color labels in the initial mixture confers more apparent competitive advantage (Figure 13-18). The absence of growth difference between *FLO11* and *flo11* Δ cells in liquid culture suggests that the spatial limitation of nutrient favors the cells that adhere to the surface and expand two-dimensionally to confer rapid expansion (Figure 5, 13).

In order to quantitatively define the competitive advantage during head-to-head competition, further computational analysis could be done to quantify the change of the sector angle along the radius normalized by the minimal competitive advantage (or disadvantage) between isogenic strains. We observed in this study that the *FLO11* sectors exhibited a delay in showing the competitive advantage when the strain was labeled with mCherry compared to non-labeled strain. Future experiments and quantitative analysis could be implemented to reveal whether the initial absence of advantage is due to the initial suppression on *FLO11* expression and pattern formation

before certain time point by RT-PCR. Linear inoculation instead of radial expansion could be done to reveal whether there is a threshold of expanding domain area for the competitive advantage to occur.

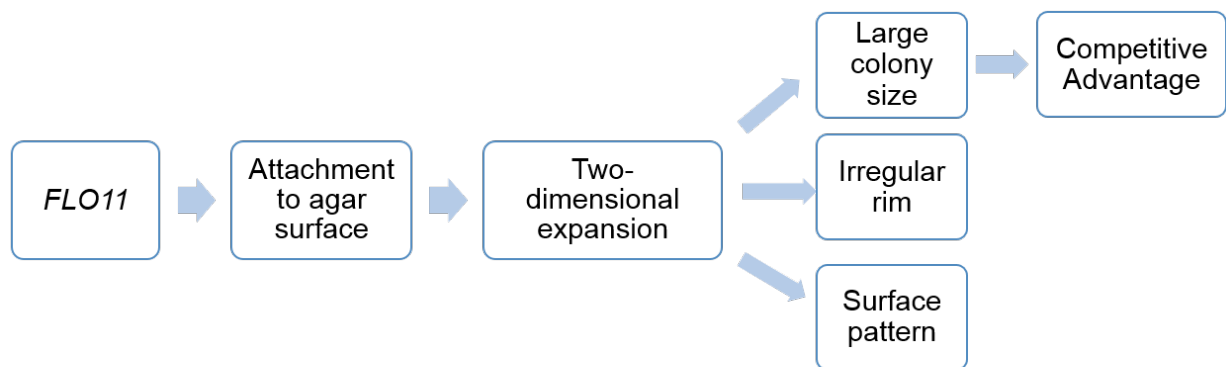


Figure 19. Summary. *FLO11* directed two-dimensional colony expansion triggered salient features.

Previous reports indicated that heterogeneously structured pattern formation conveys other functional benefits to the biofilm. The organized secondary wrinkles in *B. subtilis* increase the permeability locally to facilitate the nutrient transportation along the colony (10). Therefore, genome-wide high-throughput analysis using microarray or whole genome sequencing on the expression pattern between the spatially differentiated secondary wrinkles region and the interim region between secondary wrinkles might reveal whether *FLO11* shares similar spatial expression pattern with other functional genes related to osmolality, such as the HOG pathway, environmental signaling, such as the MAPK pathway, and drug resistance, such as the PDR5 multi-drug resistance pump (9, 247, 257, 294, 313-316).

Overall, this dissertation identified the dependence of adhesin mediated yeast distinct yeast colony expansion and the wavelengths of patterns on various glucose and agar concentrations through quantitative analysis. It also revealed the competitive advantage of *FLO11* directed two-dimensional expansion (Figure 19). The ESVS model that fitted well the experimental data suggested that the pattern is triggered through hierarchical wrinkling. The mathematical and physical models developed in this dissertation could serve as potential tools for understanding the heterogeneous modes of growth and wrinkling pattern in other microbes in response to physical stresses during complex multicellular structure development.

Reference

1. Costerton, J. W., G. G. Geesey, and K. J. Cheng. 1978. How bacteria stick. *Sci Am* 238(1): 86-95.
2. O'Toole, G., H. B. Kaplan, and R. Kolter. 2000. Biofilm formation as microbial development. *Annu Rev Microbiol* 54:49-79.
3. Serra, D. O., and R. Hengge. 2014. Stress responses go 3D - the spatial order of physiological differentiation in bacterial macrocolony biofilms. *Environ Microbiol*.
4. Costerton, J. W., K. J. Cheng, G. G. Geesey, T. I. Ladd, J. C. Nickel, M. Dasgupta, and T. J. Marrie. 1987. Bacterial biofilms in nature and disease. *Annu Rev Microbiol* 41:435-464.
5. Costerton, J. W., Z. Lewandowski, D. E. Caldwell, D. R. Korber, and H. M. Lappin-Scott. 1995. Microbial biofilms. *Annu Rev Microbiol* 49:711-745.
6. Costerton, J. W. 1995. Overview of microbial biofilms. *J Ind Microbiol* 15:137-140.
7. Lawrence, J. R., D. R. Korber, B. D. Hoyle, J. W. Costerton, and D. E. Caldwell. 1991. Optical sectioning of microbial biofilms. *J Bacteriol* 173(20): 6558-6567.
8. Gloag, E. S., M. A. Javed, H. Wang, M. L. Gee, S. A. Wade, L. Turnbull, and C. B. Whitchurch. 2013. Stigmergy: A key driver of self-organization in bacterial biofilms. *Commun Integr Biol* 6:e27331.
9. Vachova, L., V. Stovicek, O. Hlavacek, O. Chernyavskiy, L. Stepanek, L. Kubinova, and Z. Palkova. 2011. Flo11p, drug efflux pumps, and the extracellular matrix cooperate to form biofilm yeast colonies. *J Cell Biol* 194:679-687.
10. Wilking, J. N., V. Zaburdaev, M. De Volder, R. Losick, M. P. Brenner, and D. A. Weitz. 2013. Liquid transport facilitated by channels in *Bacillus subtilis* biofilms. *Proc Natl Acad Sci U S A* 110(3): 848-852.
11. Asally, M., M. Kittisopikul, P. Rue, Y. Du, Z. Hu, T. Cagatay, A. B. Robinson, H. Lu, J. Garcia-Ojalvo, and G. M. Suel. 2012. Localized cell death focuses mechanical forces during 3D patterning in a biofilm. *Proc Natl Acad Sci U S A* 109(46): 18891-18896.
12. Van Houdt, R., and C. W. Michiels. 2010. Biofilm formation and the food industry, a focus on the bacterial outer surface. *J Appl Microbiol* 109:1117-1131.
13. Walker, J. T., D. J. Bradshaw, A. M. Bennett, M. R. Fulford, M. V. Martin, and P. D. Marsh. 2000. Microbial biofilm formation and contamination of dental-unit water systems in general dental practice. *Appl Environ Microbiol* 66(8): 3363-3367.
14. Characklis, W. G., and D. B. I. B. James. 2009. Bioengineering Report. Fouling biofilm development: a process analysis. *Biotechnol Bioeng.*, Vol. XXIII, Pp. 1923-60 (1981). *Biotechnol Bioeng* 102:309, 310-347.
15. Marsh, P. D. 2005. Dental plaque: biological significance of a biofilm and community life-style. *J Clin Periodontol* 32 Suppl 6:7-15.
16. Wang, H., S. Masters, M. A. Edwards, J. O. Falkinham, 3rd, and A. Pruden. 2014. Effect of disinfectant, water age, and pipe materials on bacterial and eukaryotic community structure in drinking water biofilm. *Environ Sci Technol* 48(3): 1426-1435.
17. Tan, S. Y., S. C. Chew, S. Y. Tan, M. Givskov, and L. Yang. 2014. Emerging frontiers in

- detection and control of bacterial biofilms. *Curr Opin Biotechnol* 26C: 1-6.
18. Minandri, F., C. Bonchi, E. Frangipani, F. Imperi, and P. Visca. 2014. Promises and failures of gallium as an antibacterial agent. *Future Microbiol* 9: 379-397.
 19. Zhou, H., M. D. Weir, J. M. Antonucci, G. E. Schumacher, X. D. Zhou, and H. H. Xu. 2014. Evaluation of three-dimensional biofilms on antibacterial bonding agents containing novel quaternary ammonium methacrylates. *Int J Oral Sci*.
 20. Zheng, C. Y., J. Pan, Z. H. Wang, and Y. Wang. 2014. Effects of hydrogen peroxide-containing bleaching on the growth of *Streptococcus mutans* biofilm on enamel disc surface. *Beijing Da Xue Xue Bao* 46:30-34.
 21. Buswell, C. M., Y. M. Herlihy, L. M. Lawrence, J. T. McGuiggan, P. D. Marsh, C. W. Keevil, and S. A. Leach. 1998. Extended survival and persistence of *Campylobacter* spp. in water and aquatic biofilms and their detection by immunofluorescent-antibody and -rRNA staining. *Appl Environ Microbiol* 64(2): 733-741.
 22. Castonguay, M. H., S. van der Schaaf, W. Koester, J. Krooneman, W. van der Meer, H. Harmsen, and P. Landini. 2006. Biofilm formation by *Escherichia coli* is stimulated by synergistic interactions and co-adhesion mechanisms with adherence-proficient bacteria. *Res Microbiol* 157(5): 471-478.
 23. Silhan, J., C. B. Corfitzen, and H. J. Albrechtsen. 2006. Effect of temperature and pipe material on biofilm formation and survival of *Escherichia coli* in used drinking water pipes: a laboratory-based study. *Water Sci Technol* 54(3): 49-56.
 24. Kumpel, E., and K. L. Nelson. 2014. Mechanisms affecting water quality in an intermittent piped water supply. *Environ Sci Technol* 48(5): 2766-2775.
 25. Wang, J. J., X. Liu, T. W. Ng, J. W. Xiao, A. T. Chow, and P. K. Wong. 2013. Disinfection byproduct formation from chlorination of pure bacterial cells and pipeline biofilms. *Water Res* 47(8): 2701-2709.
 26. Pachepsky, Y., J. Morrow, A. Guber, D. Shelton, R. Rowland, and G. Davies. 2012. Effect of biofilm in irrigation pipes on microbial quality of irrigation water. *Lett Appl Microbiol* 54(3): 217-224.
 27. Abreu Acosta, N., L. E. Rodriguez Gomez, and M. Alvarez Diaz. 2012. Effect of oxygen injection in a reclaimed wastewater pipeline on the microbiological quality of water. *Environ Technol* 33(4-6): 497-505.
 28. Cernohorska, L., and P. Slavikova. 2009. Antibiotic resistance and biofilm formation in *Pseudomonas aeruginosa* strains isolated from patients with urinary tract infections. *Epidemiol Mikrobiol Imunol* 58(4): 154-157.
 29. Langmark, J., M. V. Storey, N. J. Ashbolt, and T. A. Stenstrom. 2007. The effects of UV disinfection on distribution pipe biofilm growth and pathogen incidence within the greater Stockholm area, Sweden. *Water Res* 41(15): 3327-3336.
 30. Wingender, J., and H. C. Flemming. 2004. Contamination potential of drinking water distribution network biofilms. *Water Sci Technol* 49(11-12): 277-286.
 31. Hallam, N. B., J. R. West, C. F. Forster, and J. Simms. 2001. The potential for biofilm growth in water distribution systems. *Water Res* 35(17): 4063-4071.
 32. Banning, N., S. Toze, and B. J. Mee. 2003. Persistence of biofilm-associated *Escherichia coli*

- and *Pseudomonas aeruginosa* in groundwater and treated effluent in a laboratory model system. *Microbiology* 149(Pt 1): 47-55.
33. Guven, N., and F. Kaynak Onurdag. 2014. Investigation of antimicrobial and antibiofilm effects of some preservatives used in drugs, cosmetics and food products. *Mikrobiyol Bul* 48(1): 94-105.
 34. Szewzyk, U., R. Szewzyk, W. Manz, and K. H. Schleifer. 2000. Microbiological safety of drinking water. *Annu Rev Microbiol* 54: 81-127.
 35. Gomez-Alvarez, V. 2014. Biofilm-growing bacteria involved in the corrosion of concrete wastewater pipes: protocols for comparative metagenomic analyses. *Methods Mol Biol* 1147: 323-340.
 36. Wang, W., S. Chen, K. Bao, J. Gao, R. Zhang, Z. Zhang, and N. Sugiura. 2014. Enhanced removal of contaminant using the biological film, anoxic-anaerobic-aerobic and electro-coagulation process applied to high-load sewage treatment. *Environ Technol* 35(5-8): 833-840.
 37. Mohanakrishnan, J., M. V. Kofoed, J. Barr, Z. Yuan, A. Schramm, and R. L. Meyer. 2011. Dynamic microbial response of sulfidogenic wastewater biofilm to nitrate. *Appl Microbiol Biotechnol* 91:1647-1657.
 38. Mohanakrishnan, J., K. R. Sharma, R. L. Meyer, G. Hamilton, J. Keller, and Z. Yuan. 2009. Variation in biofilm structure and activity along the length of a rising main sewer. *Water Environ Res* 81:800-808.
 39. Mohanakrishnan, J., O. Gutierrez, K. R. Sharma, A. Guisasola, U. Werner, R. L. Meyer, J. Keller, and Z. Yuan. 2009. Impact of nitrate addition on biofilm properties and activities in rising main sewers. *Water Res* 43(17): 4225-4237.
 40. Jiang, F., D. H. Leung, S. Li, G. H. Chen, S. Okabe, and M. C. van Loosdrecht. 2009. A biofilm model for prediction of pollutant transformation in sewers. *Water Res* 43(13): 3187-3198.
 41. Hood, S. K., and E. A. Zottola. 1997. Adherence to stainless steel by foodborne microorganisms during growth in model food systems. *Int J Food Microbiol* 37:145-153.
 42. Niemira, B. A., G. Boyd, and J. Sites. 2014. Cold Plasma Rapid Decontamination of Food Contact Surfaces Contaminated with *Salmonella* Biofilms. *J Food Sci*.
 43. Fox, E. M., K. Solomon, J. E. Moore, P. G. Wall, and S. Fanning. 2014. Phylogenetic profile of in-house microflora in drains at a food production facility: comparisons of *Listeria*-positive and -negative containing bacterial populations, and its implications for biocontrol. *Appl Environ Microbiol*.
 44. Faille, C., T. Benezech, G. Midelet-Bourdin, Y. Lequette, M. Clarisse, G. Ronse, A. Ronse, and C. Slomianny. 2014. Sporulation of *Bacillus* spp. within biofilms: a potential source of contamination in food processing environments. *Food Microbiol* 40:64-74.
 45. Lee, S. H., B. L. Mangolin, J. L. Goncalves, D. V. Neeff, M. P. Silva, A. G. Cruz, and C. A. Oliveira. 2014. Biofilm-producing ability of *Staphylococcus aureus* isolates from Brazilian dairy farms. *J Dairy Sci* 97:1812-1816.
 46. Latorre, A. A., J. S. Van Kessel, J. S. Karns, M. J. Zurakowski, A. K. Pradhan, K. J. Boor, B. M. Jayarao, B. A. Houser, C. S. Daugherty, and Y. H. Schukken. 2010. Biofilm in milking equipment on a dairy farm as a potential source of bulk tank milk contamination with *Listeria monocytogenes*. *J Dairy Sci* 93:2792-2802.

47. Mafu, A. A., D. Roy, J. Goulet, L. Savoie, and R. Roy. 1990. Efficiency of sanitizing agents for destroying *Listeria monocytogenes* on contaminated surfaces. *J Dairy Sci* 73:3428-3432.
48. Tang, X., S. H. Flint, R. J. Bennett, J. D. Brooks, and R. H. Morton. 2009. Biofilm growth of individual and dual strains of *Klebsiella oxytoca* from the dairy industry on ultrafiltration membranes. *J Ind Microbiol Biotechnol* 36:1491-1497.
49. Lindsay, D., V. S. Brozel, J. F. Mostert, and A. von Holy. 2002. Differential efficacy of a chlorine dioxide-containing sanitizer against single species and binary biofilms of a dairy-associated *Bacillus cereus* and a *Pseudomonas fluorescens* isolate. *J Appl Microbiol* 92:352-361.
50. Austin, J. W., and G. Bergeron. 1995. Development of bacterial biofilms in dairy processing lines. *J Dairy Res* 62:509-519.
51. Somers, E. B., and A. C. Wong. 2004. Efficacy of two cleaning and sanitizing combinations on *Listeria monocytogenes* biofilms formed at low temperature on a variety of materials in the presence of ready-to-eat meat residue. *J Food Prot* 67:2218-2229.
52. Verraes, C., S. Van Boxtael, E. Van Meervenne, E. Van Coillie, P. Butaye, B. Catry, M. A. de Schaetzen, X. Van Huffel, H. Imberechts, K. Dierick, G. Daube, C. Saegerman, J. De Block, J. Dewulf, and L. Herman. 2013. Antimicrobial resistance in the food chain: a review. *Int J Environ Res Public Health* 10:2643-2669.
53. Abdallah, M., C. Benoliel, D. Drider, P. Dhulster, and N. E. Chihib. 2014. Biofilm formation and persistence on abiotic surfaces in the context of food and medical environments. *Arch Microbiol*.
54. Allan, J. T., Z. Yan, and J. L. Kornacki. 2004. Surface material, temperature, and soil effects on the survival of selected foodborne pathogens in the presence of condensate. *J Food Prot* 67:2666-2670.
55. Allan, J. T., Z. Yan, L. L. Genzlinger, and J. L. Kornacki. 2004. Temperature and biological soil effects on the survival of selected foodborne pathogens on a mortar surface. *J Food Prot* 67:2661-2665.
56. Norwood, D. E., and A. Gilmour. 1999. Adherence of *Listeria monocytogenes* strains to stainless steel coupons. *J Appl Microbiol* 86:576-582.
57. Manios, S. G., and P. N. Skandamis. 2014. Control of *Listeria monocytogenes* in the processing environment by understanding biofilm formation and resistance to sanitizers. *Methods Mol Biol* 1157: 251-261.
58. Rema, T., J. R. Lawrence, J. J. Dynes, A. P. Hitchcock, and D. R. Korber. 2014. Chlorhexidine-tolerance in *Delftia acidovorans* biofilms: microscopic and spectroscopic analyses. *Antimicrob Agents Chemother*.
59. Perez Ibarreche, M., P. Castellano, and G. Vignolo. 2014. Evaluation of anti-*Listeria* meat borne *Lactobacillus* for biofilm formation on selected abiotic surfaces. *Meat Sci* 96(1): 295-303.
60. De Oliveira, D. C., A. Fernandes Junior, R. Kaneno, M. G. Silva, J. P. Araujo Junior, N. C. Silva, and V. L. Rall. 2014. Ability of *Salmonella* spp. to produce biofilm is dependent on temperature and surface material. *Foodborne Pathog Dis* 11(6): 478-483.
61. Rosan, B., and R. J. Lamont. 2000. Dental plaque formation. *Microbes Infect* 2:1599-1607.
62. Ritz, H. L. 1967. Microbial population shifts in developing human dental plaque. *Arch Oral Biol* 12:1561-1568.
63. Xu, P., and J. Gunsolley. 2014. Application of metagenomics in understanding oral health and

- disease. *Virulence* 5:424-432.
64. Schlafer, S., M. K. Raarup, R. L. Meyer, D. S. Sutherland, I. Dige, J. R. Nyengaard, and B. Nyvad. 2011. pH landscapes in a novel five-species model of early dental biofilm. *PLoS One* 6(9): e25299.
 65. Sutherland, I. 2001. Biofilm exopolysaccharides: a strong and sticky framework. *Microbiology* 147:3-9.
 66. Jenkinson, H. F., and R. J. Lamont. 1997. Streptococcal adhesion and colonization. *Crit Rev Oral Biol Med* 8(2): 175-200.
 67. Kolenbrander, P. E., and J. London. 1993. Adhere today, here tomorrow: oral bacterial adherence. *J Bacteriol* 175(11): 3247-3252.
 68. Whittaker, C. J., C. M. Klier, and P. E. Kolenbrander. 1996. Mechanisms of adhesion by oral bacteria. *Annu Rev Microbiol* 50:513-552.
 69. Chalmers, N. I., R. J. Palmer, Jr., J. O. Cisar, and P. E. Kolenbrander. 2008. Characterization of a *Streptococcus* sp.-*Veillonella* sp. community micromanipulated from dental plaque. *J Bacteriol* 190(24): 8145-8154.
 70. Archibald, L. K., and R. P. Gaynes. 1997. Hospital-acquired infections in the United States. The importance of interhospital comparisons. *Infect Dis Clin North Am* 11:245-255.
 71. Fridkin, S. K., S. F. Welbel, and R. A. Weinstein. 1997. Magnitude and prevention of nosocomial infections in the intensive care unit. *Infect Dis Clin North Am* 11:479-496.
 72. Goldmann, D. A., and W. C. Huskins. 1997. Control of nosocomial antimicrobial-resistant bacteria: a strategic priority for hospitals worldwide. *Clin Infect Dis* 24 Suppl 1:S139-145.
 73. Huebner, J., G. B. Pier, J. N. Maslow, E. Muller, H. Shiro, M. Parent, A. Kropec, R. D. Arbeit, and D. A. Goldmann. 1994. Endemic nosocomial transmission of *Staphylococcus epidermidis* bacteremia isolates in a neonatal intensive care unit over 10 years. *J Infect Dis* 169(3): 526-531.
 74. Weber, D. J., D. Anderson, and W. A. Rutala. 2013. The role of the surface environment in healthcare-associated infections. *Curr Opin Infect Dis* 26:338-344.
 75. Wang, R., B. A. Khan, G. Y. Cheung, T. H. Bach, M. Jameson-Lee, K. F. Kong, S. Y. Queck, and M. Otto. 2011. *Staphylococcus epidermidis* surfactant peptides promote biofilm maturation and dissemination of biofilm-associated infection in mice. *J Clin Invest* 121(1): 238-248.
 76. Veri, A., and L. E. Cowen. 2014. Progress and prospects for targeting Hsp90 to treat fungal infections. *Parasitology* 141(9): 1127-1137.
 77. Bjarnsholt, T. 2013. The role of bacterial biofilms in chronic infections. *APMIS Suppl*:1-51.
 78. Khoury, A. E., K. Lam, B. Ellis, and J. W. Costerton. 1992. Prevention and control of bacterial infections associated with medical devices. *ASAIO J* 38(3): M174-178.
 79. Litzler, P. Y., L. Benard, N. Barbier-Frebourg, S. Vilain, T. Jouenne, E. Beucher, C. Bunel, J. F. Lemeland, and J. P. Bessou. 2007. Biofilm formation on pyrolytic carbon heart valves: influence of surface free energy, roughness, and bacterial species. *J Thorac Cardiovasc Surg* 134:1025-1032.
 80. Savage, V. J., I. Chopra, and A. J. O'Neill. 2013. Population diversification in *Staphylococcus aureus* biofilms may promote dissemination and persistence. *PLoS One* 8(4): e62513.
 81. Sriramulu, D. D., H. Lunsdorf, J. S. Lam, and U. Romling. 2005. Microcolony formation: a novel biofilm model of *Pseudomonas aeruginosa* for the cystic fibrosis lung. *J Med Microbiol* 54(Pt 7):

- 667-676.
82. Drenkard, E., and F. M. Ausubel. 2002. *Pseudomonas* biofilm formation and antibiotic resistance are linked to phenotypic variation. *Nature* 416:740-743.
 83. Foxman, B. 2002. Epidemiology of urinary tract infections: incidence, morbidity, and economic costs. *Am J Med* 113 Suppl 1A:5S-13S.
 84. Hooton, T. M., and W. E. Stamm. 1997. Diagnosis and treatment of uncomplicated urinary tract infection. *Infect Dis Clin North Am* 11:551-581.
 85. Manges, A. R., J. R. Johnson, B. Foxman, T. T. O'Bryan, K. E. Fullerton, and L. W. Riley. 2001. Widespread distribution of urinary tract infections caused by a multidrug-resistant *Escherichia coli* clonal group. *N Engl J Med* 345:1007-1013.
 86. Anderson, G. G., J. J. Palermo, J. D. Schilling, R. Roth, J. Heuser, and S. J. Hultgren. 2003. Intracellular bacterial biofilm-like pods in urinary tract infections. *Science* 301:105-107.
 87. Wang, J. F., Z. Q. Xiong, S. Y. Li, and Y. Wang. 2013. Enhancing isoprenoid production through systematically assembling and modulating efflux pumps in *Escherichia coli*. *Appl Microbiol Biotechnol* 97:8057-8067.
 88. Alekshun, M. N., and S. B. Levy. 1999. The *mar* regulon: multiple resistance to antibiotics and other toxic chemicals. *Trends Microbiol* 7(10): 410-413.
 89. Brooun, A., S. Liu, and K. Lewis. 2000. A dose-response study of antibiotic resistance in *Pseudomonas aeruginosa* biofilms. *Antimicrob Agents Chemother* 44(3): 640-646.
 90. Maira-Litran, T., D. G. Allison, and P. Gilbert. 2000. An evaluation of the potential of the multiple antibiotic resistance operon (*mar*) and the multidrug efflux pump *acrAB* to moderate resistance towards ciprofloxacin in *Escherichia coli* biofilms. *J Antimicrob Chemother* 45(6): 789-795.
 91. Maira-Litran, T., D. G. Allison, and P. Gilbert. 2000. Expression of the multiple antibiotic resistance operon (*mar*) during growth of *Escherichia coli* as a biofilm. *J Appl Microbiol* 88(2): 243-247.
 92. Stewart, P. S., and J. W. Costerton. 2001. Antibiotic resistance of bacteria in biofilms. *Lancet* 358:135-138.
 93. Ceri, H., M. E. Olson, C. Stremick, R. R. Read, D. Morck, and A. Buret. 1999. The Calgary Biofilm Device: new technology for rapid determination of antibiotic susceptibilities of bacterial biofilms. *J Clin Microbiol* 37(6): 1771-1776.
 94. Anderl, J. N., M. J. Franklin, and P. S. Stewart. 2000. Role of antibiotic penetration limitation in *Klebsiella pneumoniae* biofilm resistance to ampicillin and ciprofloxacin. *Antimicrob Agents Chemother* 44(7): 1818-1824.
 95. Zahller, J., and P. S. Stewart. 2002. Transmission electron microscopic study of antibiotic action on *Klebsiella pneumoniae* biofilm. *Antimicrob Agents Chemother* 46(8): 2679-2683.
 96. Kumon, H., K. Tomochika, T. Matunaga, M. Ogawa, and H. Ohmori. 1994. A sandwich cup method for the penetration assay of antimicrobial agents through *Pseudomonas* exopolysaccharides. *Microbiol Immunol* 38(8): 615-619.
 97. Shigeta, M., G. Tanaka, H. Komatsuzawa, M. Sugai, H. Suginaka, and T. Usui. 1997. Permeation of antimicrobial agents through *Pseudomonas aeruginosa* biofilms: a simple method. *Chemotherapy* 43(5): 340-345.
 98. Meers, P., M. Neville, V. Malinin, A. W. Scotto, G. Sardaryan, R. Kurumunda, C. Mackinson, G.

- James, S. Fisher, and W. R. Perkins. 2008. Biofilm penetration, triggered release and in vivo activity of inhaled liposomal amikacin in chronic *Pseudomonas aeruginosa* lung infections. *J Antimicrob Chemother* 61(4): 859-868.
99. Tseng, B. S., W. Zhang, J. J. Harrison, T. P. Quach, J. L. Song, J. Penterman, P. K. Singh, D. L. Chopp, A. I. Packman, and M. R. Parsek. 2013. The extracellular matrix protects *Pseudomonas aeruginosa* biofilms by limiting the penetration of tobramycin. *Environ Microbiol* 15(10): 2865-2878.
100. de Beer, D., P. Stoodley, F. Roe, and Z. Lewandowski. 1994. Effects of biofilm structures on oxygen distribution and mass transport. *Biotechnol Bioeng* 43(11): 1131-1138.
101. Walters, M. C., 3rd, F. Roe, A. Bugnicourt, M. J. Franklin, and P. S. Stewart. 2003. Contributions of antibiotic penetration, oxygen limitation, and low metabolic activity to tolerance of *Pseudomonas aeruginosa* biofilms to ciprofloxacin and tobramycin. *Antimicrob Agents Chemother* 47(1): 317-323.
102. Tack, K. J., and L. D. Sabath. 1985. Increased minimum inhibitory concentrations with anaerobiasis for tobramycin, gentamicin, and amikacin, compared to latamoxef, piperacillin, chloramphenicol, and clindamycin. *Chemotherapy* 31(3): 204-210.
103. Vroom, J. M., K. J. De Grauw, H. C. Gerritsen, D. J. Bradshaw, P. D. Marsh, G. K. Watson, J. J. Birmingham, and C. Allison. 1999. Depth penetration and detection of pH gradients in biofilms by two-photon excitation microscopy. *Appl Environ Microbiol* 65(8): 3502-3511.
104. Henry-Stanley, M., D. Hess, and C. Wells. 2014. Aminoglycoside inhibition of *Staphylococcus aureus* biofilm formation is nutrient dependent. *J Med Microbiol*.
105. Bogino, P. C., L. Oliva Mde, F. G. Sorroche, and W. Giordano. 2013. The role of bacterial biofilms and surface components in plant-bacterial associations. *Int J Mol Sci* 14(8): 15838-15859.
106. Van Acker, H., P. Van Dijck, and T. Coenye. 2014. Molecular mechanisms of antimicrobial tolerance and resistance in bacterial and fungal biofilms. *Trends Microbiol*.
107. Al-Ahmad, A., H. Ameen, K. Pelz, L. Karygianni, A. Wittmer, A. C. Anderson, B. Spitzmuller, and E. Hellwig. 2014. Antibiotic resistance and capacity for biofilm formation of different bacteria isolated from endodontic infections associated with root-filled teeth. *J Endod* 40(2): 223-230.
108. Nadell, C. D., J. B. Xavier, and K. R. Foster. 2009. The sociobiology of biofilms. *FEMS Microbiol Rev* 33(1): 206-224.
109. Stoodley, P., D. Debeer, and Z. Lewandowski. 1994. Liquid flow in biofilm systems. *Appl Environ Microbiol* 60(8): 2711-2716.
110. Stanley, N. R., and B. A. Lazazzera. 2004. Environmental signals and regulatory pathways that influence biofilm formation. *Mol Microbiol* 52(4): 917-924.
111. Palmer, R. J., Jr., and D. C. White. 1997. Developmental biology of biofilms: implications for treatment and control. *Trends Microbiol* 5(11): 435-440.
112. Periasamy, S., H. S. Joo, A. C. Duong, T. H. Bach, V. Y. Tan, S. S. Chatterjee, G. Y. Cheung, and M. Otto. 2012. How *Staphylococcus aureus* biofilms develop their characteristic structure. *Proc Natl Acad Sci U S A* 109(4): 1281-1286.
113. Flemming, H. C., and J. Wingender. 2010. The biofilm matrix. *Nat Rev Microbiol* 8(9): 623-633.
114. Watnick, P. I., and R. Kolter. 1999. Steps in the development of a *Vibrio cholerae* El Tor biofilm.

- Mol Microbiol 34(3): 586-595.
115. Venugopalan, V. P., M. Kuehn, M. Hausner, D. Springael, P. A. Wilderer, and S. Wuertz. 2005. Architecture of a nascent *Sphingomonas* sp. biofilm under varied hydrodynamic conditions. *Appl Environ Microbiol* 71(5): 2677-2686.
 116. Costerton, J. W., L. Montanaro, and C. R. Arciola. 2005. Biofilm in implant infections: its production and regulation. *Int J Artif Organs* 28(11): 1062-1068.
 117. Hall-Stoodley, L., and P. Stoodley. 2002. Developmental regulation of microbial biofilms. *Curr Opin Biotechnol* 13(3): 228-233.
 118. Donlan, R. M. 2002. Biofilms: microbial life on surfaces. *Emerg Infect Dis* 8(9): 881-890.
 119. Dworkin, M. 1996. Recent advances in the social and developmental biology of the myxobacteria. *Microbiol Rev* 60(1): 70-102.
 120. Hartzell, P. L., and P. Youderian. 1995. Genetics of gliding motility and development in *Myxococcus xanthus*. *Arch Microbiol* 164(5): 309-323.
 121. O'Toole, G. A., and R. Kolter. 1998. Flagellar and twitching motility are necessary for *Pseudomonas aeruginosa* biofilm development. *Mol Microbiol* 30(2): 295-304.
 122. Ramsey, M. M., and M. Whiteley. 2004. *Pseudomonas aeruginosa* attachment and biofilm development in dynamic environments. *Mol Microbiol* 53(4): 1075-1087.
 123. Bendinger, B., H. H. Rijnaarts, K. Altendorf, and A. J. Zehnder. 1993. Physicochemical cell surface and adhesive properties of coryneform bacteria related to the presence and chain length of mycolic acids. *Appl Environ Microbiol* 59(11): 3973-3977.
 124. Ng, M., S. B. Epstein, M. T. Callahan, B. O. Piotrowski, G. L. Simon, A. D. Roberts, J. F. Keiser, and J. B. Kaplan. 2014. Induction of MRSA Biofilm by Low-Dose beta-Lactam Antibiotics: Specificity, Prevalence and Dose-Response Effects. *Dose Response* 12(1): 152-161.
 125. Atshan, S. S., M. Nor Shamsudin, L. T. Lung, Z. Sekawi, C. Pei Pei, A. Karunanidhi, J. Jeevajothei Nathan, A. Mateg Ali, E. Ghaznavi-Rad, S. A. Abduljaleel, and R. Awang Hamat. 2013. Genotypically different clones of *Staphylococcus aureus* are diverse in the antimicrobial susceptibility patterns and biofilm formations. *Biomed Res Int* 2013:515712.
 126. Brazil, G. M., L. Kenefick, M. Callanan, A. Haro, V. de Lorenzo, D. N. Dowling, and F. O'Gara. 1995. Construction of a rhizosphere pseudomonad with potential to degrade polychlorinated biphenyls and detection of bph gene expression in the rhizosphere. *Appl Environ Microbiol* 61(5): 1946-1952.
 127. Gross, M. J., and B. E. Logan. 1995. Influence of different chemical treatments on transport of *Alcaligenes paradoxus* in porous media. *Appl Environ Microbiol* 61(5): 1750-1756.
 128. Moller, S., C. Sternberg, J. B. Andersen, B. B. Christensen, J. L. Ramos, M. Givskov, and S. Molin. 1998. In situ gene expression in mixed-culture biofilms: evidence of metabolic interactions between community members. *Appl Environ Microbiol* 64(2): 721-732.
 129. Sarra, M., C. Casas, M. Poch, and F. Godia. 1999. A simple structured model for continuous production of a hybrid antibiotic by *Streptomyces lividans* pellets in a fluidized-bed bioreactor. *Appl Biochem Biotechnol* 80:39-50.
 130. Wolfaardt, G. M., J. R. Lawrence, R. D. Robarts, S. J. Caldwell, and D. E. Caldwell. 1994. Multicellular organization in a degradative biofilm community. *Appl Environ Microbiol* 60(2): 434-446.

131. Zobell, C. E. 1943. The Effect of Solid Surfaces upon Bacterial Activity. *J Bacteriol* 46(1): 39-56.
132. Zhu, Y., E. C. Weiss, M. Otto, P. D. Fey, M. S. Smeltzer, and G. A. Somerville. 2007. *Staphylococcus aureus* biofilm metabolism and the influence of arginine on polysaccharide intercellular adhesin synthesis, biofilm formation, and pathogenesis. *Infect Immun* 75(9): 4219-4226.
133. Hausner, M., and S. Wuertz. 1999. High rates of conjugation in bacterial biofilms as determined by quantitative in situ analysis. *Appl Environ Microbiol* 65(8): 3710-3713.
134. Marks, L. R., R. M. Reddinger, and A. P. Hakansson. 2012. High levels of genetic recombination during nasopharyngeal carriage and biofilm formation in *Streptococcus pneumoniae*. *MBio* 3(5).
135. Costerton, J. W., P. S. Stewart, and E. P. Greenberg. 1999. Bacterial biofilms: a common cause of persistent infections. *Science* 284(5418): 1318-1322.
136. Anwar, H., M. Dasgupta, K. Lam, and J. W. Costerton. 1989. Tobramycin resistance of mucoid *Pseudomonas aeruginosa* biofilm grown under iron limitation. *J Antimicrob Chemother* 24(5): 647-655.
137. Anwar, H., J. L. Strap, and J. W. Costerton. 1992. Establishment of aging biofilms: possible mechanism of bacterial resistance to antimicrobial therapy. *Antimicrob Agents Chemother* 36(7): 1347-1351.
138. Anwar, H., J. L. Strap, and J. W. Costerton. 1992. Susceptibility of biofilm cells of *Pseudomonas aeruginosa* to bactericidal actions of whole blood and serum. *FEMS Microbiol Lett* 71(3): 235-241.
139. Hoyle, B. D., and J. W. Costerton. 1991. Bacterial resistance to antibiotics: the role of biofilms. *Prog Drug Res* 37:91-105.
140. Nickel, J. C., I. Ruseska, J. B. Wright, and J. W. Costerton. 1985. Tobramycin resistance of *Pseudomonas aeruginosa* cells growing as a biofilm on urinary catheter material. *Prog Drug Res* 37: 91-105.
141. Wu, Q., Q. Wang, K. G. Taylor, and R. J. Doyle. 1995. Subinhibitory concentrations of antibiotics affect cell surface properties of *Streptococcus sobrinus*. *J Bacteriol* 177(5): 1399-1401.
142. Vergeres, P., and J. Blaser. 1992. Amikacin, ceftazidime, and flucloxacillin against suspended and adherent *Pseudomonas aeruginosa* and *Staphylococcus epidermidis* in an in vitro model of infection. *J Infect Dis* 165(2): 281-289.
143. Singh, P. K., M. R. Parsek, E. P. Greenberg, and M. J. Welsh. 2002. A component of innate immunity prevents bacterial biofilm development. *Nature* 417:552-555.
144. Hoffmann, N., B. Lee, M. Hentzer, T. B. Rasmussen, Z. Song, H. K. Johansen, M. Givskov, and N. Hoiby. 2007. Azithromycin blocks quorum sensing and alginate polymer formation and increases the sensitivity to serum and stationary-growth-phase killing of *Pseudomonas aeruginosa* and attenuates chronic *P. aeruginosa* lung infection in *Cftr(-/-)* mice. *Antimicrob Agents Chemother* 51(10): 3677-3687.
145. Wei, Q., and L. Z. Ma. 2013. Biofilm matrix and its regulation in *Pseudomonas aeruginosa*. *Int J Mol Sci* 14(10): 20983-21005.
146. Reynolds, T. B., A. Jansen, X. Peng, and G. R. Fink. 2008. Mat formation in *Saccharomyces cerevisiae* requires nutrient and pH gradients. *Eukaryot Cell* 7(1): 122-130.
147. Uhlich, G. A., C. Y. Chen, B. J. Cottrell, and L. H. Nguyen. 2014. Growth media and temperature

- effects on biofilm formation by serotype O157:H7 and non-O157 Shiga toxin-producing *Escherichia coli*. *FEMS Microbiol Lett*.
148. Dietrich, L. E., C. Okegbe, A. Price-Whelan, H. Sakhtah, R. C. Hunter, and D. K. Newman. 2013. Bacterial community morphogenesis is intimately linked to the intracellular redox state. *J Bacteriol* 195(7): 1371-1380.
 149. Wong, K. K., K. L. Suen, and H. S. Kwan. 1989. Transcription of *pfl* is regulated by anaerobiosis, catabolite repression, pyruvate, and *oxrA*: *pfl*::*Mu dA* operon fusions of *Salmonella typhimurium*. *J Bacteriol* 171(9): 4900-4905.
 150. Rodel, W., W. Plaga, R. Frank, and J. Knappe. 1988. Primary structures of *Escherichia coli* pyruvate formate-lyase and pyruvate-formate-lyase-activating enzyme deduced from the DNA nucleotide sequences. *Eur J Biochem* 177(1): 153-158.
 151. Fang, W., J. Hu, and S. L. Ong. 2010. Effects of phosphorus on biofilm disinfections in model drinking water distribution systems. *J Water Health* 8(3): 446-454.
 152. Wrangstadh, M., U. Szewzyk, J. Ostling, and S. Kjelleberg. 1990. Starvation-specific formation of a peripheral exopolysaccharide by a marine *Pseudomonas* sp., strain S9. *Appl Environ Microbiol* 56(7): 2065-2072.
 153. Myszka, K., and K. Czaczyk. 2009. Characterization of adhesive exopolysaccharide (EPS) produced by *Pseudomonas aeruginosa* under starvation conditions. *Curr Microbiol* 58(6): 541-546.
 154. Finkel, S. E., and R. Kolter. 2001. DNA as a nutrient: novel role for bacterial competence gene homologs. *J Bacteriol* 183(21): 6288-6293.
 155. Davies, D. G., and G. G. Geesey. 1995. Regulation of the alginate biosynthesis gene *algC* in *Pseudomonas aeruginosa* during biofilm development in continuous culture. *Appl Environ Microbiol* 61(3): 860-867.
 156. Allan, V. J., M. E. Callow, L. E. Macaskie, and M. Paterson-Beedle. 2002. Effect of nutrient limitation on biofilm formation and phosphatase activity of a *Citrobacter* sp. *Microbiology* 148(Pt 1): 277-288.
 157. Prigent-Combaret, C., O. Vidal, C. Dorel, and P. Lejeune. 1999. Abiotic surface sensing and biofilm-dependent regulation of gene expression in *Escherichia coli*. *J Bacteriol* 181(19): 5993-6002.
 158. Kapfhammer, D., E. Karatan, K. J. Pflughoeft, and P. I. Watnick. 2005. Role for glycine betaine transport in *Vibrio cholerae* osmoadaptation and biofilm formation within microbial communities. *Appl Environ Microbiol* 71(7): 3840-3847.
 159. Shi, W., C. Li, C. J. Louise, and J. Adler. 1993. Mechanism of adverse conditions causing lack of flagella in *Escherichia coli*. *J Bacteriol* 175(8): 2236-2240.
 160. Gowrishankar, J. 1985. Identification of osmoresponsive genes in *Escherichia coli*: evidence for participation of potassium and proline transport systems in osmoregulation. *J Bacteriol* 164(1): 434-445.
 161. Sarma, V., and P. Reeves. 1977. Genetic locus (*ompB*) affecting a major outer-membrane protein in *Escherichia coli* K-12. *J Bacteriol* 132(1): 23-27.
 162. Kreft, J. U., and J. W. Wimpenny. 2001. Effect of EPS on biofilm structure and function as revealed by an individual-based model of biofilm growth. *Water Sci Technol* 43(6): 135-141.

163. Hu, W., L. Li, S. Sharma, J. Wang, I. McHardy, R. Lux, Z. Yang, X. He, J. K. Gimzewski, Y. Li, and W. Shi. 2012. DNA builds and strengthens the extracellular matrix in *Myxococcus xanthus* biofilms by interacting with exopolysaccharides. *PLoS One* 7(12): e51905.
164. Mayer, C., R. Moritz, C. Kirschner, W. Borchard, R. Maibaum, J. Wingender, and H. C. Flemming. 1999. The role of intermolecular interactions: studies on model systems for bacterial biofilms. *Int J Biol Macromol* 26:3-16.
165. Allison, D. G. 2003. The biofilm matrix. *Biofouling* 19(2): 139-150.
166. Tielen, P., F. Rosenau, S. Wilhelm, K. E. Jaeger, H. C. Flemming, and J. Wingender. 2010. Extracellular enzymes affect biofilm formation of mucoid *Pseudomonas aeruginosa*. *Microbiology* 156(Pt 7): 2239-2252.
167. Gomez-Gomez, J. M., and R. Amils. 2014. Crowning: a novel *Escherichia coli* colonizing behaviour generating a self-organized corona. *BMC Res Notes* 7: 108.
168. Stoodley, P., I. Dodds, J. D. Boyle, and H. M. Lappin-Scott. 1998. Influence of hydrodynamics and nutrients on biofilm structure. *J Appl Microbiol* 85 Suppl 1:19S-28S.
169. Peterson, B. W., H. J. Busscher, P. K. Sharma, and H. C. van der Mei. 2014. Visualization of Microbiological Processes Underlying Stress Relaxation in *Pseudomonas aeruginosa* Biofilms. *Microsc Microanal*:1-4.
170. Fletcher, M., and G. I. Loeb. 1979. Influence of substratum characteristics on the attachment of a marine pseudomonad to solid surfaces. *Appl Environ Microbiol* 37(1): 67-72.
171. Guo, K., S. Freguia, P. G. Dennis, X. Chen, B. C. Donose, J. Keller, J. J. Gooding, and K. Rabaey. 2013. Effects of surface charge and hydrophobicity on anodic biofilm formation, community composition, and current generation in bioelectrochemical systems. *Environ Sci Technol* 47(13): 7563-7570.
172. Chao, Y., F. Guo, H. H. Fang, and T. Zhang. 2014. Hydrophobicity of diverse bacterial populations in activated sludge and biofilm revealed by microbial adhesion to hydrocarbons assay and high-throughput sequencing. *Colloids Surf B Biointerfaces* 114: 379-385.
173. Cerca, N., G. B. Pier, M. Vilanova, R. Oliveira, and J. Azeredo. 2005. Quantitative analysis of adhesion and biofilm formation on hydrophilic and hydrophobic surfaces of clinical isolates of *Staphylococcus epidermidis*. *Res Microbiol* 156:506-514.
174. Rossoni, R. D., J. O. Barbosa, F. E. de Oliveira, L. D. de Oliveira, A. O. Jorge, and J. C. Junqueira. 2014. Biofilms of *Candida albicans* serotypes A and B differ in their sensitivity to photodynamic therapy. *Lasers Med Sci*.
175. Rautela, R., A. K. Singh, A. Shukla, and S. S. Cameotra. 2014. Lipopeptides from *Bacillus* strain AR2 inhibits biofilm formation by *Candida albicans*. *Antonie Van Leeuwenhoek* 105(5): 809-821.
176. Fazli, M., H. Almlad, M. L. Rybtke, M. Givskov, L. Eberl, and T. Tolker-Nielsen. 2014. Regulation of biofilm formation in *Pseudomonas* and *Burkholderia* species. *Environ Microbiol*.
177. Pamp, S. J., and T. Tolker-Nielsen. 2007. Multiple roles of biosurfactants in structural biofilm development by *Pseudomonas aeruginosa*. *J Bacteriol* 189(6): 2531-2539.
178. Al-Tahhan, R. A., T. R. Sandrin, A. A. Bodour, and R. M. Maier. 2000. Rhamnolipid-induced removal of lipopolysaccharide from *Pseudomonas aeruginosa*: effect on cell surface properties and interaction with hydrophobic substrates. *Appl Environ Microbiol* 66(8): 3262-3268.
179. Zhang, Y., and R. M. Miller. 1994. Effect of a *Pseudomonas* rhamnolipid biosurfactant on cell

- hydrophobicity and biodegradation of octadecane. *Appl Environ Microbiol* 60(6): 2101-2106.
180. Angelini, T. E., M. Roper, R. Kolter, D. A. Weitz, and M. P. Brenner. 2009. *Bacillus subtilis* spreads by surfing on waves of surfactant. *Proc Natl Acad Sci U S A* 106(43): 18109-18113.
181. Ben-Jacob, E., O. Schochet, A. Tenenbaum, I. Cohen, A. Czirok, and T. Vicsek. 1994. Generic modelling of cooperative growth patterns in bacterial colonies. *Nature* 368:46-49.
182. Ben-Jacob, E., I. Cohen, and D. L. Gutnick. 1998. Cooperative organization of bacterial colonies: from genotype to morphotype. *Annu Rev Microbiol* 52:779-806.
183. Picioreanu, C., M. C. van Loosdrecht, and J. J. Heijnen. 1998. Mathematical modeling of biofilm structure with a hybrid differential-discrete cellular automaton approach. *Biotechnol Bioeng* 58:101-116.
184. St'ovicek, V., L. Vachova, M. Kuthan, and Z. Palkova. 2010. General factors important for the formation of structured biofilm-like yeast colonies. *Fungal Genet Biol* 47(12): 1012-1022.
185. Reynolds, T. B., A. Jansen, X. Peng, and G. R. Fink. 2008. Mat formation in *Saccharomyces cerevisiae* requires nutrient and pH gradients. *Eukaryot Cell* 7(1): 122-130.
186. Reynolds, T. B., and G. R. Fink. 2001. Bakers' yeast, a model for fungal biofilm formation. *Science* 291:878-881.
187. Folch, R., E. Alvarez-Lacalle, J. Ortin, and J. Casademunt. 2009. Pattern formation and interface pinch-off in rotating Hele-Shaw flows: a phase-field approach. *Phys Rev E Stat Nonlin Soft Matter Phys* 80(5 Pt 2): 056305.
188. Johnsen, O., R. Toussaint, K. J. Maloy, and E. G. Flekkoy. 2006. Pattern formation during air injection into granular materials confined in a circular Hele-Shaw cell. *Phys Rev E Stat Nonlin Soft Matter Phys* 74(1 Pt 1): 011301.
189. Praud, O., and H. L. Swinney. 2005. Fractal dimension and unscreened angles measured for radial viscous fingering. *Phys Rev E Stat Nonlin Soft Matter Phys* 72(1 Pt 1): 011406.
190. Efimenko, K., M. Rackaitis, E. Manias, A. Vaziri, L. Mahadevan, and J. Genzer. 2005. Nested self-similar wrinkling patterns in skins. *Nat Mater* 4(4): 293-297.
191. Tokudome, Y., K. Suzuki, T. Kitanaga, and M. Takahashi. 2012. Hierarchical nested wrinkles on silica-polymer hybrid films: stimuli-responsive micro periodic surface architectures. *Sci Rep* 2: 683.
192. Freed, A. D., J. Liao, and D. R. Einstein. 2014. A membrane model from implicit elasticity theory: application to visceral pleura. *Biomech Model Mechanobiol* 13(4): 871-881.
193. Pujol, T., O. du Roure, M. Fermigier, and J. Heuvingh. 2012. Impact of branching on the elasticity of actin networks. *Proc Natl Acad Sci U S A* 109(26): 10364-10369.
194. Nishi, K., M. Chijiishi, Y. Katsumoto, T. Nakao, K. Fujii, U. I. Chung, H. Noguchi, T. Sakai, and M. Shibayama. 2012. Rubber elasticity for incomplete polymer networks. *J Chem Phys* 137(22): 224903.
195. Nayar, V. T., J. D. Weiland, C. S. Nelson, and A. M. Hodge. 2012. Elastic and viscoelastic characterization of agar. *J Mech Behav Biomed Mater* 7: 60-68.
196. Abe, Y., P. Polyakov, S. Skali-Lami, and G. Francius. 2011. Elasticity and physico-chemical properties during drinking water biofilm formation. *Biofouling* 27(7): 739-750.
197. Mathieu, L., I. Bertrand, Y. Abe, E. Angel, J. C. Block, S. Skali-Lami, and G. Francius. 2014. Drinking water biofilm cohesiveness changes under chlorination or hydrodynamic stress. *Water*

- Res 55: 175-184.
198. Stovicek, V., L. Vachova, and Z. Palkova. 2012. Yeast biofilm colony as an orchestrated multicellular organism. *Commun Integr Biol* 5(2): 203-205.
 199. Gore, J., H. Youk, and A. van Oudenaarden. 2009. Snowdrift game dynamics and facultative cheating in yeast. *Nature* 459:253-256.
 200. Koschwanez, J. H., K. R. Foster, and A. W. Murray. 2011. Sucrose utilization in budding yeast as a model for the origin of undifferentiated multicellularity. *PLoS biology* 9(8): e1001122.
 201. Smukalla, S., M. Caldara, N. Pochet, A. Beauvais, S. Guadagnini, C. Yan, M. D. Vinces, A. Jansen, M. C. Prevost, J. P. Latge, G. R. Fink, K. R. Foster, and K. J. Verstrepen. 2008. FLO1 is a variable green beard gene that drives biofilm-like cooperation in budding yeast. *Cell* 135:726-737.
 202. Verstrepen, K. J., G. Derdelinckx, H. Verachtert, and F. R. Delvaux. 2003. Yeast flocculation: what brewers should know. *Appl Microbiol Biotechnol* 61(3): 197-205.
 203. Sieiro, C., N. M. Reboredo, and T. G. Villa. 1995. Flocculation of industrial and laboratory strains of *Saccharomyces cerevisiae*. *J Ind Microbiol* 14:461-466.
 204. Govender, P., J. L. Domingo, M. C. Bester, I. S. Pretorius, and F. F. Bauer. 2008. Controlled expression of the dominant flocculation genes FLO1, FLO5, and FLO11 in *Saccharomyces cerevisiae*. *Appl Environ Microbiol* 74(19): 6041-6052.
 205. Teunissen, A. W., J. A. van den Berg, and H. Y. Steensma. 1995. Localization of the dominant flocculation genes FLO5 and FLO8 of *Saccharomyces cerevisiae*. *Yeast* 11:735-745.
 206. Bidard, F., B. Blondin, S. Dequin, F. Vezinhet, and P. Barre. 1994. Cloning and analysis of a FLO5 flocculation gene from *S. cerevisiae*. *Curr Genet* 25:196-201.
 207. Verstrepen, K. J., and F. M. Klis. 2006. Flocculation, adhesion and biofilm formation in yeasts. *Mol Microbiol* 60(1): 5-15.
 208. Lo, W. S., and A. M. Dranginis. 1996. FLO11, a yeast gene related to the STA genes, encodes a novel cell surface flocculin. *J Bacteriol* 178(24): 7144-7151.
 209. Lo, W. S., and A. M. Dranginis. 1998. The cell surface flocculin Flo11 is required for pseudohyphae formation and invasion by *Saccharomyces cerevisiae*. *Mol Biol Cell* 9(1): 161-171.
 210. Lambrechts, M. G., F. F. Bauer, J. Marmur, and I. S. Pretorius. 1996. Muc1, a mucin-like protein that is regulated by Mss10, is critical for pseudohyphal differentiation in yeast. *Proc Natl Acad Sci U S A* 93(16): 8419-8424.
 211. Hilkens, J., M. J. Ligtenberg, H. L. Vos, and S. V. Litvinov. 1992. Cell membrane-associated mucins and their adhesion-modulating property. *Trends Biochem Sci* 17(9): 359-363.
 212. Patton, S., S. J. Gendler, and A. P. Spicer. 1995. The epithelial mucin, MUC1, of milk, mammary gland and other tissues. *Biochim Biophys Acta* 1241(3): 407-423.
 213. Gendler, S. J., and A. P. Spicer. 1995. Epithelial mucin genes. *Annu Rev Physiol* 57:607-634.
 214. Kufe, D. W. 2009. Mucins in cancer: function, prognosis and therapy. *Nat Rev Cancer* 9:874-885.
 215. Kang, S., and H. Choi. 2005. Effect of surface hydrophobicity on the adhesion of *S. cerevisiae* onto modified surfaces by poly(styrene-ran-sulfonic acid) random copolymers. *Colloids and surfaces. B, Biointerfaces* 46(2): 70-77.
 216. Guo, B., C. A. Styles, Q. Feng, and G. R. Fink. 2000. A *Saccharomyces* gene family involved in

- invasive growth, cell-cell adhesion, and mating. *Proc Natl Acad Sci U S A* 97(22): 12158-12163.
217. Groes, M., K. Teilum, K. Olesen, F. M. Poulsen, and A. Henriksen. 2002. Purification, crystallization and preliminary X-ray diffraction analysis of the carbohydrate-binding domain of flocculin, a cell-adhesion molecule from *Saccharomyces carlsbergensis*. *Acta Crystallogr D Biol Crystallogr* 58(Pt 12): 2135-2137.
 218. Rigden, D. J., L. V. Mello, and M. Y. Galperin. 2004. The PA14 domain, a conserved all-beta domain in bacterial toxins, enzymes, adhesins and signaling molecules. *Trends Biochem Sci* 29:335-339.
 219. Kapteyn, J. C., H. Van Den Ende, and F. M. Klis. 1999. The contribution of cell wall proteins to the organization of the yeast cell wall. *Biochim Biophys Acta* 1426(2): 373-383.
 220. Bony, M., D. Thines-Sempoux, P. Barre, and B. Blondin. 1997. Localization and cell surface anchoring of the *Saccharomyces cerevisiae* flocculation protein Flo1p. *J Bacteriol* 179(15): 4929-4936.
 221. Verstrepen, K. J., A. Jansen, F. Lewitter, and G. R. Fink. 2005. Intragenic tandem repeats generate functional variability. *Nat Genet* 37:986-990.
 222. Verstrepen, K. J., T. B. Reynolds, and G. R. Fink. 2004. Origins of variation in the fungal cell surface. *Nat Rev Microbiol* 2(7): 533-540.
 223. Goossens, K. V., and R. G. Willaert. 2012. The N-terminal domain of the Flo11 protein from *Saccharomyces cerevisiae* is an adhesin without mannose-binding activity. *FEMS Yeast Res* 12(1): 78-87.
 224. Govender, P., S. Kroppenstedt, and F. F. Bauer. 2011. Novel wine-mediated FLO11 flocculation phenotype of commercial *Saccharomyces cerevisiae* wine yeast strains with modified FLO gene expression. *FEMS Microbiol Lett* 317(2): 117-126.
 225. Douglas, L. M., L. Li, Y. Yang, and A. M. Dranginis. 2007. Expression and characterization of the flocculin Flo11/Muc1, a *Saccharomyces cerevisiae* mannoprotein with homotypic properties of adhesion. *Eukaryot Cell* 6(12): 2214-2221.
 226. Barrales, R. R., P. Korber, J. Jimenez, and J. I. Ibeas. 2012. Chromatin modulation at the FLO11 promoter of *Saccharomyces cerevisiae* by HDAC and Swi/Snf complexes. *Genetics* 191:791-803.
 227. Lo, W. S., and A. M. Dranginis. 1998. The cell surface flocculin Flo11 is required for pseudohyphae formation and invasion by *Saccharomyces cerevisiae*. *Mol Biol Cell* 9:161-171.
 228. Holmes, D. L., A. K. Lancaster, S. Lindquist, and R. Halfmann. 2013. Heritable remodeling of yeast multicellularity by an environmentally responsive prion. *Cell* 153:153-165.
 229. Lo, T. L., Y. Qu, N. Uwamahoro, T. Quenault, T. H. Beilharz, and A. Traven. 2012. The mRNA decay pathway regulates the expression of the Flo11 adhesin and biofilm formation in *Saccharomyces cerevisiae*. *Genetics* 191:1387-1391.
 230. Bumgarner, S. L., R. D. Dowell, P. Grisafi, D. K. Gifford, and G. R. Fink. 2009. Toggle involving cis-interfering noncoding RNAs controls variegated gene expression in yeast. *Proc Natl Acad Sci U S A* 106(43): 18321-18326.
 231. Davenport, K. D., K. E. Williams, B. D. Ullmann, and M. C. Gustin. 1999. Activation of the *Saccharomyces cerevisiae* filamentation/invasion pathway by osmotic stress in high-osmolarity glycogen pathway mutants. *Genetics* 153:1091-1103.

232. Andersson, J., D. M. Simpson, M. Qi, Y. Wang, and E. A. Elion. 2004. Differential input by Ste5 scaffold and Msg5 phosphatase route a MAPK cascade to multiple outcomes. *EMBO J* 23:2564-2576.
233. Lorenz, M. C., N. S. Cutler, and J. Heitman. 2000. Characterization of alcohol-induced filamentous growth in *Saccharomyces cerevisiae*. *Mol Biol Cell* 11:183-199.
234. Vinod, P. K., N. Sengupta, P. J. Bhat, and K. V. Venkatesh. 2008. Integration of global signaling pathways, cAMP-PKA, MAPK and TOR in the regulation of FLO11. *PLoS One* 3(2): e1663.
235. Cook, J. G., L. Bardwell, and J. Thorner. 1997. Inhibitory and activating functions for MAPK Kss1 in the *S. cerevisiae* filamentous-growth signalling pathway. *Nature* 390:85-88.
236. Gagiano, M., D. van Dyk, F. F. Bauer, M. G. Lambrechts, and I. S. Pretorius. 1999. Msn1p/Mss10p, Mss11p and Muc1p/Flo11p are part of a signal transduction pathway downstream of Mep2p regulating invasive growth and pseudohyphal differentiation in *Saccharomyces cerevisiae*. *Mol Microbiol* 31(1): 103-116.
237. Chin, B. L., O. Ryan, F. Lewitter, C. Boone, and G. R. Fink. 2012. Genetic variation in *Saccharomyces cerevisiae*: circuit diversification in a signal transduction network. *Genetics* 192:1523-1532.
238. Vinod, P. K., and K. V. Venkatesh. 2007. Specificity of MAPK signaling towards FLO11 expression is established by crosstalk from cAMP pathway. *Syst Synth Biol* 1:99-108.
239. Chang, M., C. M. Kang, Y. S. Park, and C. W. Yun. 2014. Rck1 up-regulates pseudohyphal growth by activating the Ras2 and MAP kinase pathways independently in *Saccharomyces cerevisiae*. *Biochem Biophys Res Commun* 444:656-661.
240. Fichtner, L., F. Schulze, and G. H. Braus. 2007. Differential Flo8p-dependent regulation of FLO1 and FLO11 for cell-cell and cell-substrate adherence of *S. cerevisiae* S288c. *Mol Microbiol* 66(5): 1276-1289.
241. van Dyk, D., I. S. Pretorius, and F. F. Bauer. 2005. Mss11p is a central element of the regulatory network that controls FLO11 expression and invasive growth in *Saccharomyces cerevisiae*. *Genetics* 169:91-106.
242. Halme, A., S. Bumgarner, C. Styles, and G. R. Fink. 2004. Genetic and epigenetic regulation of the FLO gene family generates cell-surface variation in yeast. *Cell* 116:405-415.
243. Ryan, O., R. S. Shapiro, C. F. Kurat, D. Mayhew, A. Baryshnikova, B. Chin, Z. Y. Lin, M. J. Cox, F. Vizeacoumar, D. Cheung, S. Bahr, K. Tsui, F. Tebbji, A. Sellam, F. Istel, T. Schwarzmuller, T. B. Reynolds, K. Kuchler, D. K. Gifford, M. Whiteway, G. Giaever, C. Nislow, M. Costanzo, A. C. Gingras, R. D. Mitra, B. Andrews, G. R. Fink, L. E. Cowen, and C. Boone. 2012. Global gene deletion analysis exploring yeast filamentous growth. *Science* 337:1353-1356.
244. Octavio, L. M., K. Gedeon, and N. Maheshri. 2009. Epigenetic and conventional regulation is distributed among activators of FLO11 allowing tuning of population-level heterogeneity in its expression. *PLoS Genet* 5(10): e1000673.
245. Chen, H., and G. R. Fink. 2006. Feedback control of morphogenesis in fungi by aromatic alcohols. *Genes Dev* 20:1150-1161.
246. Rupp, S., E. Summers, H. J. Lo, H. Madhani, and G. Fink. 1999. MAP kinase and cAMP filamentation signaling pathways converge on the unusually large promoter of the yeast FLO11 gene. *EMBO J* 18:1257-1269.

247. Karunanithi, S., J. Joshi, C. Chavel, B. Birkaya, L. Grell, and P. J. Cullen. 2012. Regulation of mat responses by a differentiation MAPK pathway in *Saccharomyces cerevisiae*. *PLoS One* 7(4): e32294.
248. Karunanithi, S., N. Vadaie, C. A. Chavel, B. Birkaya, J. Joshi, L. Grell, and P. J. Cullen. 2010. Shedding of the mucin-like flocculin Flo11p reveals a new aspect of fungal adhesion regulation. *Curr Biol* 20(15): 1389-1395.
249. Bou Zeidan, M., L. Carmona, S. Zara, and J. F. Marcos. 2013. FLO11 Gene Is Involved in the Interaction of Flor Strains of *Saccharomyces cerevisiae* with a Biofilm-Promoting Synthetic Hexapeptide. *Appl Environ Microbiol* 79(19): 6023-6032.
250. Zara, G., P. Goffrini, T. Lodi, S. Zara, I. Mannazzu, and M. Budroni. 2012. FLO11 expression and lipid biosynthesis are required for air-liquid biofilm formation in a *Saccharomyces cerevisiae* flor strain. *FEMS Yeast Res* 12(7): 864-866.
251. Zara, G., M. Budroni, I. Mannazzu, and S. Zara. 2011. Air-liquid biofilm formation is dependent on ammonium depletion in a *Saccharomyces cerevisiae* flor strain. *Yeast* 28:809-814.
252. Zara, G., S. Zara, C. Pinna, S. Marceddu, and M. Budroni. 2009. FLO11 gene length and transcriptional level affect biofilm-forming ability of wild flor strains of *Saccharomyces cerevisiae*. *Microbiology* 155:3838-3846.
253. Zara, S., A. T. Bakalinsky, G. Zara, G. Pirino, M. A. Demontis, and M. Budroni. 2005. FLO11-based model for air-liquid interfacial biofilm formation by *Saccharomyces cerevisiae*. *Appl Environ Microbiol* 71(6): 2934-2939.
254. Syrkina, M. S., M. A. Rubtsov, D. M. Potashnikova, Y. D. Kondratenko, A. A. Dokrunova, and V. P. Veiko. 2014. Cell Models for the Investigation of the Role of the Mucin MUC1 Extracellular Domain in Metastasizing. *Acta Naturae* 6(2): 62-70.
255. Castorina, A., and S. Giunta. 2014. Mucin 1 (MUC1) signalling contributes to increase the resistance to cell death in human bronchial epithelial cells exposed to nickel acetate. *Biometals*.
256. Vachova, L., O. Chernyavskiy, D. Strachotova, P. Bianchini, Z. Burdikova, I. Fercikova, L. Kubinova, and Z. Palkova. 2009. Architecture of developing multicellular yeast colony: spatio-temporal expression of Ato1p ammonium exporter. *Environ Microbiol* 11(7): 1866-1877.
257. Voordeckers, K., D. De Maeyer, E. van der Zande, M. D. Vincens, W. Meert, L. Cloots, O. Ryan, K. Marchal, and K. J. Verstrepen. 2012. Identification of a complex genetic network underlying *Saccharomyces cerevisiae* colony morphology. *Mol Microbiol* 86(1): 225-239.
258. Bester, M. C., D. Jacobson, and F. F. Bauer. 2012. Many *Saccharomyces cerevisiae* Cell Wall Protein Encoding Genes Are Coregulated by Mss11, but Cellular Adhesion Phenotypes Appear Only Flo Protein Dependent. *G3 (Bethesda)* 2(1): 131-141.
259. Strittmatter, A. W., C. Fischer, M. Kleinschmidt, and G. H. Braus. 2006. FLO11 mediated filamentous growth of the yeast *Saccharomyces cerevisiae* depends on the expression of the ribosomal RPS26 genes. *Mol Genet Genomics* 276:113-125.
260. Granek, J. A., and P. M. Magwene. 2010. Environmental and genetic determinants of colony morphology in yeast. *PLoS Genet* 6:e1000823.
261. Torbensen, R., H. D. Moller, D. Gresham, S. Alizadeh, D. Ochmann, E. Boles, and B. Regenber. 2012. Amino acid transporter genes are essential for FLO11-dependent and FLO11-independent biofilm formation and invasive growth in *Saccharomyces cerevisiae*. *PLoS One* 7(7): e41272.

262. Voordeckers, K., D. De Maeyer, E. van der Zande, M. D. Vences, W. Meert, L. Cloots, O. Ryan, K. Marchal, and K. J. Verstrepen. 2012. Identification of a complex genetic network underlying *Saccharomyces cerevisiae* colony morphology. *Mol Microbiol* 86(1): 225-239.
263. Purevdorj-Gage, B., M. E. Orr, P. Stoodley, K. B. Sheehan, and L. E. Hyman. 2007. The role of FLO11 in *Saccharomyces cerevisiae* biofilm development in a laboratory based flow-cell system. *FEMS Yeast Res* 7(3): 372-379.
264. Granek, J. A., D. Murray, O. Kayrkci, and P. M. Magwene. 2013. The genetic architecture of biofilm formation in a clinical isolate of *Saccharomyces cerevisiae*. *Genetics* 193:587-600.
265. Lopez, S., J. France, W. J. Gerrits, M. S. Dhanoa, D. J. Humphries, and J. Dijkstra. 2000. A generalized Michaelis-Menten equation for the analysis of growth. *J Anim Sci* 78(7): 1816-1828.
266. Douglas, L. M., L. Li, Y. Yang, and A. M. Dranginis. 2007. Expression and characterization of the flocculin Flo11/Muc1, a *Saccharomyces cerevisiae* mannoprotein with homotypic properties of adhesion. *Eukaryot Cell* 6:2214-2221.
267. Alfred, R. L., E. A. Palombo, J. F. Panozzo, and M. Bhave. 2013. The antimicrobial domains of wheat puroindolines are cell-penetrating peptides with possible intracellular mechanisms of action. *PLoS One* 8(10): e75488.
268. Ben-Jacob, E., I. Cohen, O. Shochet, I. Aranson, H. Levine, and L. Tsimring. 1995. Complex bacterial patterns. *Nature* 373:566-567.
269. Ben-Jacob, E., I. I. Cohen, O. Shochet, A. Tenenbaum, A. Czirok, and T. Vicsek. 1995. Cooperative formation of chiral patterns during growth of bacterial colonies. *Phys Rev Lett* 75(15): 2899-2902.
270. Serra, D. O., A. M. Richter, G. Klauck, F. Mika, and R. Hengge. 2013. Microanatomy at cellular resolution and spatial order of physiological differentiation in a bacterial biofilm. *MBio* 4(2): e00103-00113.
271. Massol-Deya, A. A., J. Whallon, R. F. Hickey, and J. M. Tiedje. 1995. Channel structures in aerobic biofilms of fixed-film reactors treating contaminated groundwater. *Appl Environ Microbiol* 61(2): 769-777.
272. Stewart, P. S. 2003. Diffusion in biofilms. *J Bacteriol* 185(5): 1485-1491.
273. Vandeparre, H., M. Pineirua, F. Brau, B. Roman, J. Bico, C. Gay, W. Bao, C. N. Lau, P. M. Reis, and P. Damman. 2011. Wrinkling hierarchy in constrained thin sheets from suspended graphene to curtains. *Phys Rev Lett* 106(22): 224301.
274. Vandeparre, H., and P. Damman. 2008. Wrinkling of stimuloresponsive surfaces: mechanical instability coupled to diffusion. *Phys Rev Lett* 101(12): 124301.
275. Renner, L. D., and D. B. Weibel. 2011. Physicochemical regulation of biofilm formation. *MRS Bull* 36(5): 347-355.
276. Abdallah, M., C. Benoliel, D. Drider, P. Dhulster, and N. E. Chihib. 2014. Biofilm formation and persistence on abiotic surfaces in the context of food and medical environments. *Arch Microbiol* 196:453-472.
277. Williams, V., and M. Fletcher. 1996. *Pseudomonas fluorescens* adhesion and transport through porous media are affected by lipopolysaccharide composition. *Appl Environ Microbiol* 62(1): 100-104.
278. Ridout, M. J., G. J. Brownsey, G. M. York, G. C. Walker, and V. J. Morris. 1997. Effect of o-acyl

- substituents on the functional behaviour of *Rhizobium meliloti* succinoglycan. *Int J Biol Macromol* 20(1): 1-7.
279. Villain-Simonnet, A., M. Milas, and M. Rinaudo. 2000. A new bacterial polysaccharide (YAS34). I. Characterization of the conformations and conformational transition. *Int J Biol Macromol* 27:65-75.
280. Cui, T., P. H. Liao, C. Guan, and H. C. Guo. 1999. Purification and crystallization of precursors and autoprocessed enzymes of *Flavobacterium glycosylasparaginase*: an N-terminal nucleophile hydrolase. *Acta Crystallogr D Biol Crystallogr* 55(Pt 11): 1961-1964.
281. Cerda, E., and L. Mahadevan. 2003. Geometry and physics of wrinkling. *Phys Rev Lett* 90(7): 074302.
282. Lau, P. C., J. R. Dutcher, T. J. Beveridge, and J. S. Lam. 2009. Absolute quantitation of bacterial biofilm adhesion and viscoelasticity by microbead force spectroscopy. *Biophys J* 96(7): 2935-2948.
283. Vachova, L., and Z. Palkova. 2011. Aging and longevity of yeast colony populations: metabolic adaptation and differentiation. *Biochem Soc Trans* 39(5): 1471-1475.
284. Trejo, M., C. Douarce, V. Bailleux, C. Poulard, S. Mariot, C. Regeard, and E. Raspaud. 2013. Elasticity and wrinkled morphology of *Bacillus subtilis* pellicles. *Proc Natl Acad Sci U S A* 110(6): 2011-2016.
285. Kim, J., J. E. Heindl, and C. Fuqua. 2013. Coordination of division and development influences complex multicellular behavior in *Agrobacterium tumefaciens*. *PLoS One* 8(2): e56682.
286. Hausler, S., and C. Fuqua. 2013. Biofilms 2012: new discoveries and significant wrinkles in a dynamic field. *J Bacteriol* 195(13): 2947-2958.
287. Stewart, P. S., and M. J. Franklin. 2008. Physiological heterogeneity in biofilms. *Nat Rev Microbiol* 6(3): 199-210.
288. Lenz, A. P., K. S. Williamson, B. Pitts, P. S. Stewart, and M. J. Franklin. 2008. Localized gene expression in *Pseudomonas aeruginosa* biofilms. *Appl Environ Microbiol* 74(14): 4463-4471.
289. Werner, E., F. Roe, A. Bugnicourt, M. J. Franklin, A. Heydorn, S. Molin, B. Pitts, and P. S. Stewart. 2004. Stratified growth in *Pseudomonas aeruginosa* biofilms. *Appl Environ Microbiol* 70(10): 6188-6196.
290. Borriello, G., E. Werner, F. Roe, A. M. Kim, G. D. Ehrlich, and P. S. Stewart. 2004. Oxygen limitation contributes to antibiotic tolerance of *Pseudomonas aeruginosa* in biofilms. *Antimicrob Agents Chemother* 48(7): 2659-2664.
291. Korolev, K. S., M. J. Muller, N. Karahan, A. W. Murray, O. Hallatschek, and D. R. Nelson. 2012. Selective sweeps in growing microbial colonies. *Physical biology* 9(2): 026008.
292. Hallatschek, O., P. Hersen, S. Ramanathan, and D. R. Nelson. 2007. Genetic drift at expanding frontiers promotes gene segregation. *Proc Natl Acad Sci U S A* 104(50): 19926-19930.
293. Reynolds, T. B. 2006. The Opi1p transcription factor affects expression of FLO11, mat formation, and invasive growth in *Saccharomyces cerevisiae*. *Eukaryot Cell* 5:1266-1275.
294. Aun, A., T. Tamm, and J. Sedman. 2013. Dysfunctional mitochondria modulate cAMP-PKA signaling and filamentous and invasive growth of *Saccharomyces cerevisiae*. *Genetics* 193:467-481.
295. Alexandre, H. 2013. Flor yeasts of *Saccharomyces cerevisiae*--their ecology, genetics and

- metabolism. *Int J Food Microbiol* 167:269-275.
296. Zara, S., A. T. Bakalinsky, G. Zara, G. Pirino, M. A. Demontis, and M. Budroni. 2005. FLO11-based model for air-liquid interfacial biofilm formation by *Saccharomyces cerevisiae*. *Appl Environ Microbiol* 71(6): 2934-2939.
 297. Claessen, D., D. E. Rozen, O. P. Kuipers, L. Sogaard-Andersen, and G. P. van Wezel. 2014. Bacterial solutions to multicellularity: a tale of biofilms, filaments and fruiting bodies. *Nat Rev Microbiol* 12(2): 115-124.
 298. Kaiser, D., M. Robinson, and L. Kroos. 2010. Myxobacteria, polarity, and multicellular morphogenesis. *Cold Spring Harb Perspect Biol* 2:a000380.
 299. Queller, D. C., and J. E. Strassmann. 2009. Beyond society: the evolution of organismality. *Philos Trans R Soc Lond B Biol Sci* 364:3143-3155.
 300. Queller, D. C., and J. E. Strassmann. 2013. Experimental evolution of multicellularity using microbial pseudo-organisms. *Biol Lett* 9:20120636.
 301. Cap, M., L. Vachova, and Z. Palkova. 2012. Reactive oxygen species in the signaling and adaptation of multicellular microbial communities. *Oxid Med Cell Longev* 2012:976753.
 302. Trovato, A., F. Seno, M. Zanardo, S. Alberghini, A. Tondello, and A. Squartini. 2014. Quorum vs. diffusion sensing: a quantitative analysis of the relevance of absorbing or reflecting boundaries. *FEMS Microbiol Lett* 352(2): 198-203.
 303. Solano, C., M. Echeverz, and I. Lasa. 2014. Biofilm dispersion and quorum sensing. *Curr Opin Microbiol* 18C: 96-104.
 304. Shojima, A., and J. Nakayama. 2014. Quorum Sensing in Gram-Positive Bacteria: Assay Protocols for Staphylococcal *agr* and Enterococcal *fsr* Systems. *Methods Mol Biol* 1147: 33-41.
 305. Murray, J. D. 1982. Parameter space for turing instability in reaction diffusion mechanisms: a comparison of models. *J Theor Biol* 98:143-163.
 306. Yaryura, P. M., M. Leon, O. S. Correa, N. L. Kerber, N. L. Pucheu, and A. F. Garcia. 2008. Assessment of the role of chemotaxis and biofilm formation as requirements for colonization of roots and seeds of soybean plants by *Bacillus amyloliquefaciens* BNM339. *Curr Microbiol* 56:625-632.
 307. Reynolds, T. B. 2006. The Opi1p transcription factor affects expression of FLO11, mat formation, and invasive growth in *Saccharomyces cerevisiae*. *Eukaryot Cell* 5(8): 1266-1275.
 308. Giaccia, A. J., M. C. Simon, and R. Johnson. 2004. The biology of hypoxia: the role of oxygen sensing in development, normal function, and disease. *Genes Dev* 18:2183-2194.
 309. Ben-Jacob, E., and H. Levine. 2006. Self-engineering capabilities of bacteria. *J R Soc Interface* 3:197-214.
 310. Tolker-Nielsen, T., and S. Molin. 2000. Spatial Organization of Microbial Biofilm Communities. *Microb Ecol* 40:75-84.
 311. Picioreanu, C., M. C. van Loosdrecht, and J. J. Heijnen. 1998. A new combined differential-discrete cellular automaton approach for biofilm modeling: application for growth in gel beads. *Biotechnol Bioeng* 57:718-731.
 312. Vandeparre, H., J. Leopoldes, C. Poulard, S. Desprez, G. Derue, C. Gay, and P. Damman. 2007. Slippery or sticky boundary conditions: control of wrinkling in metal-capped thin polymer films by selective adhesion to substrates. *Phys Rev Lett* 99(18): 188302.

313. Gupta, R. P., P. Kueppers, N. Hanekop, and L. Schmitt. 2014. Generating Symmetry in the Asymmetric ATP-binding Cassette (ABC) Transporter Pdr5 from *Saccharomyces cerevisiae*. *J Biol Chem* 289:15272-15279.
314. Sengupta, N., P. K. Vinod, and K. V. Venkatesh. 2007. Crosstalk between cAMP-PKA and MAP kinase pathways is a key regulatory design necessary to regulate FLO11 expression. *Biophys Chem* 125:59-71.
315. Palecek, S. P., A. S. Parikh, and S. J. Kron. 2000. Genetic analysis reveals that FLO11 upregulation and cell polarization independently regulate invasive growth in *Saccharomyces cerevisiae*. *Genetics* 156:1005-1023.
316. Wang, Q., and Z. F. Cui. 2011. Pleiotropic drug resistance ABC transporters in fungi. *Yi Chuan* 33(10): 1048-1056.

Bibliography

- **Publications**

Chen L., J. Noorbakhsh, R. M. Adams, J. Samaniego-Evans, G. Agollah, D. Nevozhay, J. Kuzdzal-Fick, P. Mehta and G. Balázsi. Two Dimensionality of Yeast Colony Expansion Accompanied by Pattern Formation. (PLoS Comp Bio, In Press)

Zhou Y., **Chen L.**, X. L. Chai, Z. N. Yu, M. Sun. Isolation of endophytic antagonistic bacterium from *Amorphophallus konjac* and research on its antibacterial metabolite. 2007. *Acta Microbiologica Sinica (Wei Sheng Wu Xue Bao)* 47 (6):1076-9.

- **Poster Presentations**

Chen L., D. Nevozhay, P. Mehta, G. Balázsi. Growth advantage associated with robust pattern formation in expanding yeast colonies. Poster session presented at Q-bio conference; 2012 Aug; Santa Fe, NM

Chen L., G. Agollah, D. Nevozhay and G. Balázsi. Characterization of pattern formation in *S.cerevisiae* in response to various agar and glucose levels. Poster session presented at 9th Annual Computational&Theoretical Biology Symposium; 2011 Dec; Houston, TX

Chen L., J Qu, K. L. Myhr. The potassium channel Kv4.2 is expressed in subtypes of retinal ganglion cells. Poster session presented at Society for Neuroscience (SFN) Annual Conference; 2008 Nov; Washington DC.

Vita

Lin Chen was born in Changsha, China, and obtained the Bachelor's Degree in Applied Biotechnology at Huazhong Agricultural University in Wuhan, China, then received a Master of Sciences Degree at Wayne State University in Detroit, Michigan. She worked at the Department of Neuroscience at Baylor College of Medicine before pursuing a Ph.D degree at the University of Texas Health Science Center at Houston Graduate School of Biomedical Sciences since 2011.